

Inaugural dissertation
for
obtaining the doctoral degree
of the
Combined Faculty of Mathematics, Engineering and Natural Sciences
of the
Ruprecht - Karls - University
Heidelberg

presented by

M.Sc. Hongxiang Li

born in: Linyi, Shandong, People's Republic of China

Oral examination: 14.12.2022

The functional evolution of photolyase related to DNA repair and
circadian clock in vertebrates

Referees: Prof. Dr. Nicholas S. Foulkes

Prof. Dr. Uwe Strähle

Acknowledgements

Time is so fast. My four years PhD life will come to the end. Here, I want to express all my sincere gratitude to all the people that supported me during my whole PhD and thanks all of you to have made my life colorful.

Firstly, I want to thank my supervisor, Prof. Dr. Nicholas S. Foulkes for giving me this valuable opportunity to start my PhD in your lab. Many thanks and appreciations to you for your continuous guidance and patience, even for the English speaking, slides preparation and basic knowledge of projects, you are always correcting me, guiding me and telling me. I am really grateful for that and that is really helpful for a research beginner. I am pretty sure that it was you who led me into the world of science that I am interested in. I never forget at the beginning of my PhD, everytime when we talked about the experiments and results, you always wrote a paper with all the detailed information that we just talked about, which really helped me a lot to understand my projects and let me develop good research habits. Thank you so much!

I also want to thank Dr. Daniela Vallone for kindly help in my daily lab life and critical suggestions for experiments and presentations. I still remember once when there were some people talking near my bench and occupying it, and when you saw me come into lab and just wait there, you came to me and asked if I needed space for experiments, which is really warm and inspired me. I really appreciate your friendly daily help.

I also want to thank Nathalie Geyer for perfect technical assistance and support. Many thanks for teaching me and showing me experimental skills and the lab rules. Without your support, I could not start my projects successfully. Also thank you for the preparation of birthday presents, which is really meaningful for me.

Besides, I want to thank all my lab former and present members: Haiyu Zhao, Juan Du, Rima Siauciunaite, Yuhang Hong, Alessandra Boiti, Gennaro Ruggiero, Shaun Wright, Felicia Sangermano, Patrizia Birner, Noah Schumann. Thank you all for the support and great time in my lab life. Thanks Haiyu for bringing me to the lab on the first day and

handing over all the lab materials to me. Thanks Juan for showing me how to culture cells and experimental skills. Thanks Yuhang for accompanying me for lunch every day, and we really have a great time during lunch, since we talk a lot about life, experiments, projects, and so on. It is really a good memory and I appreciate that.

In addition, I also want to show my gratitude and appreciation to my parents. Thanks a lot for supporting me all the time and encouraging me do what I am interested in. It is really the best gift for me to be your son. Your love, encouragement and support always keep me going.

Last but not least, I want to express my gratitude from the bottom of my heart to my wife, Xiaodi Hu, and my daughter, Caiwei Li. No amount of thanks and appreciation can equal to one percent of the love you gave to me. Xiaodi, thank you for being my wife and respecting and following every decision I made. It is really my great honor to be your husband. We have been hand-in-hand for more than ten years and have experienced a lot of joy and sadness. What I can do is always be with you and bring you happiness to show my gratitude. Caiwei, my daughter, thank you for being my daughter. You are the best gift for me and your mom. You always bring us endless joy and fun in life, enrich our PhD life, and help us through tough periods. We never regret to bring you to Germany and you also have an amazing time here, since you are very strong and confident. We really thank you for accompanying us to get our PhD degrees in Germany. You will never know how proud we are of you.

Table of Contents

Acknowledgements.....	5
Publication	10
Abbreviations	11
Abstract	15
Zusammenfassung	17
1. Introduction	19
1.1 Sunlight: a key environmental factor	19
1.2 DNA damage and repair	21
1.2.1 UV-induced DNA damage.....	21
1.2.2 Photoreactivation and photolyases.....	21
1.2.3 Photoreactivation of UV-induced CPD photoproducts.....	24
1.2.4 Photoreactivation of UV-induced 6-4pp photoproduct	25
1.2.5 Triple Tryptophan Electron Transfer Chain (TTETC)	26
1.2.6 NER repairs UV-induced DNA damage in mammals.....	27
1.2.7 Oxidative DNA damage	29
1.2.8 BER repairs oxidative DNA damage.....	30
1.2.9 Dark CPD.....	32
1.3. The circadian clock	34
1.3.1 Overview of the circadian clock	34
1.3.2 Molecular circadian clock mechanism	36
1.3.3 Light input to the clock in vertebrates.	39
1.3.4 PAR and E4BP4 bZip transcription factors and circadian clock regulation.	42
1.4 Links between DNA repair and circadian clocks.....	45
1.4.1 Cryptochrome/photolyase family (CPF)	45
1.4.2 Bifunctional CPF members	47
1.4.3 Nocturnal bottleneck theory.....	48
1.5 Comparative fish models for studying the circadian clock and DNA repair.	51
1.6 Aims.....	56
2. Materials and Methods.....	58
2.1 Medaka fish maintenance and dissection of tissues.....	58
2.2 Fish and mammalian cell culture and transfection	58
2.3 Light sources, UV radiation and H ₂ O ₂ treatment	59
2.4 Cell viability assay.....	60
2.4.1 MTT assay.....	60
2.4.2 AHM assay	60
2.5 Immunofluorescence assay.....	61
2.5.1 Immunofluorescence assay in cells.....	61
2.5.2 Immunofluorescence assay in fish fin clips	62
2.5.3 Image analysis	62
2.6 ELISA assay	63
2.7 Construction and expression of gain of function mammalian cell lines	63
2.7.1 Establishment of gain-of-photolyase-function 3T3 cells	63

2.7.2 Site-directed mutagenesis.....	64
2.7.3 Western Blotting (WB) analysis.....	64
2.8 Coding sequence characterization and cloning.....	65
2.8.1 Alignment of coding sequences	65
2.8.2 Plasmid cloning	66
2.9 Gene expression analysis	66
2.9.1 RNA extraction	66
2.9.2 Reverse transcription (cDNA synthesis) and control PCR.....	67
2.9.3 Real-time PCR (qRT PCR)	69
2.10 Luciferase reporter gene assay.....	70
2.10.1 <i>In vitro</i> luciferase assay	70
2.10.2 <i>In vivo</i> luciferase assay (Real-time bioluminescence assay).....	71
2.10.3 Luciferase assay plasmids.....	71
2.11 Statistical analysis.....	72
3.Results.....	73
3.1 Loss of function of CPD photolyase.....	73
3.1.1 CPD photolyase function and oxidative stress	75
3.1.2 Cell viability in response to oxidative stress.....	78
3.2 Gain of CPD photolyase function in mammalian cells	81
3.2.1 Establishing a 3T3 cell line ectopically expressing CPD photolyase	81
3.2.2 Cell viability response to UV-C exposure in 3T3 cell lines.	82
3.2.3 Cellular DNA damage upon oxidative stress in 3T3 cells.....	83
3.2.4 3T3 CPD cell viability response to oxidative stress.....	85
3.3 Impact of light on ROS-induced DNA damage repair.....	88
3.3.1 Impact of light on cellular DNA damage repair upon oxidative stress	88
3.3.2 Impact of light on cell viability upon oxidative stress in medaka cells.....	90
3.4 Kinetics of DNA damage and repair	95
3.4.1 Kinetics of UV-induced DNA damage and repair.....	95
3.4.2 Kinetics of ROS-induced DNA damage and repair.....	97
3.4.3 ROS-induced 8-OHdG DNA damage and repair.....	99
3.5 Gain of function with CPD photolyase mutants	101
3.5.1 Construction of mammalian cell lines expressing CPD photolyase mutants	102
3.5.2 Validating loss of photoreactivation of UV-damaged DNA.....	102
3.5.3 Cell viability response to oxidative stress.....	104
3.6 Circadian clock gene expression upon loss of photolyase function	108
3.6.1 Circadian clock gene expression in loss of photolyase function cell lines.....	108
3.6.2 Circadian clock gene expression in loss of photolyase function mutant fish.	111
3.7 Circadian clock gene regulation by 6-4 photolyase.....	115
3.7.1 Circadian oscillation of <i>per1b</i> upon loss of 6-4 photolyase function.	115
3.7.2 Light impact on D-box in loss of 6-4 photolyase mutants	115
3.8 Regulation of the E-box enhancer by 6-4 photolyase.	117
3.9 Regulation of the D-box enhancer by 6-4 photolyase.....	119
4. Discussion.....	123
4.1 Activator for CPD photolyase "dark" DNA repair function.....	124

4.2 Molecular mechanism of 6-4 photolyase in light-dependent transcriptional control.	125
4.3 Co-evolution of cryptochrome (circadian clock) and photolyase (DNA repair)	127
4.4 Why is CPD photolyase (but not 6-4 and DASH photolyase) conserved in Somalian cavefish?	128
4.5 Perspectives	130
5. References:.....	131

Publication

Haiyu Zhao, **Hongxiang Li**, Juan Du, Giuseppe Di Mauro, Sebastian Lungu-Mitea, Nathalie Geyer, Daniela Vallone, Cristiano Bertolucci, **Nicholas S Foulkes***. Regulation of ddb2 expression in blind cavefish and zebrafish reveals plasticity in the control of sunlight-induced DNA damage repair. *PLoS Genet.* 2021;17(2): e1009356. Published 2021 Feb 5.

Abbreviations

6-4 PPs	(6-4) photoproducts of pyrimidine dimers
6-4 phr	6-4 photolyase
8-HDF	8-hydroxy-5-deazaflavin
8-oxoG	8-oxo-7,8-Dihydroguanine
8-OHdG	8-hydroxydeoxy-guanosine
AHM	automated high-throughput microscopy
ANOVA	Analysis of variance
AP-1	Activator Protein 1
APE1	AP-endonuclease 1
ATF	activating transcription factor
BER	Base Excision Repair
BET	back electron transfer
bZIP	Basic Leucine Zipper domain
BMAL	Brain and muscle ARNT-like
bp	base pair
BSA	Bovine Serum Albumin
bHLH	basic helix-loop-helix
BF	Bright field
CCGs	Clock-Controlled Genes
cDNA	complementary DNA
CLOCK	Circadian Locomotor Output Cycles Kaput
CPD	Cyclobutane Pyrimidine Dimer
CPD phr	CPD photolyase
CPF	cryptochrome/photolyase family
cps	counts per second
CRY	Cryptochrome
C-terminus	Carboxyl-terminus
CRISPR	Clustered regularly interspaced short palindromic repeats
Cas9	CRISPR-associated proteins 9
CREB	cAMP responsive element-binding protein
C/EBP	CAAT/enhancer-binding protein
CAR	constitutive androstane receptor
DAPI	4',6-diamidin-2-fenilindolo
DASH	(Drosophila, Arabidopsis, Synechocystis, Human)-type
DASH phr	DASH photolyase
D-box	D-box enhancer element
DBP	albumin D-site-Binding Protein
DMSO	Dimethylsulfoxide
DNA	Deoxyribonucleic acid
DTT	Dithiothreitol

DD	Constant darkness
DDB2	Damage-Specific DNA Binding Protein 2
DSB	DNA double strands break
dCPD	Dark CPD
E4BP4	E4 Binding Protein 4
E-box	E-box enhancer element
ECL	Enhanced chemiluminescence
EDTA	Ethylenediaminetetraacetic acid
ELISA	Enzyme-Linked ImmunoSorbent Assay
FAD	Flavin Adenine Dinucleotide
F	Phenylalanine
FEN1	Flap-endonuclease 1
FRET	Förster resonance energy transfer
FEO	food-entrained circadian oscillator
GG-NER	global genome NER
HLF	Hepatic Leukemia Factor
H ⁺	proton
H ₂ O ₂	hydrogen peroxide
h	hour
IPTG	Isopropyl-β-D-1-thiogalaktopyranosid
iCPD	incident CPD
kb	kilo base
kDa	kilo Dalton
KO	knockout
LB	Luria-Bertani Broth
LED	Light-Emitting Diode
Luc	Luciferase
LD	Light-dark cycle
LEO	light-entrained oscillator
MAPK	Mitogen-Activated Protein Kinase
ml	milliliter
mM	millimolar
MTHF	5,10-methenyltetrahydrofolate
mRNA	Messenger RNA
MTT	3-(4,5-dimethylthiazol-2-yl)-2,5-diphenyltetrazolium bromide
MgCl ₂	Magnesium chloride
Maf	musculoaponeurotic fibrosarcoma oncogene
NER	Nucleotide Excision Repair
NLS	Nuclear Localization Signal
ng	nanogram
nm	nanometer
NaCl	Sodium Chloride
NFIL3	nuclear factor, interleukin 3 regulated

NOS	Nitric oxide synthase
NOX	NADPH oxidases
NO•	nitric oxide
NF-κB	nuclear factor kappa-light-chain-enhancer of activated B
NF-E2	nuclear factor erythroid-derived 2
Opn4m2	Opsin 4 mammalian-like 2
O ₂ • ⁻	superoxide
•OH	hydroxyl radicals
ONOO ⁻	oxidant peroxynitrite
PI	propidium iodide
PCNA	proliferating cell nuclear antigen
PAS	Per-Arnt-Sim domain
PAGE	Polyacrylamide gel electrophoresis
PAR	Proline and acidic amino-acid-residue rich
PBS	Phosphate Buffered Saline
PBST	Phosphate Buffered Saline plus Tween
PBTX	Phosphate Buffered Saline plus Triton x 100
PCR	Polymerase Chain Reaction
PER	Period
PFA	Paraformaldehyde
qRT-PCR	quantitative real-time PCR
RNA	Ribonucleic acid
ROS	Reactive Oxygen Species
RT	Reverse Transcription
Ser	Serine
ssDNA	Single strand DNA
SDS	Sodium dodecyl sulphate
SCN	Suprachiasmatic nucleus
SD	Standard Deviation
SDS	Sodium Dodecyl Sulphate
SE	Standard Error
TEF	Thyrotroph Embryonic Factor
TC-NER	transcription-coupled repair
TMT	Teleost Multiple Tissue
Tris	Tris(hydroxymethyl)aminomethane
TTETC	Triple Tryptophan Electron Transfer Chain
T<>T	thymine-thymine dimer
TTFL	transcription-translation negative feedback loop
UV	Ultraviolet
μg	microgram
μl	microliter
WT	Wild type
W/Trp	Tryptophan

XRCC1	X-ray repair cross-complementing protein 1
XPC	Xeroderma Pigmentosum, Complementation Group C
ZT	Zietgeber

Abstract

The cryptochrome/photolyase family (CPF) is a group of highly conserved flavoproteins that harness sunlight to enable various biological processes including photoreception, DNA damage repair and circadian clock entrainment. Photoreactivation, one of the principal DNA repair systems is catalysed by the flavoprotein enzymes called photolyases. These use light as a driving force to repair UV-induced DNA damage and are encountered in almost all prokaryotes and eukaryotes with the notable, strange exception of placental mammals. The Foulkes lab's previous work has demonstrated that the Somalian cavefish, *Phreatichthys andruzzii*, which has evolved in a perpetually dark subterranean environment for millions of years, has greatly attenuated photoreactivation as the result of accumulating truncation mutations in the 6-4 and DASH photolyase genes. However, the CPD photolyase gene remains intact and encodes a protein that can still catalyze DNA repair. Is there selective pressure acting to maintain CPD photolyase function despite the complete absence of sunlight? Here I have used a comparative approach involving photolyase mutant lines generated in medaka as well as zebrafish and cavefish, to reveal that CPD photolyase confers increased cell survival and enhanced DNA repair capacity upon exposure of cells to oxidative stress. Furthermore, I demonstrate that light does not influence CPD photolyase-induced protection against ROS-induced mortality. Interestingly, in the absence of light, ROS can induce limited CPD production however, it remains unclear whether CPD photolyase may be able to catalyze the repair of this DNA damage under constant darkness. My results may account for why the CPD photolyase gene is conserved in the Somalian cavefish. Furthermore, this may provide clues as to how and why photolyase genes have been lost during placental mammal evolution.

It has been documented that in various organisms, many CPF flavoproteins possess a bifunctional property, specifically being not only implicated in DNA repair but also serving as circadian clock components. In this study, I have shown that the loss of 6-4 photolyase function disrupts rhythmic expression of certain clock genes in a gene- and

tissue-specific manner. Furthermore, I have shown that 6-4 photolyase participates in the transcription control of circadian clock genes via repression of transactivation of the CLOCK-BMAL complex occurring at E-box enhancer elements and via enhancing TEF transactivation at light-responsive D-box enhancer elements. However, the precise nature of the physical interaction between 6-4 photolyase and the CLOCK-BMAL heterodimer and the TEF protein remains unclear. My discovery provides new insight into the basis of the divergent function of CPF members in vertebrates. Furthermore, more generally the results obtained in this project reveal how the evolution of the CPF family of flavoproteins may have been shaped by adaptation to extreme environmental conditions.

Keywords: photolyase, photoreactivation, oxidative stress, cryptochrome, circadian clock, cavefish, evolution

Zusammenfassung

Die Cryptochrom-/Photolyase-Familie (CPF) ist eine Gruppe hochkonservierter Flavoproteine, die Sonnenlicht nutzen, um verschiedene biologische Prozesse zu ermöglichen. Dies beinhaltet Photorezeption, die Reparatur von DNA-Schäden und Entrainment der circadianen Uhr. Die Photoreaktivierung, eines der wichtigsten DNA-Reparatursysteme, wird durch Flavoprotein-Enzyme, die Photolyasen genannt werden, katalysiert. Diese verwenden Licht als treibende Kraft, um UV-induzierte DNA-Schäden zu reparieren. Sie kommen in fast allen Prokaryoten und Eukaryoten vor. Eine bemerkenswerte Ausnahme sind hierbei die Plazentasäuger. Vorausgehende Arbeit des Foulkes-Labors hat gezeigt, dass beim somalische Höhlenfisch, *Phreatichthys andruzzii*, der sich seit Millionen von Jahren in einer dauerhaft dunklen unterirdischen Umgebung entwickelt hat, die Photoreaktivierung durch Anhäufung von Trunkierungsmutationen in 6-4- und DASH-Photolyase-Genen stark abgeschwächt vorliegt. Das CPD-Photolyase-Gen ist jedoch intakt geblieben und codiert ein Protein, das weiterhin die DNA-Reparatur katalysieren kann. Gibt es einen selektiven Druck, um die CPD-Photolyase-Funktion trotz völliger Abwesenheit von Sonnenlicht aufrechtzuerhalten? Hier habe ich einen vergleichenden Ansatz zwischen Medaka-Photolyase-Mutationslinien, Zebrafischen und Höhlenfischen verwendet, um aufzuzeigen, dass die CPD-Photolyase ein erhöhtes Zellüberleben und eine verbesserte DNA-Reparaturkapazität bewirkt, wenn Zellen oxidativen DNA-Schäden ausgesetzt werden. Darüber hinaus zeige ich, dass der CPD-Photolyase-induzierte Schutz vor ROS-induzierter Mortalität nicht von Licht beeinflusst wird. Interessanterweise kann ROS in Abwesenheit von Licht die CPD-Produktion veranlassen. Es bleibt jedoch unklar, ob die CPD-Photolyase in der Lage sein könnte, die Reparatur dieses DNA-Schadens bei konstanter Dunkelheit zu katalysieren. Diese Ergebnisse könnten erklären, warum das CPD-Gen im somalischen Höhlenfisch trotz Millionen von Jahren der Evolution in ewiger Dunkelheit konserviert ist. Außerdem kann dies Hinweise darauf liefern, wie und warum Photolyase-Gene während der Evolution von Plazenta-Säugetieren verloren gegangen sind.

Es wurde demonstriert, dass viele Vertreter der CPF in unterschiedlichen Organismen eine bifunktionelle Eigenschaft besitzen und somit nicht nur mit der DNA-Reparatur verknüpft sind, sondern auch als Komponenten der circadianen Uhr dienen. In dieser Studie habe ich gezeigt, dass der Verlust der 6-4 Photolyase-Funktion die rhythmische Expression von uhrregulierten Core-Clock-Genen auf gen- und gewebespezifische Weise stört. Darüber hinaus habe ich gezeigt, dass 6-4 Photolyase an der Transkriptionskontrolle von circadianen Uhrgenen über die Repression der Transaktivierung des CLOCK-BMAL-Komplexes an E-Box-Enhancer-Elementen und über die Verstärkung der TEF-Transaktivierung an lichtempfindlichen D-Box-Enhancer-Elementen beteiligt ist. Die genaue Art der physikalischen Wechselwirkung zwischen 6-4 Photolyase und dem CLOCK-BMAL-Heterodimer und dem TEF-Protein bleibt jedoch unklar. Diese Entdeckung liefert neue Einblicke in die Grundlage der divergierenden Funktion von CPF-Photolyase-Vertretern in Wirbeltieren. Darüber hinaus zeigen die in diesem Projekt erzielten Ergebnisse ganz allgemein, wie die Evolution der CPF-Familie von Flavoproteinen durch die Anpassung an extreme Umweltbedingungen geprägt worden sein könnte.

Stichwörter: Photolyase, Photoreaktivierung, oxidativer Stress, Kryptochrom, zirkadiane Uhr, Höhlenfisch, Evolution

1. Introduction

1.1 Sunlight: a key environmental factor

Sunlight represents a dominating environmental factor for most organisms on earth. Animals and plants have evolved different strategies to perceive sunlight and to effectively mobilize it as a primary source of energy. For example, plants harness light energy to generate sugar from carbon dioxide and water by the process of photosynthesis, while via their visual systems, animals sense light to distinguish their orientation in the environment, locate their food and escape from predators. Furthermore, the daily variation in sunlight contributes to a crucial timing system for the optimum temporal organization of activity and physiology. Specifically, numerous biochemical, physiological, and behavioural processes are controlled by the so-called circadian clock, which is present in most organisms ranging from bacteria to humans^{1,2}. The term “Circadian” refers to their property that under constant conditions, this clock generates a rhythm that is approximately (*Circa*) one day (*diem*) in length. This rhythm enables organisms to anticipate the progression of the day-night cycle and so have sufficient time to make appropriate adaptations to meet the changing challenges of their environment according to the time of day. In order to synchronize this clock with the environmental 24 hours day-night cycle, organisms perceive daily changes in the intensity and spectrum of sunlight via dedicated photoreceptors and thereby reset the phase of the clock according to the time of day.

Sunlight also represents an environmental stressor. Exposure to ultraviolet (UV) radiation from sunlight can have deleterious effects on organisms, since it elicits the formation of genotoxic, mutagenic as well as carcinogenic DNA lesions^{3,4}. These predominantly include cyclobutane pyrimidine dimers (CPDs) and (6-4) photoproducts of pyrimidine dimers (6-4PPs). In order to survive these genetic changes, organisms have evolved a self-defense system termed photoreactivation, a DNA repair system that specifically removes UV-induced DNA lesions. Photoreactivation is a light-

dependent process that is mediated by enzymes termed DNA photolyases^{5,6}. These harvest blue light energy to catalyse the repair of UV-induced DNA damage⁷. The photolyases belong to a large family of highly conserved flavoproteins, the cryptochrome/photolyase family (CPF) which includes cryptochromes. Cryptochromes represent central components of the circadian clock mechanism which are involved in the light-dependent and light-independent modulation of circadian clock function. Exposure to sunlight can also induce the production of reactive oxygen species (ROS), which can result in oxidative damage of macromolecules, including DNA. Apart from having these deleterious effects, ROS can also potentially function as a "second messenger" involved in signaling pathways which participate in the regulation of cell growth, proliferation and apoptosis⁸.

Although sunlight dominates life on earth, there are many organisms which inhabit extreme, constant dark environments such as subterranean caves or abyssal regions of oceans. Such environments are extremely challenging for sustaining life since they cannot support photosynthesis or complex plant-based ecosystems. Therefore, they are frequently nutrient poor environments which pose particular challenges for animals to navigate, feed and reproduce. One classical example of animals that have adapted to life in the complete absence of sunlight are species of cavefish, which have evolved in perpetually dark, subterranean aquatic habitats in some cases for millions of years.

1.2 DNA damage and repair

1.2.1 UV-induced DNA damage

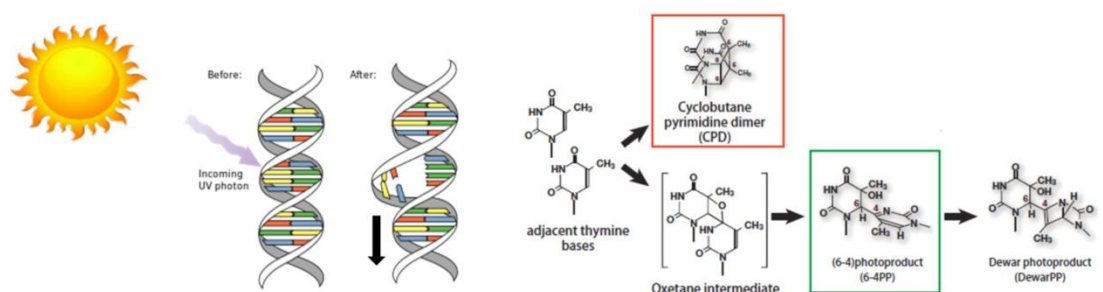


Figure 1.1 Ultraviolet (UV) irradiation from sunlight induces DNA damage and predominantly produces cyclobutane pyrimidine dimers (CPDs) and (6-4) photoproducts of pyrimidine dimers (6-4PPs)⁹.

The ultraviolet wavelengths of sunlight represent an important source of macromolecular damage, notably inducing mutations in DNA. Exposure to UV-C (200-280nm) and UV-B (280-320nm) is able to convert two adjacent pyrimidines (thymines and cytosines), to cyclobutane pyrimidine dimers (CPDs), (6-4) photoproducts of pyrimidine dimers (6-4PPs) and Dewar valence isomers, the photo isomerisation product of (6-4) photoproducts formed after 6-4PPs formation¹⁰ (Figure 1.1). CPDs represent the most abundant photoproducts arising from sunlight exposure (70-80%), while 6-4PPs are responsible for 20-30% of UV-induced DNA damage and the most cytotoxic lesions^{11,12}. These lesions result in distortion of the DNA double helix and thereby influence DNA replication as well as transcription resulting in mutations which can ultimately lead to carcinogenesis and cell death¹³.

1.2.2 Photoreactivation and photolyases

To preserve genome integrity, organisms have developed a battery of DNA repair pathways to detect different types of damage and initiate appropriate repair. One of them is photoreactivation, referring to the utilization of light as a source of energy to

repair ultraviolet-damaged DNA under the action of photolyases⁶. Three main classes of photolyase have been identified, CPD photolyase, 6-4 photolyase and Cry-DASH photolyase, which repair distinct types of UV-induced DNA damage^{9,14,15}. Specifically, CPD photolyase is involved in repairing the CPD photoproduct in the context of double-strand DNA, while 6-4 photolyase is engaged in repairing (6-4) photoproducts within double-strand DNA. Cry-DASH photolyase instead shows a high degree of specificity for repairing CPD photoproducts in single-strand DNA¹⁶ and it has also been reported that in the fungus *Mucor circinelloides*, Cry-DASH photolyase is able to repair CPD photoproducts in double-strand DNA, thereby acting like CPD photolyase¹⁷.

The structure of all photolyases incorporates two chromophores which absorb blue light, named flavin adenine dinucleotide (FAD) and methenyltetrahydrofolate (MTHF) or 8-hydroxy-5-deazaflavin (8-HDF)^{18,19}. The chromophores enable the photolyases to harvest light energy which is required to break the two abnormal bonds cross-linking the thymines in the various UV-induced photoproducts and consequently convert the pyrimidine dimers back to two separate canonical pyrimidines²⁰.

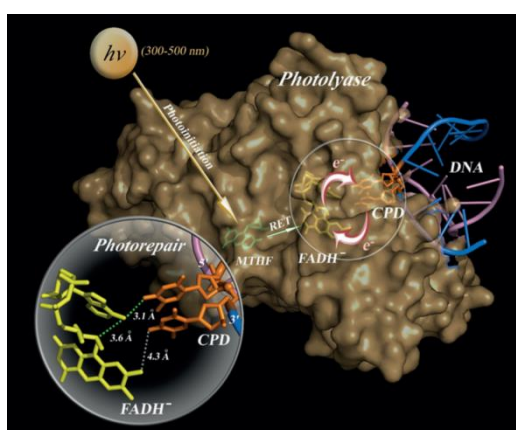


Figure 1.2 Reaction mechanism of photolyase. Photolyase recognizes and binds to the phosphate residues of the damaged DNA strand and flips out the thymine dimer dinucleotide into the active site cavity. Thereafter, photoactivation is initiated by the reduction of FADH^o to catalytically competent FADH⁻ by effectively accepting a photon and concomitantly, electron transfer from FADH^{*} to the pyrimidine dimers in order to separate them to reform two canonical thymines. The inset indicates the distances between the represented atoms of FADH⁻ and the cyclobutane pyrimidine dimer (CPD)^{21,22}.

Generally, photoreactivation consists of three main steps^{20,23-25}: recognition, photoactivation and photorepair. For the first step, due to the distortion of the DNA backbone caused by the pyrimidine dimers, photolyases are able to efficiently recognize and bind to DNA which incorporates abnormal photo-crosslinked pyrimidines. Following binding to the damage sites, photolyases flip the photoproducts out from within the helix and bury them in the core active site of the photolyase according to ionic interactions between the positively charged groove on the photolyase protein surface and the negatively charged DNA phosphodiester backbone. Thereafter, the pyrimidine dimers are connected with the FADH^o molecule by Van der Waals's forces. This binding between photolyase and damaged DNA is not light-dependent and can occur under darkness⁶. In the subsequent photoactivation step, semi-reduced flavin (FADH^o) is reduced to catalytically competent FADH⁻ by effectively accepting a photon in 2 alternative ways. The first way is via the blue light-absorbing antenna molecule, MTHF or 8-HDF, which upon absorbing a photon, transfers the excitation energy to semi-reduced flavin (FADH^o) by Förster resonance energy transfer (FRET) and thereby reduces it to FADH⁻^{21,22}. The second way is that FADH^o can receive a photon from the Three Tryptophan Electron Transfer Chain resulting in it achieving a fully reduced state. This triad of highly conserved Tryptophan residues within the photolyase active site can also harvest photons and thus transfer an electron to FADH^o, which will be discussed in detail later. The final process is photorepair, involving the complete reduction step from FADH⁻ to FADH^{-*} by accepting a 300-500 nm photon, and electron transfer from FADH^{-*} to the pyrimidine dimers, which results in them being separated into two canonical pyrimidines. After splitting of the pyrimidine dimers, electron transfer is reversed back to FADH⁻, and afterwards the photolyase dissociates from DNA, which closes the catalytic cycle. Subsequently the photolyase protein can continue searching for other DNA damage and implement the entire photoreactivation process once again (Figure 1.2)²⁶. It has been elucidated that based on the determination of the rates of energy transfer from chromophore to FADH^o, electron transfer from photoexcited FADH^{-*} to pyrimidine dimers, C5-C5' and C6-C6' bond cleavage, bond formation and electron return to the transiently formed

flavin radical FADH^\bullet in real-time and with picosecond resolution^{19,21–23,27–29}, the whole catalytic cycle is accomplished in 1.2 ns, and the photolyases repair pyrimidine dimers with a quantum yield of 0.9^{21,23,29}.

1.2.3 Photoreactivation of UV-induced CPD photoproducts

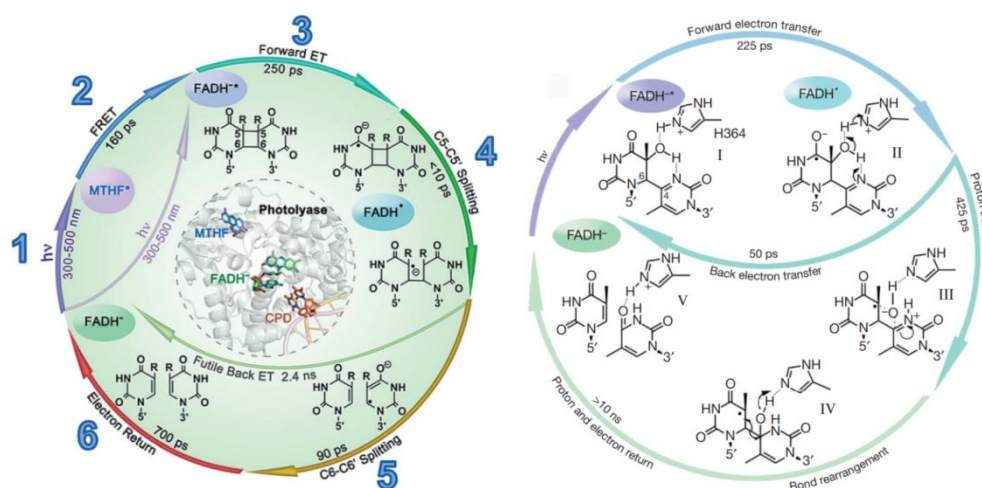


Figure 1.3 Dynamic repair mechanism of CPD and 6-4pp by CPD photolyase and 6-4pp photolyase, respectively. The left panel denotes repair kinetics of CPD photoproduct²², while the right panel indicates the dynamic repair of the 6-4pp photoproduct³⁰. All of the fundamental processes in photoreactivation are represented together with the reaction times.

The UV-induced CPD photoproduct is repaired by CPD photolyase under a cyclic electron-transfer radical mechanism, consisting of electron-tunneling pathways and cyclobutane ring splitting. Specifically, FADH^- is fully reduced to FADH^{\bullet} by accepting excitation energy from MTHF (or 8-HDF) or the Three Tryptophan Electron Transfer Chain, and then FADH^{\bullet} donates an electron to the CPD photoproduct with an intervening adenine moiety to result in a $\text{FADH}^\bullet + \text{T}^{\bullet}$ state. Subsequently, the C5-C5' bond is cleaved and then there are two possible outcomes: in the first scenario (without repair functionality), the electron transfers back to FADH^\bullet (back electron transfer, BET) to permit FADH^- to stay in a fully reduced FADH^- state to complete photoreactivation at other DNA damage sites; while in the other scenario (related to repair capacity), the C6-C6' bond is split as a result of electron transfer and thereafter,

the electron returns to FADH° which is reduced to FADH^- . During the entire process, the electron from FADH^* tunnels through the adenine moiety of FAD to the CPD photoproduct and the adenine moiety of FADH^- plays a crucial role in modulating forward electron transfer toward the 5' side of the CPD photoproduct and dictates the rate of electron transfer through a super exchange mechanism (Figure 1.3)^{6,22,28,31-35}.

1.2.4 Photoreactivation of UV-induced 6-4pp photoproduct

In *E.coli*, the process of photoreactivation of the 6-4pp photoproduct encompasses forward electron transfer, proton transfer, bond rearrangement and proton and electron return. Specifically, FADH^- receives excitation energy (a photon) and is fully reduced to FADH^* , donating an electron to the 6-4pp photoproduct. Thereafter, the photo induced electron transfer activates the catalytic and neighbouring proton transfer between the Histidine 364 residue in the active site of the 6-4 photolyase and 6-4pp photoproduct. This essential proton transfer step is a key step in the repair photocycle, which is stimulated by the initial electron transfer step, strongly competes with the back electron transfer from the 6-4pp photoproduct and assists the photoreaction repair to proceed effectively. After protonation and a battery of atomic rearrangements with bond cleavage and formation, the proton reversely transfers back to the Histidine 364 residue located in the active site of the 6-4 photolyase and the electron returns back to FADH° , reconstituting the 6-4 photolyase into its active state and converting the 6-4pp photoproduct into two canonical pyrimidines. The entire process is quite rapid, taking approximately ten nanoseconds (Figure 1.3)^{6,28,30,36-39}.

harvesting and electron transfer during photoactivation (Figure 1.4).

1.2.6 NER repairs UV-induced DNA damage in mammals

In addition to photoreactivation, organisms possess other, highly conserved DNA repair pathways for the repair of various other types of DNA damage induced by sunlight exposure, such as Nucleotide Excision Repair (NER), Base Excision Repair (BER). Strikingly, while photoreactivation is encountered in most organisms ranging from bacteria, fungi, plants to higher vertebrates, placental mammals lack photolyase genes and the function of the efficient photoreactivation pathway. Instead, placental mammals employ the versatile, evolutionary highly conserved and more complex NER DNA repair pathway to repair UV-induced DNA damage, indicating that during evolution of mammalian ancestors, selective pressure operated to eliminate light-dependent photolyase function.

The NER system incorporates 2 subpathways named global genome NER (GG-NER) and transcription-coupled repair (TC-NER). GG-NER provides whole genome-wide surveillance for a range of different types of DNA damage, but repairs certain types of DNA damage with reduced efficiency. TC-NER represents a complementary NER pathway which detects stalled RNA polymerases on the template strand of actively transcribed DNA, stalling that is associated with the presence of pyrimidine dimers along the DNA strand. Both NER subpathways represent complex multi-step processes that require a battery of concerted procedures involving approximately 30 proteins to sequentially implement damage recognition, chromatin remodeling, damage site excision, gap-filling DNA synthesis, and strand ligation^{11,42-45}.

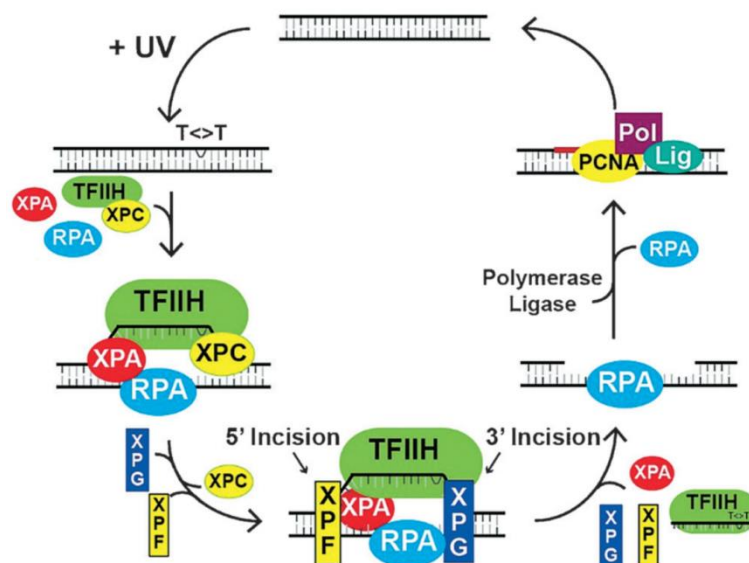


Figure 1.5 Reaction mechanism of the nucleotide excision repair system. The recognition of and binding of particular recognition factors (e.g. XPC) to DNA lesions triggers NER. Following the unwinding of the DNA double helix at the lesion region, short oligonucleotides are removed. Ultimately, DNA replication seals the gap, and DNA ligase ligates the nicks²⁰.

More specifically, for the GG-NER pathway, the DDB1-DDB2 complex (DDB2 is also known as XPE) is able to recognize DNA lesions and kinked damaged DNA directly to enable recognition by XPC. Afterwards, XPC recognizes helix-distorting DNA lesions and recruits the TFIIH complex, which contains the XPB and XPD helicase subunits which facilitate the opening of the damaged DNA. In contrast, in the case of TC-NER, CSB (ERCC6) recognizes the damage-stalled RNA polymerase and stimulates forward movement of this polymerase. In turn, the CSA (ERCC8), UVSSA and USP7 proteins are involved in regulating this process. Subsequently, the mechanisms of DNA incision and gap filling for both GG-NER and TC-NER are identical. The endonuclease XPF-ERCC1 heterodimer recruited by XPA cleaves the DNA at a position 5' of the lesion, while XPG recruited by XPA cleaves 3' of the lesion. Thereafter, DNA polymerase δ and ϵ convert the ssDNA gap to form double stranded DNA and the final nicks in both DNA strands are sealed by DNA ligase 1 (Figure 1.5)^{20,46,47}.

1.2.7 Oxidative DNA damage

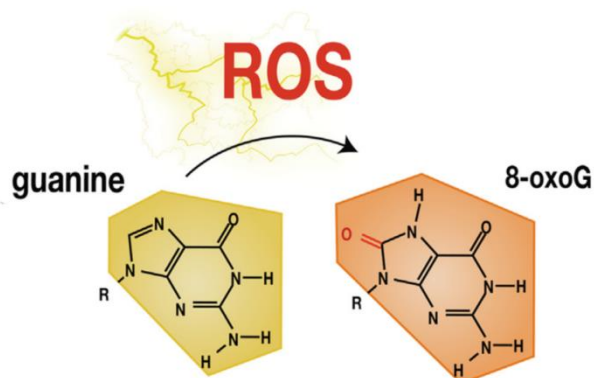


Figure 1.6 8-oxo-7,8-Dihydroguanine (8-oxoG). 8-oxoG is produced when reactive oxygen species (ROS) alters guanine under oxidative stress⁴⁸.

Besides UV-induced DNA damage, there exist many other types of DNA damage in organisms that can be induced upon prolonged exposure to sunlight. One of them is oxidative DNA damage, arising from elevated production of reactive oxygen species (ROS), comprising peroxides (e.g., H_2O_2), superoxide ($\text{O}_2^{\cdot-}$), hydroxyl radicals ($\cdot\text{OH}$) and singlet oxygen ($^1\text{O}_2$)⁴⁹. These can originate from a variety of external and internal sources, including endogenous chemical activity through the cells' own metabolism and enzymatic activity⁵⁰, inflammatory disorders^{51,52}, toxins⁵³, or radiation⁵⁴⁻⁵⁶. Exposure to UV can also induce cellular oxidative stress and consequent DNA damage in addition to the direct effects of UV on pyrimidine dimer formation. If left unrepaired, ROS-induced oxidative DNA damage can trigger the disruption of cellular function, mutations and ultimately cell death. The oxygen free radicals give rise to a variety of DNA lesions, incorporating oxidized bases, abasic (AP) sites, and DNA double strand breaks. Notably, one major site which is sensitive to oxidative reactions is the 8 position of guanine which when oxidized results in the formation of 7,8-dihydro-8-oxoguanine (8-oxoG) (Figure 1.6)^{57,58}. 8-oxoG has the propensity to mispair with A residues, giving rise to an increased frequency of spontaneous transversion mutations from G·C to T·A in repair-deficient organisms^{59,60}. 8-oxoG is able to disrupt intracellular functionality through two main routes. It can disrupt the binding between DNA and

proteins to consequently hinder^{61–66} or stimulate^{67–71} transcription. 8-oxoG can also alter the secondary structure of DNA and lead to dysfunctional genomic maintenance by influencing telomere length and genome instability^{72–75} and may also contribute to interfering with base lesion clusters at the replication fork⁷⁶, which potentially contributes to extra genome stability.

1.2.8 BER repairs oxidative DNA damage

To repair DNA damage which involves 8-oxoG base modifications, the Base Excision Repair (BER) pathway plays a pivotal role. At the onset, 8-oxoG is excised by 8-oxoguanine DNA glycosylase (OGG1) and consequently leaves an apurinic site (AP site). At this site, the DNA backbone is cleaved by AP-endonuclease 1 (APE1). Afterwards, for long patch base excision repair, the polymerase δ and ϵ as well as proliferating cell nuclear antigen (PCNA) are involved in converting the resulting single stranded portion into double stranded DNA, and then the old strand is removed by Flap-endonuclease 1 (FEN1) and sequentially the ligase I (Lig I) ligates the DNA backbone together. Meanwhile, for short patch base excision repair, polymerase β replaces the single missing base, ligase III (Lig III) ligates the DNA backbone back together and X-ray repair cross-complementing protein 1 (XRCC1) promotes the process and acts as a scaffold for additional components^{48,77} (Figure 1.7).

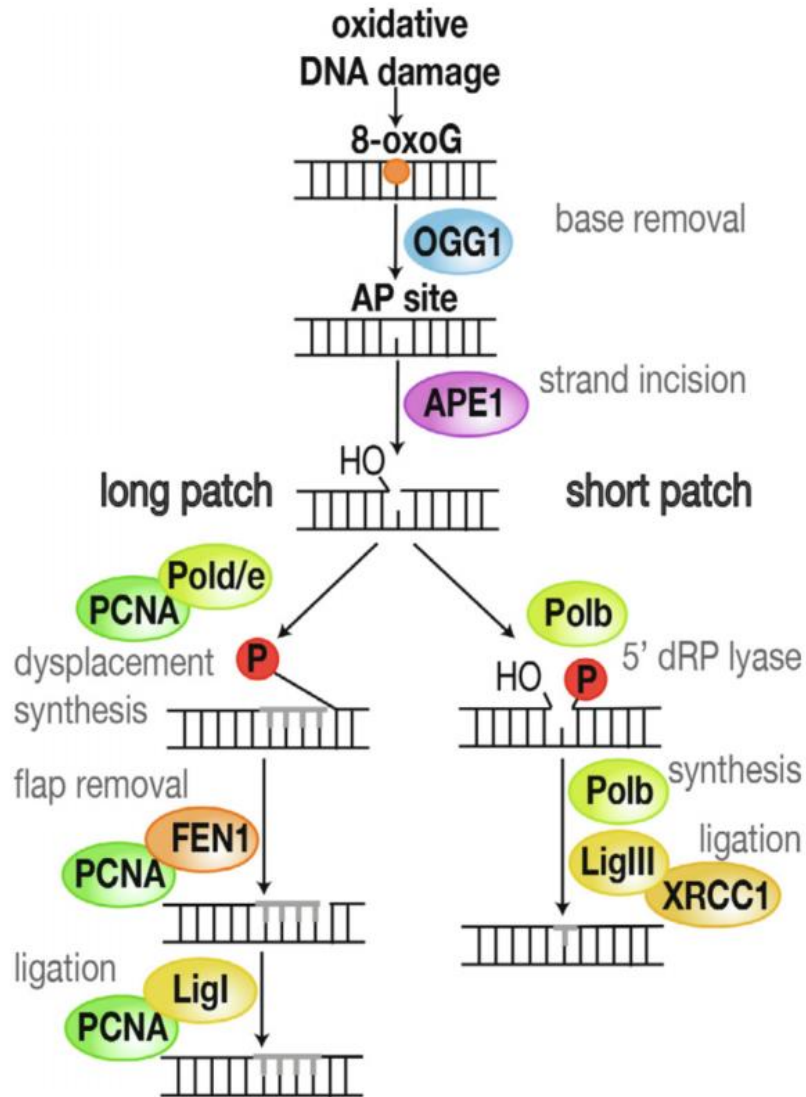


Figure 1.7 Base excision repair (BER) of 8-oxo-7,8-dihydroguanine (8-oxoG). Base excision repair (BER) uses a number of repair intermediates to remove oxidative DNA damage. It is possible to create a reactive apurinic site (AP site) by removing the oxidised base. A single strand break is formed by breaking the strand, and the damaged area is subsequently repaired using either a short or long patch BER⁴⁸.

1.2.9 Dark CPD

Based on our current understanding of the chemistry of UV-induced DNA damage, it would seem a reasonable prediction that upon elimination of UV exposure, CPD generation would be halted. However, it has been revealed that for several hours following UV exposure, CPD continues to be produced even in complete darkness, and this has been termed "dark CPD" (dCPD)⁷⁸. For example, in hairless albino mouse epidermis, the level of production of CPD at 2-4h in darkness following UV exposure is much higher than the CPD levels measured immediately following irradiation with UV light⁷⁹. Another study revealed that in human unstimulated lymphocytes, the CPD content shows a maximum level at 4h after UV exposure⁸⁰. Additionally, the kinetics of dCPD formation in mouse melanocytes have been assayed. The production of CPD increases with time and reaches a peak at 3h after the completion of UV exposure and then the CPD content decreases to a relatively low level at 5h following the UV pulse⁷⁸. While thymine-thymine dimers (T<>T) represent the most prevalent type of CPD generated during UV light exposure, thymine-thymine dimers (T<>T) constitute approximately 70% of dCPD, the remaining 30% consisting of cytosine-containing CPD, namely cytosine-thymine (C<>T) and thymine-cytosine (T<>C)⁷⁸.

There has been much speculation about how UV radiation may indirectly contribute to dCPD formation. As previously mentioned, UV irradiation also results in an increase in ROS levels. ROS can obstruct NF- κ B signaling pathways, which increases pro-inflammatory cytokines and lowers levels of cytoprotective proteins and antioxidants. This exaggerates the oxidative stress and concomitantly leads to increased levels of oxidatively generated modifications of DNA, protein and lipids⁸¹⁻⁸⁵. It is conceivable that UV-induced oxidative stress is a contributing factor to the production of dCPD. Furthermore, a "melanin chemiexcitation" theory has been proposed to account for the continued production of dCPD in the absence of UV radiation. Specifically, UV irradiation is able to activate nitric oxide synthase (NOS), NADPH oxidase (NOX) and melanin synthase and thereby induces the production of nitric oxide (NO^{*}) and

superoxide ($O_2^{\cdot-}$). Reaction of these radicals results in the release of the oxidant peroxynitrite ($ONOO^-$). Peroxynitrite degrades melanin into fragments and through an excited triplet state, melanin-carbonyls produce dCPD in the absence of UV light exposure⁷⁸. Nevertheless, some studies have reported that even in the absence of melanin, cells still produced CPD, indicating that other mechanisms may be responsible for the generation of dCPD (Figure 1.8)^{86,87}.

To cope with dCPD DNA damage, it has been reported that cells show different repair mechanisms, not involving light or photoreactivation repair⁸⁶. Specifically, in mammals, while the NER pathway participates in repairing incident CPD (iCPD) with a reduced repair efficiency⁸⁸, dCPD is repaired by the NER pathway with rapid kinetics⁸⁹.

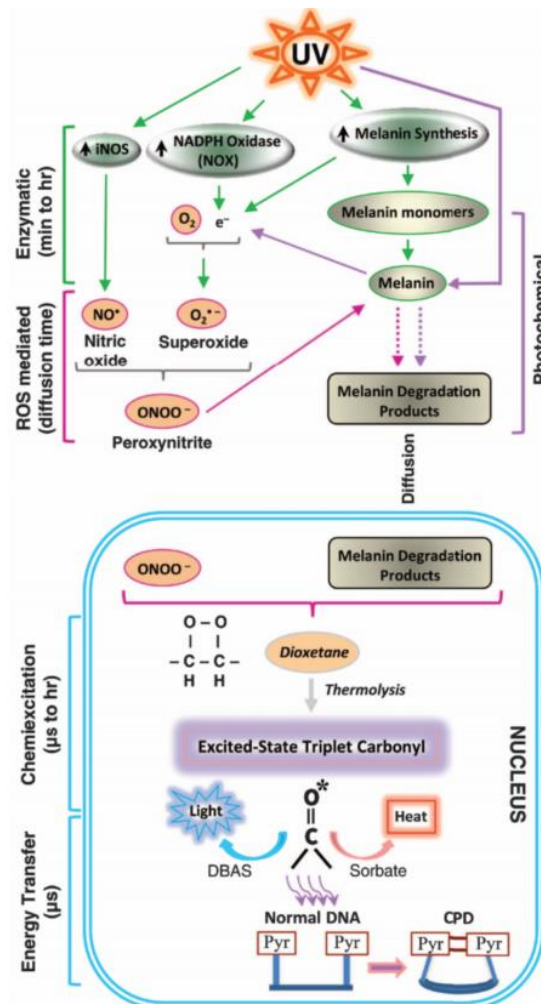


Figure 1.8 Melanin chemiexcitation. A mechanistic framework whereby melanin plays a key role in the chemiexcitation-induced production of dark CPD in melanocytes⁷⁸.

1.3. The circadian clock

1.3.1 Overview of the circadian clock

The spinning of our planet on its axis results in the 24 hours day-night cycle that dominates life on earth. In order to adapt to the day-night cycle, organisms have evolved a highly conserved mechanism to anticipate the associated regular environmental challenges. A key element of this mechanism is an endogenous timing system, termed the circadian clock, that enables organisms to optimally coordinate their physiology and behaviour to match their changing needs according to the time of day⁹⁰. The circadian clock mechanism is highly conserved among organisms, ranging from unicellular organisms and fungi to plants and animals⁹¹. Characteristically, even under constant darkness, the circadian clock mechanism still continues to function, generating a rhythmic output with a period of approximately 24 hours. Therefore, another vital property of the clock is that it is reset on a daily basis by environmental signals, primarily light, which are indicative of the time of day (named "zeitgebers" or time givers), so that the clock can remain synchronized with the 24 hours day-night cycle^{92,93}. The pathways that relay zeitgeber information to the core clock are termed "Input" pathways. In turn, the clock mechanism communicates with physiological and behavioural control systems by a range of different pathways, termed "Output" pathways^{94,95}(Figure 1.9). Circadian clocks are present in most cell types and represent cell autonomous mechanisms based on interacting dynamic networks of clock genes and their clock protein products, that generate circadian rhythms. At the organismal level the circadian clock is characterized by a hierarchical organization. Certain clocks termed "Central" or "Master" pacemakers are located in specialized tissues and coordinate the function of the clocks which are located in other cells and tissues, the so-called "peripheral" clocks. The links between the central pacemakers and the peripheral clocks are formed by a complicated battery of cycling systemic signals^{96,97}. In mammals, the suprachiasmatic nucleus (SCN) of the hypothalamus acts as a central circadian pacemaker, while in fish, reptiles, amphibia and birds, the pineal gland plays

this role⁹⁸.

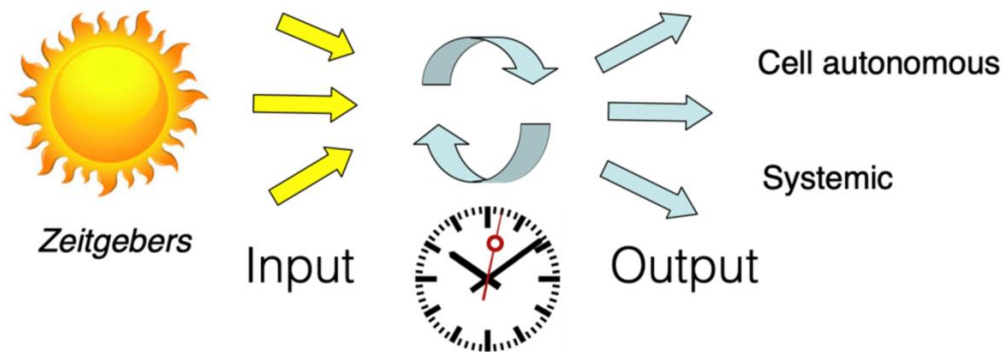


Figure 1.9 Schematic representation of input and output pathways of the circadian clock. The circadian clock system in organisms receives inputs (zeitgebers), such as light to synchronize the circadian clock, which regulates rhythmic outputs including gene expression and other cellular and molecular processes.

Given the central role played by the circadian clock in coordinating physiology, regular disruption of clock function has been associated with increased incidence of complex pathologies such as cardiovascular diseases, neurodegenerative diseases and cancer^{99–101}. Furthermore, the circadian clock system is tightly interconnected with metabolism and the disruption of daily circadian rhythms is now widely recognized to be linked with various metabolic disorders. For example, diabetes and hypoinsulinaemia are associated with the disruption of the core clock components: CLOCK and BMAL1¹⁰². Additionally, the loss of CLOCK protein leads to metabolic syndrome and obesity¹⁰³.

1.3.2 Molecular circadian clock mechanism

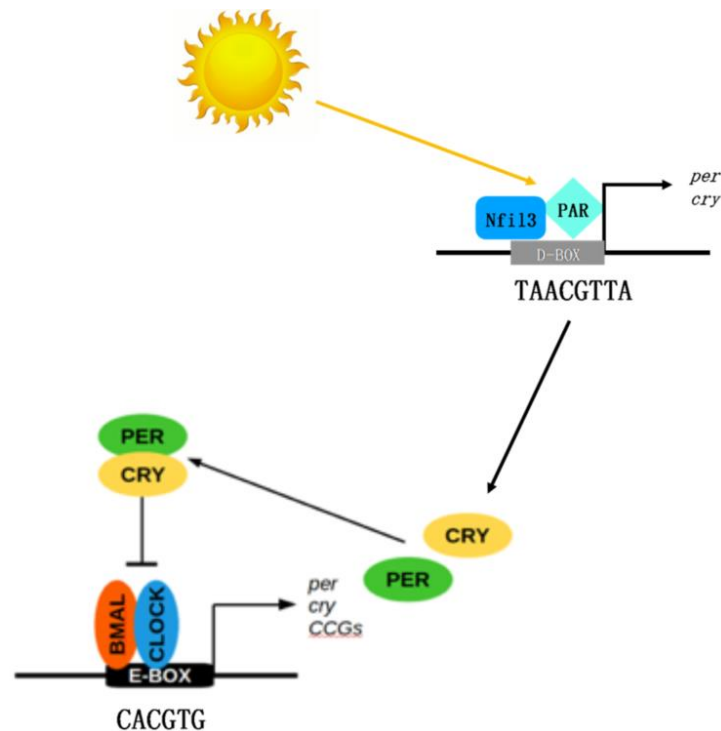


Figure 1.10 Molecular circadian clock mechanism (Transcription-translation feedback loop) in zebrafish. CLOCK and BMAL proteins can form a heterodimer and thereby bind directly to the E-Box enhancer in the promoters of the *per* and *cry* clock genes as well as, more generally, other clock control genes (CCGs) to activate transcription. PERIOD (PER) and CRYPTOCHROME (CRY) proteins translocate into the nucleus and interact physically with the CLOCK-BMAL heterodimer to inhibit the transactivation of CLOCK-BMAL complex. As a consequence, the levels of the PER and CRY proteins decrease until a critical threshold when the CLOCK-BMAL heterodimer is able once again to activate transcription. This entire process takes approximately 24 hours to complete one cycle. In the case of the zebrafish, light regulates and synchronizes the endogenous circadian clock at the molecular level through directing transcriptional activation via the D-box enhancer located in the promoters of light inducible genes, which include a subset of *per* and *cry* genes¹⁰⁴.

Much of what is currently understood about the molecular mechanism of the vertebrate circadian clock has been learned from forward genetic analysis in the mouse and comparison with clock mechanisms in other genetic models notably, the well-studied *Drosophila* clock. In vertebrates, at the molecular level, the core of the

circadian clock is constituted by a transcription-translation negative feedback loop (TTFL)¹⁰⁵. Specifically, 2 critical circadian clock components: the CLOCK and BMAL proteins, belonging to the bHLH PAS (basic helix-loop-helix PER-ARNT-SIM) family of transcription factors, form a heterodimer through interactions between their PER-ARNT-SIM (PAS) domains and bind directly to the E-Box enhancer thereby activating transcription. E-boxes are located in the promoters of two other types of clock gene which serve as negative elements within the clock machinery, namely the *period* (*per*) and *cryptochrome* (*cry*) genes. Upon activation of their transcription by the CLOCK-BMAL heterodimer, the PER and CRY proteins accumulate in the cytoplasm and then translocate into the nucleus and interact physically with the CLOCK-BMAL heterodimer to repress the transactivation of this complex. This results in a reduction in the levels of expression of PER and CRY, and as a result, a reduction in the negative regulation of the CLOCK-BMAL complex. At a certain critical threshold, the CLOCK-BMAL is released to once again activate *per* and *cry* transcription and the cycle restarts. This regulatory cycle takes approximately 24 hours to be completed and is the origin of circadian rhythmicity. Certain key steps in this cycle, such as the rate of translocation of PER and CRY into the nucleus as well as tightly controlled stability of the various protein complexes, confers the relatively long duration of this feedback loop and ensures the stability of its timing function¹⁰⁴(Figure 1.10).

Regarding the physical interaction between CRY and CLOCK-BMAL in the regulation of the circadian clock, it has already been shown that in mammals CRY1 can interact physically with the C-terminus of BMAL in the CLOCK-BMAL heterodimer complex^{106,107} and potentially suppress the activity of the CLOCK-BMAL heterodimer in the absence of PER^{108,109}. Meanwhile, in zebrafish, it has been demonstrated that CLOCK and BMAL can form a heterodimer via the basic helix-loop-helix (bHLH) and PAS B domains, with little or no interaction between the two PAS A domains, and sequentially, CRY1a is able to bind tightly to the PAS B domain of CLOCK and multiple domains of BMAL, containing the bHLH, PAS B and C-terminus domains to block the formation of the CLOCK-BMAL heterodimer¹¹⁰ (Figure 1.11). The inhibition by CRY1a

of E-box-driven CLOCK-BMAL transactivation of clock controlled genes in zebrafish operates in 2 ways: the first way is to suppress the transactivation of CLOCK-BMAL heterodimer directly by interaction with the C-terminus of BMAL, and the second way is that CRY1a is able to competitively bind to the bHLH and PAS B domains of BMAL and the PAS B domain of CLOCK, where CLOCK and BMAL themselves interact directly to form an active heterodimer.

Consistent with the widespread presence of circadian clocks, clock genes are expressed with characteristic circadian rhythms of mRNA and protein in most cell types and tissues. Interestingly, for the clock genes constituting the transcription-translation feedback loop, namely *clock*, *bmal*, *per* and *cry*, each gene is represented by several copies in mammals and fish and each copy has distinct oscillation rhythms in different tissues¹¹¹. For example, in zebrafish, the expressed peak of *cry2* gene appears in the early morning, while the *cry1* and *cry3* genes display highest expression levels at midday¹¹². In addition, the expression of *clock* and *bmal* genes peaks at dusk and the early part of the night^{113,114}, while the peak of *per2* gene expression occurs in the morning or around midday¹¹⁵. The functional significance of the gene copy-specific differences in the timing of rhythmic expression remains poorly understood. However, it is tempting to speculate that they may confer diversity in clock regulatory function.

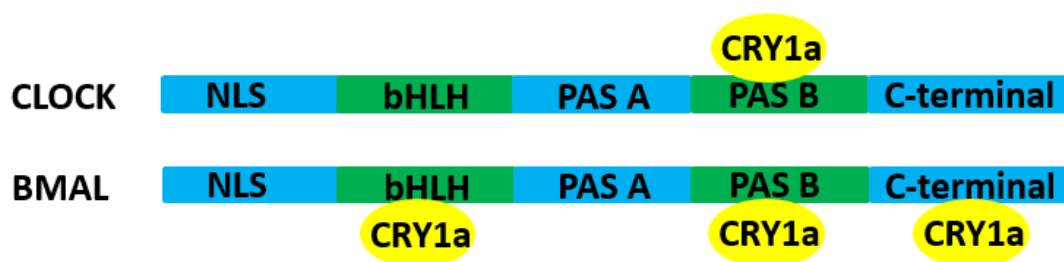


Figure 1.11 Schematic representation of light-induced interactions between CRY1a and the CLOCK-BMAL heterodimer in zebrafish. CRY1a is able to interact directly with the PAS B domain of CLOCK1 and the bHLH, PAS B, and C-terminal domains of BMAL1¹¹⁰.

1.3.3 Light input to the clock in vertebrates.

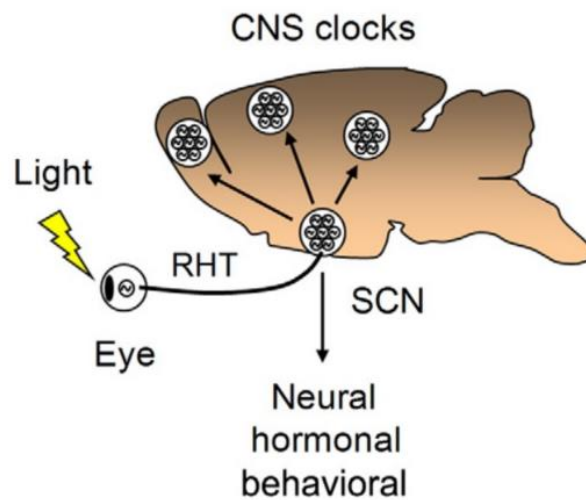


Figure 1. 12 The central circadian pacemaker in mammals. The central circadian pacemaker located in the SCN is entrained by the external light–dark cycle through light input signals from the retina transmitted through the RHT¹¹⁶.

The mechanisms whereby light exposure regulates the circadian clock has been studied extensively in mammals. Specifically, the suprachiasmatic nuclei (SCN) of the hypothalamus play a central role in the generation and maintenance of circadian rhythms in mammals, and the loss of the SCN gives rise to behavioural arrhythmicity^{117–119}. It has been demonstrated that light signals from the environment regulates the SCN clock via the retina to set its phase so that it remains synchronized with the 24 hours environmental day-night cycle – a biological process named photoentrainment^{120–122}. Dedicated photoreceptor cells in the retina transmit photic signals as nerve impulses to the master circadian pacemaker in SCN through the retinohypothalamic tract (RHT). Specifically, retinal photoreceptors including photosensitive rods, cones and intrinsically photosensitive retinal ganglion cells (ipRGCs)^{123,124} are able to detect light and relay this information to the SCN clock. ipRGCs express melanopsin as their photopigment and thereby mediate a wide range of non-image-forming response to light^{125–127}. Melanopsin is encoded by the *Opn4* gene¹²⁸ and appears to serve as the primary photoreceptor in the nonvisual, circadian

clock response to light of ipRGCs^{127,129}. Its synthesis in the ipRGCs is under the control of a circadian oscillator, which results in elevated synthesis during the night and reduced expression during the day. Stimulation of the melanopsin photopigment by light causes the downstream activation of a membrane-bound signaling cascade^{130–132}. Although ipRGCs are intrinsically photosensitive, they also accept input from rods and cones via the bipolar cells and amacrine cells of the retina. Thereby, they serve as a conduit for conveying rod and cone signals to the SCN¹³³. Despite the fact that melanopsin, rod, and cone-driven signals can all induce entrainment on their own, it appears that each of them is specialized to detect and encode different aspects of the light signal, enabling a robust and flexible detection of daily light levels^{134–136}(Figure 1.12).

Glutamate and PACAP^{137,138}, the principal neurotransmitters of the RHT, have the capacity to activate a variety of kinase-based signaling pathways in the SCN¹³⁹. The CREB (cAMP response element binding protein) transcription factor represents a convergence point for these signaling pathways; upon phosphorylation at Ser133 and Ser142, CREB binds to cAMP response elements (CRE) in the promoter of light responsive genes such as the mammalian *per1* and *per2* genes^{140,141}. The CREB-mediated activation of *per* gene transcription is clock phase-dependent and consequently, the ensuing alterations in PER proteins change the phase of the circadian clock¹⁴². Therefore, in mammals, light indirectly regulates the circadian timing system via anatomically distinct, specialized photoreceptive structures.

In contrast, in fish such as the zebrafish, light is able to regulate the clock at a cell autonomous level. Specifically, direct exposure of peripheral clocks to light results in entrainment of the clock^{143,144}. This predicts the widespread expression of photoreceptors that are connected with circadian clock in fish tissues. Consistently, 42 opsin light genes have been described in zebrafish which are expressed in a wide range of tissues outside the retina, with the brain itself expressing more than 20 nonvisual opsins¹⁴⁵. Since most of them have been revealed to possess a photoreceptive function, they seem to be a good source of candidates for the function of peripheral

photoreceptors. Furthermore, a key step in entrainment is the light induced expression of a subset of *period* and *cryptochrome* clock genes and notably the two clock genes: *period2 (per2)* and *cryptochrome1a (cry1a)*^{146,147}. CRY1a is known as a potent repressor of CLOCK-BMAL heterodimer activation¹¹⁰ and PER2 serves as either a transcriptional activator or corepressor depending upon its transcriptional regulatory targets¹⁴⁸. The induction of PER2 and CRY1a by light is assumed to elicit resetting of the phase of the clock. Particularly, it has been demonstrated that in the promoter regions of these light-regulated genes of zebrafish, there is an enrichment of the D-box enhancer sequence^{146,147} and the integrity of the D-box enhancer is crucial for light-regulated gene expression^{149,150}. Interestingly, in the *per2* promoter the D-box is situated near an E-box enhancer, and both D- and E-boxes are critical for light-induced gene expression¹⁴⁹. In addition, light exposure can also induce the production of ROS, which has been implicated in directing the activation of clock gene expression in zebrafish cells through the activation of the MAPK pathway. Furthermore, ROS has a regulatory impact on the immediate early transcriptional factors c-Fos and c-Jun, and thus on the regulation of genes which are controlled by AP1 enhancer function¹⁵¹. The D-box enhancer also activates transcription in response to elevated levels of ROS as well as upon exposure to UV¹⁵². Therefore, the D-box represents a convergence point for transcriptional regulation in response to the direct and indirect effects of sunlight exposure^{150,152–155}.

Interestingly, in the mammalian clock mechanism the D-box enhancer element serves as a key clock output target and is encountered in the promoters of clock genes as well as various clock-controlled genes. In the mouse, the D-box serves to relay timing information from the circadian clock to generate rhythms of transcription in output genes. Therefore, it appears that during vertebrate evolution, the function of the D-box enhancer has altered considerably according to its function within the circadian timing system.

1.3.4 PAR and E4BP4 bZip transcription factors and circadian clock regulation.

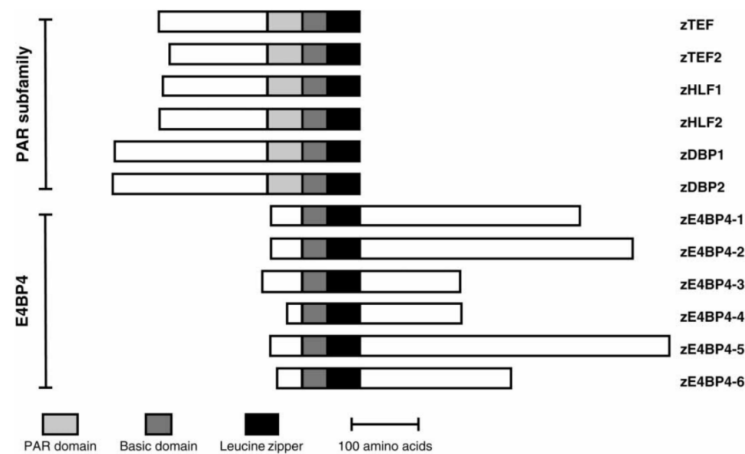


Figure 1.13 Primary structure of the zebrafish PAR subfamily and E4BP4 bZip transcription factors¹⁵⁶.

D-box regulated transcriptional activation is mediated by a group of so-called PAR (proline and acidic amino acid-rich) transcription factors, TEF (thyrotroph embryonic factor), HLF (hepatic leukemia factor-1) and DBP (D-box-binding protein) which specifically bind to D-box elements in homo and heterodimeric combinations. Interestingly, according to studies of DBP-deficient mice, TEF and HLF accumulate to a lesser extent in hepatocyte nuclei of DBP-deficient animals than in those of wild-type mice¹⁵⁷, suggesting that heterodimerization of TEF and HLF with DBP is central to PAR factor regulation of the D-box¹⁵⁸. A second group of transcription factors termed NFIL3 (also known as E4BP4, E4-binding protein 4) is involved in repressing D-box regulated transcription.

The D-box binding, PAR family of transcription factors belong to the large group of basic Leucine Zipper transcription factors which all share a protein-protein interaction domain that includes a leucine zipper. This consists of an amphipathic alpha-helix distinguished by a periodic repeat of leucine residues, which generates coiled-coil domains with hydrophobic surfaces that allow dimerization^{159,160}. The leucine zipper

in turn maintains the correct orientation of an adjacent domain rich in basic amino acids which directly contact the DNA helix. The bZip family, based on DNA binding specificity and similarities of amino acid sequences principally in the bZip domain, is comprised of 6 conserved subfamilies termed ATF/CREB (activating transcription factors/cAMP responsive element-binding proteins), AP-1 (activating protein-1), C/EBP (CAAT/enhancer-binding protein), NF-E2 (nuclear factor erythroid-derived 2), Maf (musculoaponeurotic fibrosarcoma oncogene) and the PAR (proline and acidic amino acid-rich) subfamily^{154,161}. The PAR subfamily is also characterized by a proline and acidic amino acid-rich region, positioned adjacent to the basic region, which is involved in protein-protein interactions and transcriptional activation^{162,163}. While the E4BP4 transcription factors share the conserved basic and leucine zipper domains of the PAR factor family, they lack the PAR domain (Figure 1.13). Both groups of transcription factors are able to competitively bind to the D-box element of clock-controlled genes' promoters to regulate transcription¹⁵⁶.

The PAR factor genes are rhythmically expressed as the result of regulation by the CLOCK-BMAL heterodimer via E-box mediated activation¹⁶⁴. Subsequently, the circadian expression of downstream genes is controlled by these clock-controlled transcription factors, affecting a variety of physiological processes. E4BP4 factors are involved in complementing the PAR factors' modulation of clock genes in a reciprocating process, which means that E4BP4 factors inhibit the transcription of target genes through physical interaction with D-boxes, while PAR proteins compete for the same binding sites to activate them at different times of the day^{165,166}.

Analysis of mice carrying loss of function mutations in TEF, DBP and HLF have revealed a key role for these factors in the regulation of metabolism of vitamin B6, which has an effect on the balance of neurotransmitters in the brain, and the loss of PAR activity results in spontaneous and sound-induced epilepsies that normally lead to death¹⁵⁴. Moreover, it has been reported that in the liver and kidney of mice, PAR factors are also able to activate the expression of genes that are implicated in detoxification and drug metabolism, for example carboxylesterases, cytochrome P450 enzymes and

constitutive androstane receptor (CAR). Mice carrying loss of function mutations for all three PAR factors are more hypersensitive to and deficient in xenobiotic detoxification, possibly contributing to the high morbidity, premature death, and accelerated aging observed in these animals¹⁶⁷.

In addition to functioning as clock output factors, these factors are also able to feed back on the core clock through binding to the D-box of clock genes. For example, DBP contributes to an additional accessory loop by activating the *per1* promoter in the mouse¹⁶⁸. Meanwhile, E4BP4 factors have also been implicated in regulating expression of *per2*, the core clock gene, and the light entrainment of circadian clock^{166,169}.

While in mouse, there are single genes for each type of PAR factor, in zebrafish, there are multiple gene orthologs. Specifically, the zebrafish PAR subfamily consists of *tef-1*, *tef-2*, *hlf-1*, *hlf-2*, *dbp-1* and *dbp-2*, (Figure 1.13). Interestingly, phylogenetic analysis points to a higher conservation between *tef* and *hlf* orthologs, while *dbp* displays less sequence conservation owing to its later emergence during evolution¹⁵⁴. Furthermore, there are 6 E4BP4 homologs in zebrafish suggesting additional complexity in E4BP4 function in these species, which not only enables competitive binding to the D-box elements of clock-controlled gene promoters to regulate transcription¹⁵⁶, but also acts as a survival factor in heart which is critical for normal embryonic heart development^{170,171}. In the case of fish, exposure of cells to light regulates the endogenous circadian clock at the molecular level by activating the transcription of a subset of negatively-acting clock genes via D-box enhancers. Light-regulated gene expression mediated by D-boxes is also observed in other classes of gene such as many DNA damage repair genes as well as many genes involved in mitochondrial function^{146,147}. Therefore, light induced, D-box mediated gene expression represents part of a broader cellular strategy to survive the effects of sunlight.

1.4 Links between DNA repair and circadian clocks

There is considerable evidence for tight interconnections between the circadian clock and DNA repair systems. Indeed, it has been speculated that one of the selective pressures that led to the evolution of the circadian clock was to ensure optimization of the timing of DNA damage repair to match the changing conditions of the day-night cycle^{172,173}. Indeed, there are many known links between the circadian clock and key DNA repair elements. For example, in mice, the CRYs which serve as core circadian clock components regulate the rhythmic expression of the *xpa* gene, a recognition factor for the NER repair pathway. This periodically modulates the activity of the entire excision repair system, an important step in avoiding the development of invasive skin carcinoma in mice^{172,173}. Therefore, the CRY proteins which are closely associated with circadian clock function, also have a prominent impact on the regulation of DNA repair systems. Other evidence for links between clocks and DNA repair comes from the presence of proteins or groups of proteins which share functions of both DNA repair and the circadian clock. One key example is the group of cryptochrome and photolyase flavoproteins.

1.4.1 Cryptochrome/photolyase family (CPF)

As discussed previously, the photolyases utilize light to repair UV-induced DNA damage, while cryptochromes act as circadian clock components. They physically interact with and thereby inhibit transactivation by the CLOCK-BMAL heterodimer which binds to E-box elements in the promoters of clock-controlled genes. Cryptochromes are regarded as photolyase-like proteins which lack DNA photolyase activity. Photolyases and cryptochromes both share a conserved FAD binding domain, which is crucial for harvesting light energy. Therefore, photolyases and cryptochromes both exhibit the structural features of blue light photoreceptors^{7,174-177}. The animal and plant cryptochrome genes are not close relatives¹⁷⁵ and from phylogenetic analysis, plant cryptochromes exhibit a higher degree of sequence similarity with CPD photolyase¹⁷⁸,

while animal cryptochromes are more closely related to 6-4 photolyase^{179,180} (Figure 1.14).

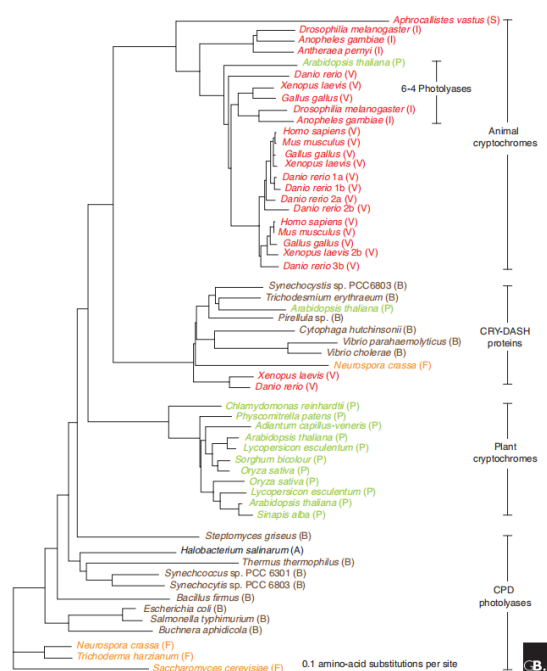


Figure 1.14 A phylogenetic tree of the cryptochrome/photolyase family as well as subfamilies indicated on the right. Abbreviations: A, archaea; B, bacteria; F, fungi; I, insects; P, plants; S, sponges; V, vertebrates ¹⁷⁴.

In animals, cryptochromes regulate the circadian clock in a light-dependent and light-independent manner. Specifically, it has been reported that in cultured *Drosophila* S2 cells, CRY is able to inhibit the repression of PER and TIM, negative regulators of the central oscillator in a light-dependent manner¹⁸¹. In addition, in mouse, CRY1 and CRY2 proteins are able to interact physically with PER proteins and translocate to the nucleus to repress the transcription of clock-controlled genes driven by the CLOCK-BMAL complex via direct binding to the CLOCK-BMAL heterodimer. This negative regulation by CRY is light independent¹⁸². On the contrary, in *Arabidopsis*, CRY1 and CRY2 as well as phytochromes have been demonstrated to play a crucial role in circadian entrainment¹⁸³. Specifically, the C-terminal domain of CRYs can interact with COP1, functioning as a component of an E3 ubiquitin ligase, in a light-dependent manner and then COP is able to interact physically with the HY5 protein, a bZIP transcription factor

that regulates the promoters of multiple genes that are expressed during photomorphogenesis. In darkness, the physical interaction between COP1 and HY5 stimulates proteasome-regulated degradation of HY5, whereas CRY inhibits the ubiquitin ligase activity of COP1 by harvesting light energy and sequentially, the proteasome-regulated degradation of HY5 is suppressed and HY5 content increases. Consequently, there exists a CRY-COP1-HY5 heterotrimeric complex involved in the modulation of photomorphogenesis and within this context, CRY acts as a photoreceptor^{184,185}. Moreover, in plants, CRYs are implicated in the modulation of seedling growth, flowering, and development^{186–188}.

1.4.2 Bifunctional CPF members

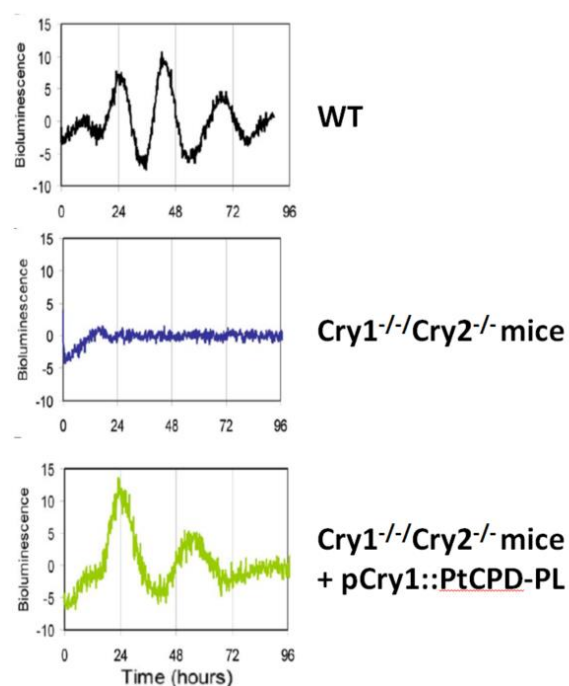


Figure 1.15 *Potorous tridactylus* CPD photolyase rescues circadian clock function in the liver of CRY-deficient mice¹⁸⁹.

Certain CPF members have evolved functionalities involving both DNA repair and circadian clock regulation. Specifically, in the marine diatom, *Phaeodactylum tricornutum*, a member of the CPF family termed PtCPF1, exhibits DNA repair activity

for 6-4 photoproducts, but not CPD photoproducts and furthermore, this protein represses transactivation of CLOCK-BMAL heterodimer in the context of the circadian clock¹⁹⁰. In addition, in the green alga, *Ostreococcus tauri*, two members of the CPF family, called OtCPF1 and OtCPF2 also exhibit dual functions. Specifically, OtCPF2 possesses photolyase activity for repairing CPD photoproducts, while OtCPF1 repairs 6-4 photoproducts. OtCPD1 is also implicated in circadian clock function by mediating the CLOCK-BMAL-activated transcription at the E-box enhancer located in the promoter of clock-controlled genes¹⁹¹. There is also evidence for bifunctional CPF family members in mammals. Ectopic expression of the marsupial *Potorous tridactylus* PtCPD (*Potorous tridactylus* CPD) is able to restore circadian rhythmicity in the liver of CRY1/CRY2-deficient mice during a period in constant darkness, indicating that rhythmically expressed photolyase can functionally substitute for CRY proteins in the mammalian circadian oscillator¹⁸⁹ (Figure 1.15).

It has been widely assumed that DNA photolyase was the common ancestor for the animal and plant cryptochromes. However, in *Synechocystis* the redox-regulated transcriptional regulator CRY appears to have evolved from a photolyase. This observation raises the possibility of a light-dependent redox reaction mediated by an ancestral flavoprotein that did not involve photolyase activity. Therefore, ancestral cryptochrome-like proteins may represent the evolutionary forerunners of both cryptochromes and photolyases¹⁹².

1.4.3 Nocturnal bottleneck theory

One of the most curious observations regarding the cryptochrome/photolyase family is that although these proteins are widely encountered throughout prokaryotes and eukaryotes, the only species that lack photolyase genes belong to the small group of placental mammals. This result has led to much speculation about the evolutionary selective pressure that resulted in the eventual loss of these key light-dependent DNA repair enzymes in such a well-defined phylogenetic group.



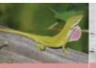




	teleost	amphibian	reptile	bird	monotreme	marsupial	eutherian
							
<div style="display: flex; flex-direction: column; align-items: center;"> <div style="margin-bottom: 10px;">non-visual opsins</div> <div style="margin-bottom: 10px;">visual opsins</div> </div>	exorhodopsin	Y	N	N	N	N	N
	RH1	Y	Y	Y	Y	Y	Y
	RH2	Y	N	Y	Y	N	N
	SWS2	Y	Y	Y	Y	Y	N
	SWS1	Y	Y	Y	Y	N	Y
	LWS	Y	Y	Y	Y	Y	Y
	pinopsin	N	Y	Y	Y	N	N
	VA	Y	Y	Y	Y	N	N
	parietopsin	Y	Y	Y	N	N	N
	parapinopsin	Y	Y	Y	N	N	N
	TMT	Y	Y	Y	Y	Y	N
	OPN3	Y	Y	Y	Y	Y	Y
	OPN5	Y	Y	Y	Y	Y	Y
	peropsin	Y	Y	Y	Y	Y	Y
	RGR	Y	Y	Y	Y	Y	Y
	OPN4X	Y	Y	Y	Y	N	N
	OPN4M	Y	Y	Y	Y	Y	Y
		non-mammals				mammals	

Figure 1.16 A summary list demonstrating the existence of opsin orthologs in contemporary members of the major vertebrate classes, from bony fish to mammals. It displays whether a specific opsin class is present (yes, Y, green shading) or absent (no, N, red shading), with a vertical red line denoting the boundary between reptiles and mammals. The nocturnal bottleneck hypothesis accounts for the significant loss of opsin genes during vertebrate evolution¹⁹³.

One popular theory to explain this pattern of evolution is the so-called "nocturnal bottleneck theory" which was originally based on a comparison of opsin photoreceptors of birds, reptiles and all three extant taxa of the mammalian lineage, containing the monotremes, marsupials and placentals (included in the eutherians). This theory accounts for an apparent reduction in opsin gene diversity during early mammalian evolution and predicts that in order to avoid predation by dinosaurs, the dominant taxon at that time, the ancestors of placental mammals became predominantly nocturnal animals, possibly sleeping in underground burrows during the day when dinosaurs are predicted to have been predominantly active¹⁹⁴. This nocturnal lifestyle led to various adaptations which limited the animals need to expose themselves fully at the surface to be able to sense environmental lighting conditions for setting the phase of their clocks. One such adaptation included changes to eye function and a restriction of circadian photoreceptors to the retina rather than being

widely expressed throughout the body. Specifically, the peripheral clocks of mammals could only be synchronized by light via the central clock of the suprachiasmatic nucleus (SCN) in the hypothalamus since tissues and cells from mammals were no longer light responsive. However, these peripheral clocks could still be entrained by systemic timing signals originating from the hypothalamus including acute changes in temperature and serum composition to enable communication between the central and peripheral clocks^{195–197}. This ultimately led to a reduction in the number of opsin genes, even though all the 5 subtypes of opsin genes were still represented^{198,199} (Figure 1.16).

Can the nocturnal bottleneck theory explain the loss of photolyase function in placental mammal ancestors after the divergence of marsupials and placental mammals?^{200,201} This question is particularly relevant given that photoreactivation DNA repair represents the most efficient mechanism for the repair of UV-induced DNA damage. Indeed, ectopic expression of marsupial CPD photolyase in transgenic mice resulted in the transgenic cells exhibiting improved resistance to UV-induced damage^{42,202}. In the context of the nocturnal bottleneck theory, if placental mammal ancestors were exclusively nocturnal animals and possibly also occupying a subterranean niche, then they would not normally experience significant levels of UV radiation and also they would not experience sufficient visible light to drive the photoreactivation reaction catalyzed by the photolyases. For this reason, there might be only weak selective pressure to maintain photoreactivation as well as photolyase genes.

Although an attractive theory, there is currently limited evidence to support it. One valuable strategy to test the merits of this theory would be to examine photolyase function and evolution in extant species inhabiting extreme photic environments completely lacking sunlight. In this regard, comparing photolyase function in species of blind cavefish with related surface-dwelling fish would potentially be of great interest.

1.5 Comparative fish models for studying the circadian clock and DNA repair.



Figure 1.17 Fish models for studying the DNA repair and circadian clock mechanisms. Zebrafish (*Danio rerio*), Somalian cavefish (*Phreatichthys andruzzii*) and medaka (*Oryzias latipes*).

In this project, I have followed a comparative approach involving a set of fish models, specifically zebrafish (*Danio rerio*), medaka (*Oryzias latipes*), and the blind Somalian cavefish (*Phreatichthys andruzzii*), to investigate the biological mechanisms underlying DNA repair and the circadian clock and how these two key processes have been shaped by the photic environment (Figure 1.17). Both zebrafish and medaka provide a large repertoire of genetic and screening tools for functional investigation of DNA repair and circadian clock. Furthermore, they possess all of the normal DNA repair systems, including photoreactivation. In addition, besides their eyes and visual functions, zebrafish and medaka have a photosensitive pineal gland, deep brain photoreceptors and light-responsive dermal melanophores to sense light²⁰³. The peripheral clocks of tissues of zebrafish and medaka are also entrained by direct exposure to light²⁰⁴, which contrasts with mammals where circadian clock photoreceptors are restricted to the retina.

Teleosts represent the largest and most diverse group of vertebrates, inhabiting a broad range of aquatic environments. The ambient illumination conditions in each of these habitats can vary dramatically. For example, day length, optical properties of the water, as well as the wavelengths and intensity of light that fish are exposed to can all vary and have a substantial impact on fish biology²⁰⁵. Extreme examples are perpetual

dark fresh water and marine aquatic environments such as subterranean caves or abyssal ocean habitats, which represent uniquely challenging habitats for fish species. Fish which have evolved in these environments exhibit dramatic changes in anatomy and physiology with a classical example of this being species of blind cavefish.

Cavefish, so-called hypogean fish, represent a group of fish inhabiting subterranean environments, typically living in freshwater aquifers such as phreatic layers, cave waters and wells, and including approximately 200 species worldwide²⁰⁶. They exhibit a set of particular phenotypes known as “Troglomorphisms”, consisting of regressive and constructive traits. Regressive features include eye loss (anophthalmia) and depigmentation, while constructive traits include enhanced longevity and non-visual sensory systems and tolerance of starvation to adapt to the typically nutrient-poor environments which are unable to support photosynthesis^{207–209}. The selective pressure underlying eye loss in cavefish has been a subject of great debate over many years. One theory proposes the “energy-saving” advantages of an eyeless phenotype, since generally, the maintenance of eyes has been considered as a phenotype that is highly energy demanding.

Importantly, two species of cavefish have received significant attention: the Somalian cavefish, *Phreatichthys andruzzii* and the Mexican tetra, *Astyanax mexicanus*. *P. andruzzii* is remarkable in that it possess one of the more extreme troglomorphic phenotypes. Indeed, this species has been completely isolated in constant dark phreatic layers deep beneath the Somalian desert for millions of years, and there are no surface-dwelling forms. On the contrary, *A. mexicanus* inhabits cave systems in the mountainous regions of Northeastern part of Mexico. This species is represented by many isolated populations which can be separated into 2 types: surface fish which do not show troglomorphisms and blind cavefish which inhabit particular caves and exhibit troglomorphisms²¹⁰. However, these adaptations are less extreme than those in *P. andruzzii* since the fish are frequently not completely isolated from surface populations and have not been isolated for as long as *P. andruzzii*. Importantly these different *A. mexicanus* populations all represent a single species and so are able to

mate with each other to produce fertile F1 offspring. They can also be maintained in the laboratory and so have been used for various advanced genetic studies to explore the mechanisms underlying troglomorphisms²¹⁰.

It is logical to assume that since the cavefish *P. andruzzii* has been exposed to perpetual darkness over the course of millions of years in a relatively constant environment, there would be no selective pressure to maintain a functional circadian clock, photoreceptors or light dependent DNA damage repair mechanisms in this species. Indeed, in *P. andruzzii*, central and peripheral tissues as well as a primary cell line derived from fin clips show arrhythmic locomotor activity and clock gene expression when exposed to artificial LD cycles²¹¹. However, *P. andruzzii* cell lines do still possess peripheral circadian clocks although they tick with an aberrant 40 hours, infradian rhythm²¹¹. Moreover, at the molecular level, the “blindness” of the circadian clocks of these cavefish is attributed to loss of function mutations in 2 nonvisual opsins, the melanopsin homolog (Opn4m2) and the teleost multiple tissue (TMT) opsin that are both broadly expressed in fish tissues^{211,212}. Interestingly, while light-entrained circadian oscillation in *P. andruzzii* has been lost they do retain a normal food-entrained circadian oscillator (FEO), which is entrained by the periodic availability of food and which directs a feeding activity rhythm, where the fish become generally more active just before the arrival of food, thereby enabling them to more efficiently exploit the limited food supply²¹¹.

In the case of *A. mexicanus*, while the surface fish show light-induced expression of *per2* and *cry1a* genes, the cave strains exhibit remarkably reduced light induction of these clock genes but with much higher basal expression levels²¹². Moreover, while the surface fish in the field display similar *per1* oscillations to those in the lab, the cavefish in the wild show inhibition of clock function which may result from the elevated expression levels of *per2* and *cry1a*²¹⁰. Hence, being arrhythmic rather than having daily rhythms of activity and metabolic processes may provide some selective advantage for cavefish.

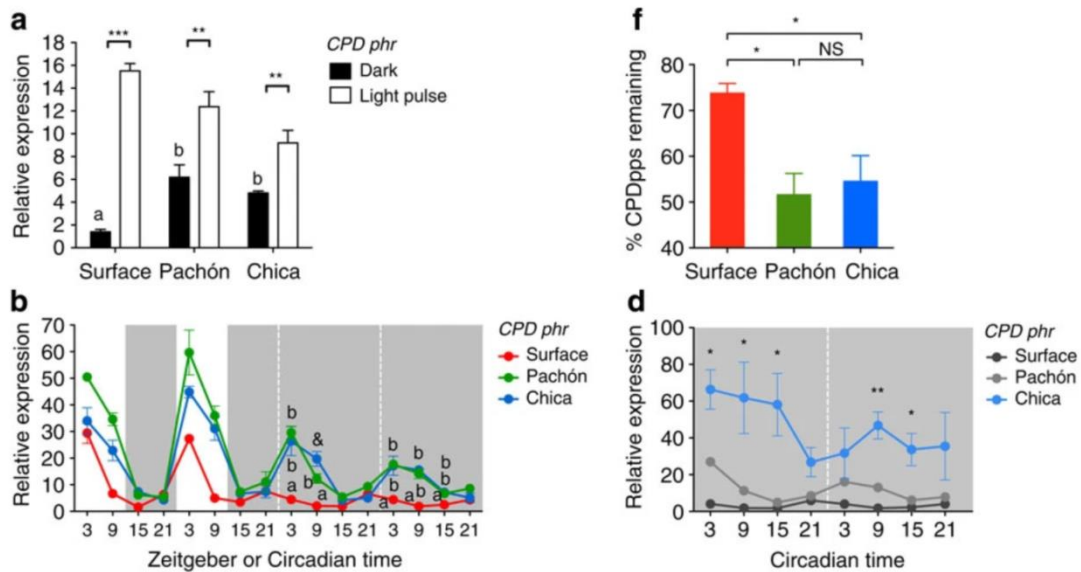


Figure 1.18 *Astyanax mexicanus* cavefish show enhanced DNA repair gene expression and activity in the dark. (a) Adult fish were entrained to a LD cycle and given a 3-hour light pulse at ZT16. CPD photolyase expression levels were measured in light-pulsed and dark control fin samples by qPCR. (b, d) mRNA levels of CPD photolyase in *Astyanax mexicanus* surface and cavefish were measured by qPCR. (f) CPD remaining in genomic DNA extracted from adult fins after a UV light pulse²¹⁰.

Additionally, it is critical to note that the cave environment is complex and not merely characterized by an absence of light. Each subterranean habitat is unique in terms of geology, water properties and connection with surface water. One potentially important factor is hypoxia of the water supply, which may induce oxidative DNA damage as well as affecting dCPD production. Interestingly, it has been revealed that comparing *A. mexicanus* surface fish, the cave forms (Pachón and Chica) have notably elevated basal levels of CPD photolyase (Figure 1.18 b, d). Although the expression of CPD photolyase in cavefish is induced by light, this occurs with a lower magnitude than the light induced expression of CPD photolyase observed in surface fish (Figure 1.18 a). Moreover, ELISA analysis of *A. mexicanus* revealed that compared with surface fish, the cavefish display substantially lower DNA damage and therefore higher DNA repair activity even in darkness, indicating that the elevated levels of CPD photolyase gene expression in cavefish is associated with an enhanced capacity to repair DNA damage²¹⁰ (Figure 1.18 f).

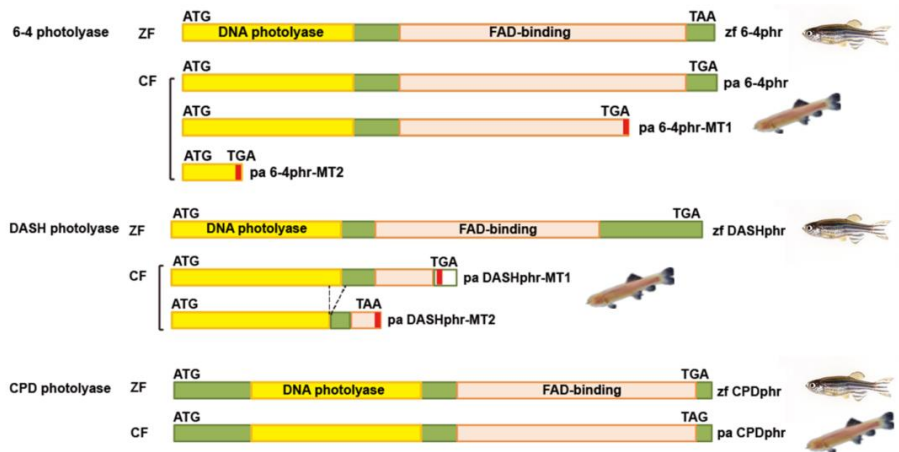


Figure 1.19 Comparison of the photolyase genes between zebrafish and Somalian cavefish. The C-terminal FAD binding domain is shaded pink while the conserved N-terminal photolyase domain is yellow. Red boxes signify premature termination codons¹⁵².

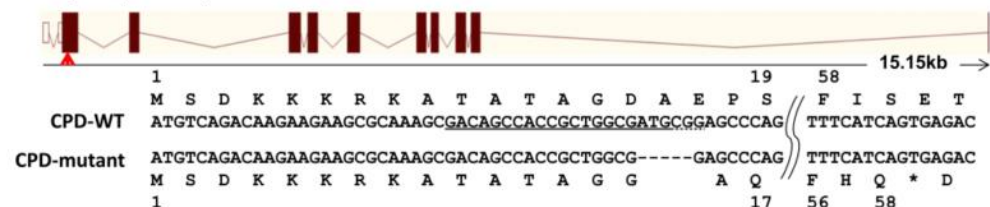
The Foulkes lab's previous work has documented that *P. andruzzii* has lost photoreactivation DNA repair function and this loss partly derives from loss of function mutations of DASH and 6-4 photolyase DNA repair genes. Specifically, in *P. andruzzii*, C-terminal truncations of the DASH and 6-4 photolyase proteins restrict these proteins to the cytoplasm and are predicted to interfere with protein binding to the Flavin co-factor. Surprisingly, the comparison of photolyase genes between zebrafish and cavefish indicates that *P. andruzzii* still possesses a normal CPD photolyase gene which shares high similarity with zebrafish CPD photolyase and furthermore, the encoded protein is able to perform normal photoreactivation in an *in vitro* assay¹⁵² (Figure 1.19).

Together, the results and findings related to CPD photolyase in these two species of cavefish might seem rather counterintuitive. Classically, photolyases employ light as a source of energy to repair UV-induced DNA damage but light is completely absent in the cave environment. Furthermore, the fish in the cave environment will not be exposed to UV damage and so levels of UV-induced CPD photoproducts should be extremely low. However, the conservation and elevated expression of CPD photolyase suggests there is some selection for maintaining its function, even in the absence of sunlight.

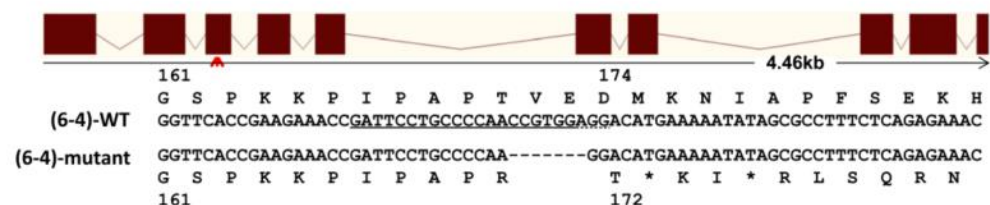
1.6 Aims

The overarching aim of this thesis is to provide new insight into how DNA repair function of photolyases in vertebrates has been shaped over the course of evolution. This project is divided into two main sections. Firstly, I address the observation that in *P. andruzzii*, while the 6-4 and DASH photolyase genes exhibit multiple loss of function mutations, CPD photolyase is highly conserved. I aim to explore how vertebrate photolyase structure and function has changed during evolution in an extreme, perpetually dark environment. Specifically, I hypothesize that CPD photolyase has a light-independent DNA repair function that would account for it being conserved in an animal that has not been exposed to sunlight for millions of years. In the second section of this project, as described in the previous sections of this Introduction, photolyases and cryptochromes are close relatives, and it has been established that cryptochromes are essential circadian clock components but can also share photolyase DNA repair function. Therefore, my aim is to explore whether photolyases are able to serve as circadian clock regulatory elements in fish.

CPD phr (exon2)



(6-4) phr (exon3)



cry-dash (exon3)

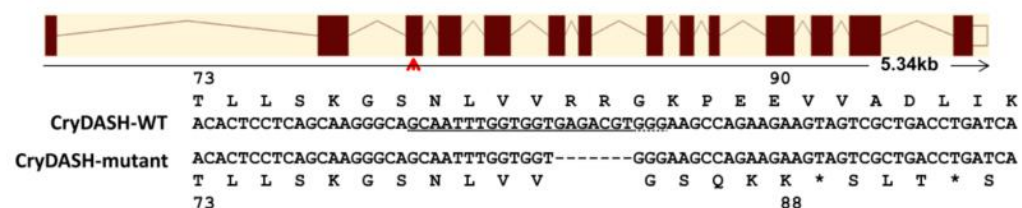


Figure 1.20 Genes for CPD photolyase, 6-4 photolyase, and Cry-DASH photolyase were mutated in medaka by CRISPR/Cas9. The upper portion of each panel displays the exon-intron structure of the CPD photolyase, 6-4 photolyase, and Cry-DASH photolyase genes. The nucleotide sequences, translated amino acid sequences, and acquired deletion mutations of the CRISPR target site are displayed in the lower section of each pane ²¹³ I.

In order to tackle these projects, I initially studied cell lines derived from medaka and made available to me by the Todo lab (Osaka University, Japan), that via CRISPR/Cas9-induced mutagenesis carry loss of function mutations in the CPD photolyase, 6-4 photolyase, and Cry-DASH photolyase genes²¹³ (Figure 1.20). These mutants show a significant impairment of photoreactivation DNA repair even under light-dark cycle (LD) conditions²¹³. I then used a series of gain and loss of function cell culture systems as well as the fish from which the cell lines were derived, to study in depth the functionality of CPD photolyase that is independent of light exposure.

2. Materials and Methods

2.1 Medaka fish maintenance and dissection of tissues

Wild type (iCab) and photolyase mutant medaka (*Oryzias latipes*) were maintained in the fish facility of the Institute of Biological and Chemical Systems, Biological Information Processing (IBCS-BIP) at the Karlsruhe Institute for Technology (KIT). The mutant fish generated by CRISPR-Cas9 were a kind gift from Takeshi Todo's lab (Osaka University, Japan)²¹³. All fish were reared in a water circulation system at 26°C under a 14 hours light and 10 hours dark cycle and fed manually twice per day. Fish were crossed in a circulating water tank holding 5 females and 1 male and the eggs were collected from the female fish's belly. The experiments using fish were all conducted according to European Legislation for the Protection of Animals used for Scientific Purposes (Directive 2010/63/EU) and the German animal protection standards.

For fin clip experiments in medaka, fish were anesthetized in 0.02% Tricaine (Sigma Aldrich) for 2-3 minutes, and then a small part of the fin was cut using a scalpel. For recovery, the fish were transferred to ERM medium containing methylene blue. The cut fin segments were washed in 1 X PBS and Leibovitz's L-15 medium 3 times, separately, and afterwards, treated following the experimental design.

For the dissection of multiple tissues (eye, brain, heart, liver, muscle, skin, fin clip) medaka were incubated in ice water until they were dead, and the various tissues were dissected and frozen in liquid nitrogen immediately and then stored at -80°C until further treatment.

2.2 Fish and mammalian cell culture and transfection

The cell line derived from 36 hours old zebrafish embryos (PAC-2), medaka wild type and mutant cell lines derived from medaka embryos (CPD/DASH/6-4 WT/KO) and cavefish cell lines derived from *P. andruzzii* embryos (EPA) were cultured in Leibovitz's L-15 medium (Gibco) supplemented with 15% (zebrafish cells) or 20% (medaka and

cavefish cells) Fetal Bovine Serum (FBS) (Gibco), 100 units/ml penicillin, 100 µg/ml streptomycin and 100 µg/ml gentamicin (Gibco). All these cell lines were incubated in an atmospheric CO₂, non-humidified cell culture incubator at 26°C.

The mouse cell line (NIH 3T3) and the stably transfected, photolyase-expressing cell lines (3T3 CPD/DASH/6-4pp) were cultured in DMEM medium (Gibco) supplemented with 10% Fetal Bovine Serum (FBS) (Gibco), 100 units/ml penicillin, 100 µg/ml streptomycin (NIH 3T3 cells) or 250 µg/ml neomycin (stable 3T3 lines expressing photolyases) (Gibco). Mammalian cells were maintained in a 5% CO₂, humidified cell culture incubator at 37°C

All of these cell lines were transfected in accordance with the manufacturer's instructions using FuGene HD transfection reagent (Promega). The ratio of FuGene (µl) and plasmid DNA (µg) was 4:1, and cells were incubated with the FuGene / DNA mixture overnight at 26°C (Fish cells) or 37°C (3T3 cells).

2.3 Light sources, UV radiation and H₂O₂ treatment

All light exposure experiments were conducted by using one of the following light sources at a constant temperature of 26°C (fish cells) or 37°C (mammalian cells).

- Laboratory UV-C light (VETTER GmbH, 254nm)
- White light emitting diodes (LED, Kopa, 440 nm-690 nm)
- Monochromatic red light emitting diodes (LED, Kopa, 665 nm)
- Monochromatic blue-light-emitting diodes (LED, Kopa, 468 nm)

All UV treatments were carried out using UV-C, which is commonly applied in laboratory research due to its maximum absorption by DNA and more effective photoproduct formation than UVA or UVB radiation. Due to the weak penetration of UVC, medium was removed from the plate before UV-C treatment and immediately after UV-C pulse exposure, the medium was replaced.

Hydrogen peroxide (H₂O₂, Sigma Aldrich) treatment was carried out according to the manufacturer's instructions, by simply adding H₂O₂ to the medium in the wells and incubating at various times depending on the experimental design. Subsequently, the H₂O₂ containing medium was discarded and replaced by fresh medium for recovery.

2.4 Cell viability assay

2.4.1 MTT assay

The MTT (3(4,5dimethylthiazol-2yl)2,5diphenyltetrazolium bromide, Sigma Aldrich) assay was employed to determine cell viability as previously described²¹⁴. Specifically, wildtype and photolyase mutant medaka cells were planted at a density of 3 x 10⁴ cells/well in 96-well plates and maintained until confluency for two days in the dark. Subsequently, cells were treated with various concentrations of H₂O₂ for a certain time and then the H₂O₂ containing medium was replaced with fresh medium. After discarding the medium, 0.5 mg/ml MTT dissolved in L-15 medium was added for 4 hours at 26°C or 37°C. After removing the MTT medium, DMSO was applied to dissolve the purple formazan crystals. Subsequently, the plate was measured using a test wavelength of 590 nm and a reference wavelength of 620 nm on a SpectraMax iD3 Microplate Reader.

2.4.2 AHM assay

This assay was initially established in the lab of Dr. Carsten Weiss at IBCS-BIP and the lab members initially guided me in the practical use of the automated microscopy set-up and the methods used for the analysis of data. 8 x 10³ cells (medaka cells) or 1.5 x 10³ cells (mammalian cells) were plated per well of a 96 well plate for automated high-throughput microscopy (AHM) measurement of cell number and the proportion of living and dead cells. The cells were incubated in darkness for 2 days and then treated with various doses of H₂O₂ or UV-C pulse exposure. After that, the cell medium was refreshed for recovery for 1 or 2 days. Following recovery, analysis was performed

according to a previously described protocol^{215,216}. Cells were stained with Hoechst 33342 and propidium iodide (PI) at 0.3 g/mL and 0.5 g/mL, respectively. Bright field (BF) and fluorescence pictures were acquired from four areas of each well using an automated Olympus IX81 fluorescence microscope and a 10-objective lens after 30 minutes incubation in the dark (Olympus, Hamburg, Germany). Excitation and emission wavelengths of 350 and 450 nm, respectively, were used to detect the Hoechst dye. At 488 nm and 590 nm, respectively, PI dye was identified. As previously reported^{215,216}, the acquired images were processed by using scan[^]R analysis software (version 2.7.3, Olympus, Hamburg, Germany) to identify the number of living or dead cells (combination of Hoechst and PI channel).

2.5 Immunofluorescence assay

2.5.1 Immunofluorescence assay in cells

Immunofluorescence assays were performed as previously described²¹⁷ with some modifications. Cells were seeded at a density of 1×10^5 per well in a 24-well plate and incubated in the dark for 2 days. Following treatment, cells were fixed by the addition of 4% PFA in PBS for 20 minutes and washed with PBS 3 times (5 minutes each wash) and with PBST (1x PBS + 0.1% Tween) 2 times (10 minutes each wash). Cells were permeabilized by treatment with 0.5% Triton X100 in PBS for 5-10 minutes with slow tilting agitation of the plate. Subsequently, cells were blocked by exposure to PBS + 0.1% Tween +1% BSA for at least 1 hour at room temperature and incubated with primary antibody diluted in blocking buffer overnight at 4°C. The primary antibody used was the Phospho-Histone H2A.X (Ser 139) (20E3) Rabbit monoclonal antibody (Cell Signaling). The following day, cells were washed 3 times with PBST (5 minutes each wash) rinsed briefly with blocking buffer and then incubated with the secondary fluorescent antibody diluted in blocking buffer for 1 hour at room temperature. After incubation, cells were washed with PBST and PBS separately 3 times (10 minutes each wash) and then stained with DAPI for 5 minutes. Finally, samples were mounted in

mounting medium (Dako, fluorescent mounting medium S3023) and imaged by scanning using a laser scanning confocal microscope (Leica TCS SP5).

2.5.2 Immunofluorescence assay in fish fin clips

Medaka fin clips were cut gently from fish and washed with PBS and Leibovitz's L-15 medium (20% FBS supplemented) (Gibco) several times. Samples were incubated in darkness for a few hours and then treated with hydrogen peroxide according to the experimental design. The fins were fixed with 1ml Carnoy's solution at 4 °C overnight. Carnoy's solution is a fixative incorporating 60% ethanol, 30% chloroform and 10% acetic acid. On the next day, fin clips were washed 3 times with 100% methanol and hydrated in 5 minutes series: 75% methanol + 25% PBTX (1 x PBS + 0.3% Triton X100), 50% methanol + 50% PBTX and 25% methanol + 75% PBTX. Following 2 brief rinses with PBTX, fin clips were blocked by incubation in blocking buffer (PBTX + 0.25% BSA) for 4 hours and then treated in darkness with the primary antibody at 4 °C overnight on a rotator. The primary antibody used was the Phospho-Histone H2A.X (Ser 139) (20E3) Rabbit monoclonal antibody (Cell Signaling). On the 3rd day, samples were washed 4 times, each wash for 25 minutes with PBTX (then a last wash in blocking buffer) and then incubated with the secondary antibody at 4 °C overnight on a rotator. Subsequently, following 3 x 20 minutes washes with PBTX, fin clips were stained with DAPI for 10 minutes and washed 3 x 10 minutes in PBTX. Eventually, samples were washed in 5 minutes series: 33% glycerin + 67% PBTX, 66% glycerin + 33% PBTX and 86% glycerin and then coated on microscopy slides with the mounting medium (Dako, fluorescent mounting medium S3023). Samples were imaged using a confocal microscope (Leica TCS SP5).

2.5.3 Image analysis

In order to quantify the degree of DNA damage caused by oxidative stress, the confocal images obtained from the immunofluorescence analysis with the Phospho-Histone

H2A.X (Ser 139) antibody were processed by Fiji/ImageJ software and for quantification, the cell number and fluorescence intensity of H2A.X were counted and calculated.

2.6 ELISA assay

ELISA (Enzyme-Linked ImmunoSorbent Assay) assays were employed to directly measure the levels of DNA damage and the progress of repair following UV-C light and oxidative stress exposure. The ELISA kits used in this project were OxiSelect™ UV-Induced DNA Damage ELISA Kit (CPD Quantitation) and OxiSelect Oxidative DNA Damage ELISA Kit (8-OHdG Quantitation) (Cell Biolabs) in order to quantify the content of CPD and 8-OHdG respectively. Cells were plated at a density of 6×10^5 cells/well (CPD Quantitation) in a 6-well plate or 2×10^6 cells/dish (8-OHdG Quantitation) in a 10 cm petri dish and cultured in darkness for 2 days. Samples were then treated according to the experimental design. Following treatment, cells were harvested and genomic DNA was extracted using a GeneJET Genomic DNA Purification Kit (Thermo Fisher). In the case of 8-OHdG Quantitation, samples were completely digested to nucleotides by nuclease P1 and dephosphorylated by alkaline phosphatase. Subsequently, samples were applied to a plate supplied with the kit that was coated with a specific conjugate by the manufacturers and then finally the treated plate was scanned on a SpectraMax iD3 Microplate Reader at a wavelength of 450 nm.

2.7 Construction and expression of gain of function mammalian cell lines

2.7.1 Establishment of gain-of-photolyase-function 3T3 cells

Mammalian cells were planted at a density of 4×10^5 cells/well in a 6-well plate and on the next day were co-transfected with expression vectors for wild type CPD photolyase or CPD photolyase carrying specific amino acid substitution mutations and

an empty pcDNA vector carrying a neomycin resistance cassette. After 2 days incubation, the culture medium was replaced with fresh medium supplemented with neomycin to select for stably transfected cells and after around 1 week, all the control cells (without transfection) were dead. The remaining viable cells were trypsinized, the cell density was measured and then the cells were aliquoted into individual wells of a 96 well plate, to ensure that each well of the 96-well plate carried only 1 cell. Eventually, after several weeks, multiple single clone cell lines expressing various amounts of photolyase proteins were obtained and levels of ectopic photolyase expression were quantified in each clone by western blot assay using an anti-Myc epitope tag antibody.

2.7.2 Site-directed mutagenesis

In order to explore whether key amino acids in catalyzing the photoreactivation reaction might also contribute to the CPD photolyase "dark" DNA repair function, I chose to generate the following mutations: W310F and W400F (disrupting the Three Tryptophan Electron Transfer Chain) in zebrafish CPD photolyase by using the Q5 Site-Directed Mutagenesis Kit (New England Biolabs) precisely according to the manufacturer's instructions. The primers and mutated plasmids used for the mutagenesis reactions are presented in the following table ([Table 2.1](#)).

[Table 2.1](#) Primers used for mutagenesis of the Three Tryptophan Electron Transfer Chain of zebrafish CPD photolyase

Plasmid name	Primers
zf CPD photolyase W310F mutation	F: CCTCTCCCCATTTCATTCATGCTGG R: TGGCTAACGGCGTCAGAG
zf CPD photolyase W400F mutation	F: TGACCAATTGTTAATGCTGCACAGC R: TGAGTTTCGGCGCTCTCC

2.7.3 Western Blotting (WB) analysis

Cells were seeded in a 6-well plate at a density of 4×10^5 cells per well. After 2 days incubation, culture medium was discarded and cells were washed twice with cold 1 x

PBS. Then 200 μ l 1 x Laemmli (6% SDS, 20% glycerol, 0.01% bromophenol blue and 125 mM Tris, pH = 6.8 and 0.1 M DTT) was added to the wells in order to lyse the cells which were then harvested by scraping after 2 minutes incubation in the 1 x Laemmli buffer at room temperature. A Bio-Rad mini-protean 3 chamber equipment was used for SDS-PAGE (Sodium dodecyl-sulfate polyacrylamide gel electrophoresis) and then the gel was prepared for transfer of the proteins to an ImmunBlot PVDF membrane (Millipore) by electroblotting. After primary and secondary antibody incubation and washing, the Clarity Western ECL substrate (Bio-Rad) was applied to the PVDF membrane and the membrane was visualized using the ChemiDoc™ Imaging System (Bio-Rad). The primary antibody used was the mouse Anti-Myc Tag monoclonal antibody (Millipore), while the second antibody was a Goat Anti-mouse polyclonal antibody (Cell Signaling). Images were viewed and evaluated using the ImageLab™ software (Bio-Rad).

2.8 Coding sequence characterization and cloning

2.8.1 Alignment of coding sequences

The alignment of CPD photolyase coding sequence among zebrafish, cavefish and medaka fish was conducted by using DNAMAN software 7 (Lynnon Corporation). The following table ([Table 2.2](#)) presents the Genbank accession numbers for the CPD photolyase protein sequences of these 3 species.

Table 2.2 Genbank accession number of CPD photolyase sequences

Genes	Accession No.
zebrafish CPD photolyase	NP_957358.1
cavefish CPD photolyase	AYN44215.1
Medaka CPD photolyase	NP_001098271.1

2.8.2 Plasmid cloning

All the plasmids employed this project were from the Foulkes lab's plasmids collection and were re-transformed for further use. All of the freshly re-transformed plasmids were tested by appropriate restriction enzyme from mini preparation (QIAGEN) samples and sequenced from midi or maxi preparation (QIAGEN) samples by a commercial supplier (Microsynth Seq Lab). The NanoDrop Spectrophotometer (PeqLab) was used to determine the concentration and purity of all the plasmids.

2.9 Gene expression analysis

2.9.1 RNA extraction

Medaka wild type and photolyase-mutant fish were dissected to acquire multiple tissues (eye, liver, brain, heart, muscle, skin, fin clips) and these tissues were lysed by addition of 500 μ l Trizol Reagent (Invitrogen) and homogenous grinding using a micropestle. Afterwards, these samples were kept at -80°C until RNA extraction. Cell cultures were seeded at a density of 1×10^6 cells in a 10 cm petri dish and maintained under LD (12 hours light and 12 hours dark) cycle conditions for 4 days. Subsequently, 250 μ l Trizol Reagent (Invitrogen) was added to the cell layer for lysis, then the lysate was recovered with the help of a cell scraper, transferred to 1.5ml Eppendorf tubes before freezing the samples at -80°C until further use.

Both tissue samples and cell samples were homogenized by sucking at least 10 times through a 1 ml single-use syringe with a 24 G (cells) or 26 G (tissue) needle. After addition of Chloroform (at 1/5 of the Trizol volume), the samples were mixed by rapid inversion, incubated on ice for 3 minutes and then centrifuged for 15 minutes at 12000 rpm at 4°C . Afterwards, the aqueous phase was transferred to a new eppendorf tube, Isopropanol was added (at 1/2 of the Trizol volume), mixed well by inversion and incubated on ice for 10 minutes. After centrifugation for 15 minutes at 12000 rpm at 4°C for the precipitation of RNA, the supernatant was discarded carefully and 100 μ l

80% Ethanol was added for washing. Later, after centrifugation for 5 minutes at 12000 rpm at 4°C, all the liquid was removed and the pellet was dried briefly at room temperature for approximately 10 minutes until the pellet became transparent. Thereafter, the pellet was dissolved in nuclease-free water (Promega) and the RNA concentration was quantified using a NanoDrop ND-100 Spectrophotometer (PeqLab). The integrity of the ribosomal 28S, 18S and 5S RNA bands was examined by electrophoresis on a 1% agarose gel to evaluate the quality and quantity of the total RNA.

2.9.2 Reverse transcription (cDNA synthesis) and control PCR

1 µg of total RNA was used for synthesis of cDNA and digested with 1 µl RQ1 DNase supplemented with 1 µl RQ1 10X DNase buffer and 0.25 µl RNase Inhibitor to remove contaminating genomic DNA. After incubation for 30 minutes at 37°C, 1 µl RQ1 DNase Stop Solution was applied for inactivation of DNase and incubated at 65°C for 10 minutes. Then, 1 µl Random Primer solution was added to the mixture and incubated for 5 minutes at 70°C. Subsequently, 10 µl of PCR master mix (3 µl nuclease-free water + 4 µl 5 X RT Buffer + 2 µl 10mM dNTPs + 1 µl RevertAid RT Enzyme) was prepared and added to the 12 µl cDNA mixture and then incubated according to the following program: 25°C 10 minutes, 42°C 60 minutes and 70°C 15 minutes. Finally, cDNA was diluted 1:10 by adding 200 µl nuclease-free water and stored at -20°C.

In order to evaluate the quality of synthesized cDNA, a control PCR was prepared and the reagents and cycling conditions are presented below:

Reagents	20 μ l reaction
cDNA	4 μ l
Taq DNA Polymerase	0.25 μ l
10 μ M β -actin forward + reverse primer	2 μ l
10mM dNTPs	0.5 μ l
5X Taq DNA Polymerase Buffer	4 μ l
Nuclease-free water	9.25 μ l

Step	Temp	Time
Initial Denaturation	95°C	2 minutes
25 Cycles	95°C	1 minute
	54°C	30 seconds
	72°C	30 seconds
Final Extension	72°C	5 minutes
Hold	4°C	

A 1% agarose gel was prepared for electrophoresis and 10 μ l of each PCR reaction was loaded. The cDNA should have one distinct band on the gel per sample.

2.9.3 Real-time PCR (qRT PCR)

The quantitative Real-time PCR was performed using the StepOnePlus™ Real-Time PCR System (Thermo Fisher) following the manufacturer's instructions and the reactions were prepared as summarized below:

Reagents	25µl reaction
cDNA	4µl
2 X SYBR Green	10µl
10µM forward + reverse primer	2µl
Nuclease- free water	9µl

The primer sequences used for qRT PCR are listed on [Table 2.3](#)

[Table 2.3](#) Primers for qRT-PCR

Medaka Gene	Primer sequence
<i>per1b</i>	F: GGGGAGAGTCGTGTACGTGT R: TGCTGCTGTAGAAGGTGCTG
<i>per2</i>	F: CACGAGGATGTAGAGATGG R: TGAGACTGACTGCTGGAA
<i>per3</i>	F: CGGTGCTCCTTTATCTTTTACTACA R: CTTTCAGAGTGGTTGAGTCCAGT
<i>cry1a</i>	F: CTGCCGCTCTTTACTTCA R: GCTCTCCATCTTGTCGAAGC
<i>cry5</i>	F: TTAGTTCTTTCAAGACCTGG R: ATGGGAGATTTGTAGATGAC
<i>clock1b</i>	F: AGGCTATCTACCATTTGAGGTTCTT R: AGATCCACTGTTGACCTTTTGTAG
<i>Mitochondrial ribosomal protein S18B</i>	F: TCCCCGAGAAATCCAGCAT R: CTCCTCCGTTAGCTCTCCAG
<i>β-actin</i>	F: GAAGATCTGGCACACACCTTCTACAATGAG R: GGGCGACGTAGCACAGCTTCTCCTTGATGTC

Medaka mitochondrial ribosomal protein S18B or β-actin mRNA expression was employed as a normalization to calculate the relative mRNA expression levels of interested genes by the $2^{-\Delta\Delta CT}$ method.

2.10 Luciferase reporter gene assay

2.10.1 *In vitro* luciferase assay

Cells were plated in a 24-well plate at a density of 1×10^5 (fish cells) or 5×10^4 (mammalian cells) per well and on the following day were transfected with various plasmids of interest by FuGene HD transfection reagent (Promega). 250 ng of the luciferase reporter plasmid, 50 ng β -galactosidase expression vector (pcDNA3.1/Myc-His/lacZ, Invitrogen), and a variable quantity of transcription factor expression plasmids were employed for each single well transfection. The final DNA quantity was adjusted by the addition of varying amounts of empty pCS2-MTK or pcDNA 3.1 plasmids to ensure equal amounts of total DNA were included in each transfection sample. After 1 or 2 days incubation in darkness, cells were washed by 1 X PBS twice and lysed by the addition of 70 μ l 1 X firefly luciferase lysis buffer (0.1 M Tris acetate (pH=7.5), 2 mM EDTA, 1% Triton X 100). The plate was held on a vortexer for a maximum of 2 minutes and then a scraper was used to scrape the remaining cells off the surface of the plate and the resulting cell lysate was transferred to a pre-cooled eppendorf tube on ice. Thereafter, the samples were centrifuged 5 minutes at 12000 rpm at 4°C and the supernatant was transferred to a new pre-cooled tube on ice. The lysate was kept at -80°C until used for *in vitro* luciferase assay and β -galactosidase assay.

For the *in vitro* luciferase assay, 2 pump solutions were prepared according to the manufacturer's instruction. The firefly solution contained 2 mM ATP, 1 mM DTT and Gly Gly -/- solution, while the substrate was prepared with luciferin and Gly Gly -/- at a volume ratio of 1:4. Afterwards, 70 μ l firefly solution and 20 μ l substrate were applied to 20 μ l lysate in each well of a 96-well plate and the plate was scanned by a Victor Light Luminescence Plate Reader (Perkin Elmer).

For the β -galactosidase assay, 3 solutions (Solution A, B, C) were prepared according to the manufacturer's instructions. Solution A consisted of 0.2 M Na_2HPO_4 , 0.2 M NaH_2PO_4 and water, while Solution B was 4 mg/ml ONPG dissolved in 0.1 M NaH_2PO_4

(pH=7.5). Solution C contained 1 M MgCl₂, 14 M β-mercaptoethanol and water. All 3 solutions were mixed and added to 20 μl lysate in each well of the 96-well plate and the plate was incubated at 37°C in an incubator until the mixture turned light yellow. Subsequently, the plate was measured on a SpectraMax iD3 Microplate Reader at a wavelength of 420 nm.

2.10.2 *In vivo* luciferase assay (Real-time bioluminescence assay)

Zebrafish or medaka cells were seeded at a density of 3 X 10⁴ cells/well in a 96-well plate (Perkin Elmer) and incubated in darkness for 24 hours. For transfection, the cells were transfected with different plasmids of interest using FuGene HD transfection reagent (Promega) according to the manufacturer's instructions and cultured in darkness for 1 day. Subsequently, 80 ng of the luciferase reporter plasmid and 25 ng of expression vector plasmids (if necessary) were added for each well. Thereafter, the transfection medium was replaced by luciferin medium including 0.5 mM beetle luciferin potassium salt solution (Promega) (luciferin:medium = 1:250) and the plate was sealed with plastic sealing foil and a barcode was added on the right side of the plate. The plates were then transferred to a plate stacker unit and the real-time bioluminescence values were detected by a Topcount NXT automatic scintillation counter (Perkin Elmer) for several days under different lighting conditions (light/dark cycle or constant darkness). The data was analyzed by the I-and-A Excel plug-in (S. Kay, Scripps Research Institute).

2.10.3 Luciferase assay plasmids

All the plasmids used for the luciferase assays are listed on [Table 2.4](#)

Table 2.4 Plasmids used for luciferase assay

Insert	Vector
<i>15xD-box_{cry1a}-Luc</i>	pTAL/pLuc
<i>4xE-box_{per4}-Luc</i>	pLUC MCS
<i>zf per1b promoter-Luc</i>	pGL3 basic
<i>zf clock1</i>	pcDNA 3.1
<i>zf bmal1</i>	pcDNA 3.1
<i>zf 6-4 photolyase</i>	pCS2-MTK
<i>zf CPD photolyase</i>	pCS2-MTK
<i>zf DASH photolyase</i>	pCS2-MTK
<i>zf cry1a</i>	pCS2-MTK
<i>zf tef-1</i>	pCS2-MTK
<i>zf tef-2</i>	pCS2-MTK
<i>zf hlf-1</i>	pCS2-MTK
<i>zf hlf-2</i>	pCS2-MTK
<i>zf dbp-1</i>	pCS2-MTK
<i>zf dbp-2</i>	pCS2-MTK
<i>zf e4bp4-1</i>	pCS2-MTK
<i>zf e4bp4-2</i>	pCS2-MTK
<i>zf e4bp4-3</i>	pCS2-MTK
<i>zf e4bp4-4</i>	pCS2-MTK
<i>zf e4bp4-5</i>	pCS2-MTK
<i>zf e4bp4-6</i>	pCS2-MTK

2.11 Statistical analysis

All the data were calculated and represented as mean \pm SEM. In addition, all data were plotted by using GraphPad Prism 5 (GraphPad Software Inc.) and analyzed by SPSS Statistics 19.0 (IBM). To identify statistically significant differences, either a Student's t-test or an analysis of variance (ANOVA) was used, and thereafter applied Sidak's multiple comparison post-test. Statistics were considered to be significant when the p value was less than 0.05 and the statistical differences of $p < 0.05$, $p < 0.01$, $p < 0.001$ are denoted by *, ** or ***, respectively.

3.Results

3.1 Loss of function of CPD photolyase

While in Somalian cavefish, 6-4 and DASH photolyase function is being lost as a result of accumulating several loss-of-function mutations in these two cavefish genes, CPD photolyase is highly conserved¹⁵². Does CPD photolyase have a light-independent DNA repair function that would account for it being conserved in a species that has been evolving for millions of years isolated from sunlight? A critical consideration is that even in the absence of sunlight, there are still many potential sources of DNA damage in cave and subterranean environments. One example is oxidative stress, that originates from exposure to the hypoxic conditions which have been well documented to characterize the water in many cave environments²¹⁸. Therefore, I decided to initially focus on exploring whether there were any links between CPD photolyases and the repair of oxidative damaged DNA under constant darkness.

To initially address this issue, I examined the phenotype of a unique set of 3 medaka CRISPR-Cas9-generated mutants which carry loss of function mutations in each of the three photolyase genes that were generated in the laboratory of Takeshi Todo (Osaka University, Japan)²¹³. Specifically, I studied cell lines derived from these mutants as well as 3 corresponding wild type control lines. My initial phylogenetic analysis of medaka photolyase genes revealed that they share high sequence similarity with zebrafish photolyase genes and for certain functional domains, they are close to 100% identical (Table 3.1 and Figure 3.1).

CPD phr protein	Protein sequence similarity
zebrafish and medaka	62.48%
zebrafish and cavefish	84.50%
cavefish and medaka	64.99%
zebrafish, cavefish and medaka	80.92%

Table 3.1 Protein sequence comparison of CPD photolyase among zebrafish (*Danio rerio*), Somalian cavefish (*Phreatichthys andruzzii*) and medaka (*Oryzias latipes*).

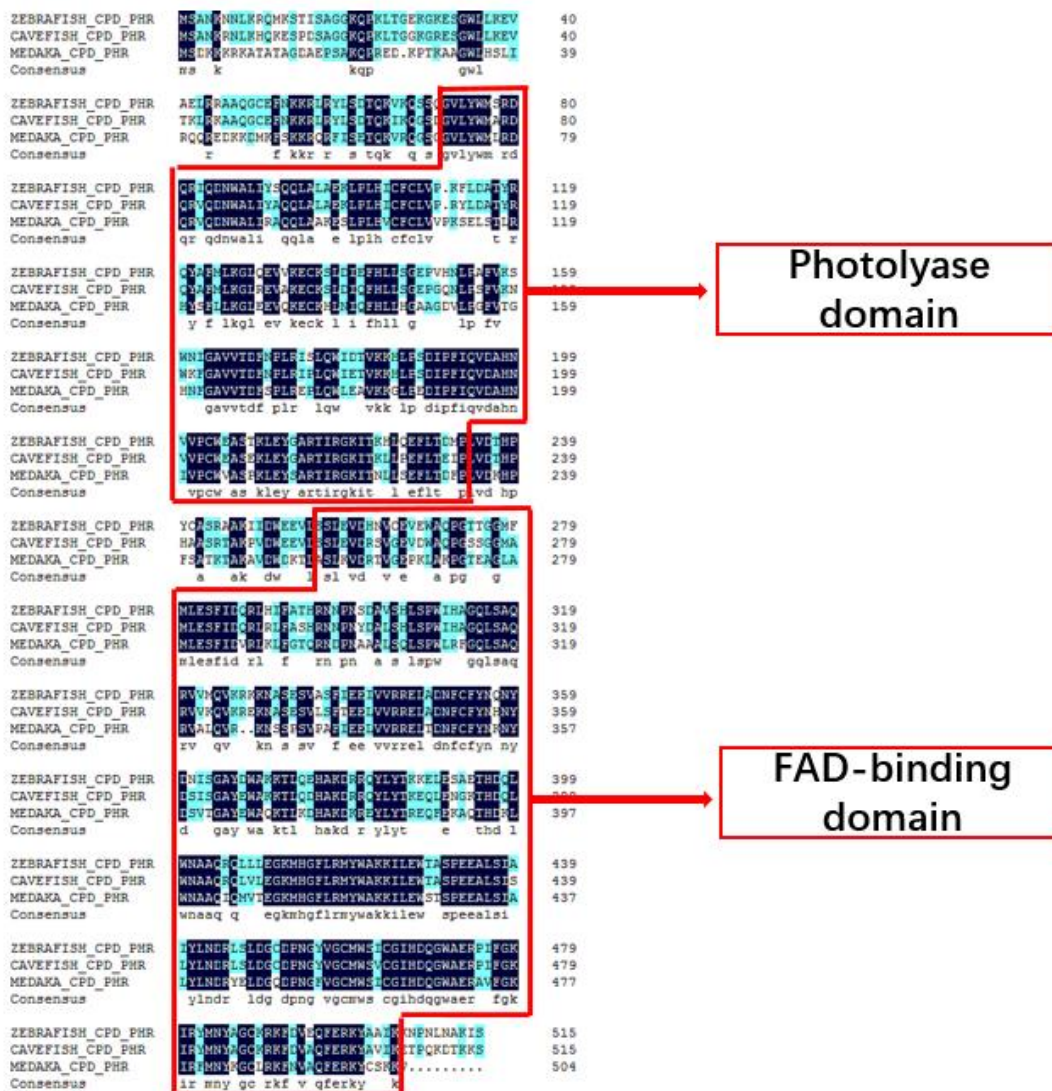


Figure 3.1 Alignment of CPD photolyase amino acid sequences from zebrafish (*Danio rerio*), Somalian cavefish (*Phreatichthys andruzzii*) and medaka (*Oryzias latipes*).

3.1.1 CPD photolyase function and oxidative stress

3.1.1.1 Increased DNA damage upon loss of CPD photolyase function.

In order to explore the levels of DNA damage induced by oxidative stress, I initially exposed cells to hydrogen peroxide in order to elevate intracellular ROS levels and then performed an immunofluorescence assay using a Phospho-Histone H2A.X (Ser139) monoclonal antibody (Cell Signaling) to detect the endogenous levels of phosphorylated H2A.X. H2A.X is a histone H2A variant that is rapidly phosphorylated at Ser139 by PI3K-like kinases at sites of DNA damage resulted from UV-light, ionizing radiation, or radiomimetic agents and therefore represents an indirect indicator or proxy of DNA damage. I exposed fully confluent cell cultures of the mutant cell lines as well as wild type controls to a range of hydrogen peroxide concentrations for 1 hour and thereafter refreshed the medium for recovery for 1 hour. I performed all the steps in darkness in order to avoid photoreactivation function. Subsequently, I fixed cells with 4% PFA, and then examined them by confocal microscopy.

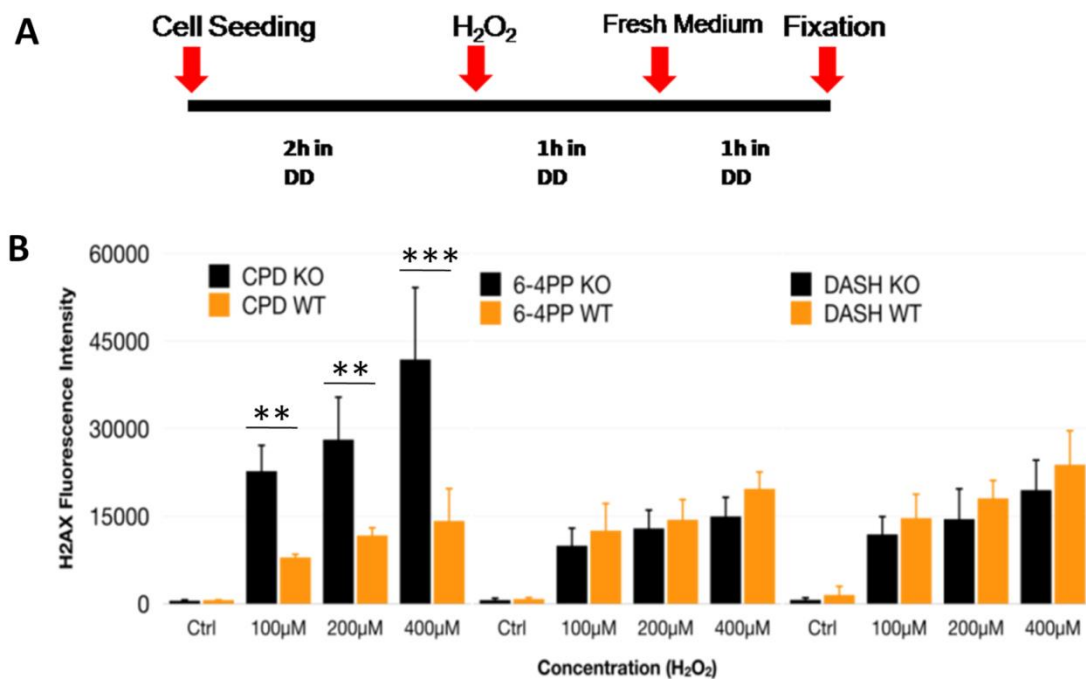


Figure 3.2 Cell signaling from DNA damage induced by oxidative stress in medaka WT and photolyase mutant cell lines. (A) Schematic representation of experimental design for immunofluorescence assay. (B) Medaka wild type (WT) and photolyase

mutant (KO) cells were treated with various hydrogen peroxide concentrations (μ M) indicated on the x-axes, and then recovered in darkness. H2A.X fluorescence intensity is plotted on the y-axes. Data represents the mean \pm SEM (n=4) and each WT and photolyase mutated cell lines were conducted independently at least 3 times. Fluorescence intensity was compared between WT and mutant groups by using Student's t-test (unpaired, two tailed) and statistical differences of $p < 0.05$, $p < 0.01$, $p < 0.001$ are represented by *, ** or ***, respectively.

My results show that there are no prominent differences between wild type and loss of function DASH and 6-4 photolyases cell lines, whereas there is a significant increase in H₂O₂ induced H2A.X levels in the CPD photolyase mutant cell line (Figure 3.2).

3.1.1.2 Cellular DNA damage upon oxidative stress *in vivo*

In order to confirm these initial *in vitro* results I next tested whether explanted cultures of fin clips from adult photolyase mutant fish would also show elevated levels of phosphorylated H2A.X compared with wild type controls when exposed to H₂O₂. I excised the medaka WT and photolyase-mutant fish fin clips and incubated them in darkness for 3 hours. Then, I treated these clips with 1mM hydrogen peroxide for 1 hour in an analogous approach to that used in the previous cell culture assays and allowed them to recover in fresh medium for 1 hour followed by fixation. I finally stained the fin clips with the Phospho-Histone H2A.X (Ser139) antibody to detect endogenous levels of phosphorylated H2A.X in the medaka fish fin clips. Consistent with the previous cell culture results, I observed a substantial increase in H₂O₂ induced H2A.X levels in the CPD knockout fin clips compared with wild type fins. Furthermore, in DASH and 6-4 mutant fins wild type levels of H2A.X staining were obtained (Figure 3.3).

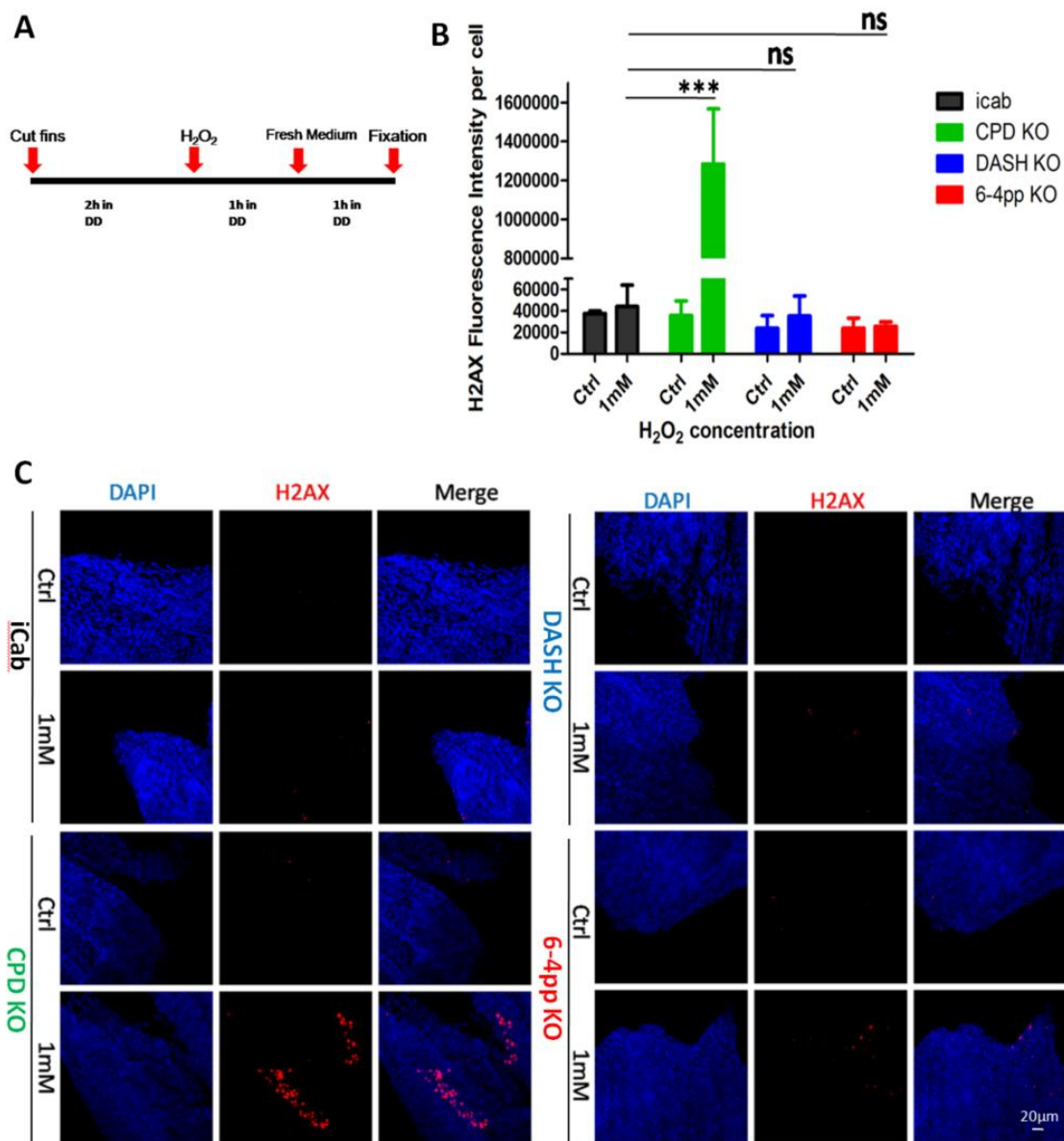


Figure 3.3 DNA damage induced by oxidative stress in medaka WT and photolyase mutant fish fin clips. (A) Schematic representation of experimental design for immunofluorescence assay. (B) Wild type medaka (iCab) and photolyase mutant (KO) fish fin clips were treated with 1mM hydrogen peroxide as indicated on the x-axis, and then recovered in darkness. H2A.X fluorescence intensity per cell is plotted on the y-axis. Data represents the mean \pm SEM (n=4) and each WT and photolyase mutated fish fin clips were repeated independently at least 3 times. Fluorescence intensity was compared between WT and mutant groups by using Student's t-test (unpaired, two tailed) and statistical differences of $p > 0.05$, $p < 0.05$, $p < 0.01$, $p < 0.001$ are represented by ns, *, **, or ***, respectively. (C) Representative images from immunofluorescence assay of H2A.X following exposure of medaka WT and photolyase mutant fish fin clips to 1mM hydrogen peroxide. Nuclear staining (DAPI, Blue), H2A.X staining (Red) and the merged images of DAPI and H2A.X staining are indicated.

medium and allowed the cells to recover for 1 day. Subsequently, I added MTT solution and measured the plate using a test wavelength of 590 nm on a Microplate Spectrophotometer. My results demonstrate that compared with the DASH and 6-4 photolyase mutants, the viability of the CPD photolyase mutant cells was significantly reduced upon hydrogen peroxide treatment (Figure 3.4)

In order to confirm this result, following initial technical training by the Carsten Weiss lab at IBCS-BIP, I next used an automated high-throughput microscopy (AHM) assay to measure the viability of WT and photolyase mutant cells following oxidative stress. In the AHM assay, cells are scored as belonging to distinct stages, specifically living cells, early-apoptotic cells, late-apoptotic cells or necrotic cells based on their staining with Hoechst and PI staining dye and morphology. The intensity and cell status were determined automatically using Scan[^]R analysis software.

I seeded medaka WT and CPD photolyase mutant cells in 96-well plates and subsequently, incubated them in darkness for 2 days. Thereafter, I treated the cells with a range of H₂O₂ concentrations for 1 hour and replaced the old culture medium with fresh medium for 1 day. Subsequently, I stained the cells with Hoechst and PI and then analysed them by automated Olympus IX81 fluorescence microscopy. My results confirmed the findings from the MTT assays. Specifically, that compared with wild type cells, the CPD photolyase mutant cells have reduced cell survival upon elevated oxidative stress (Figure 3.5).

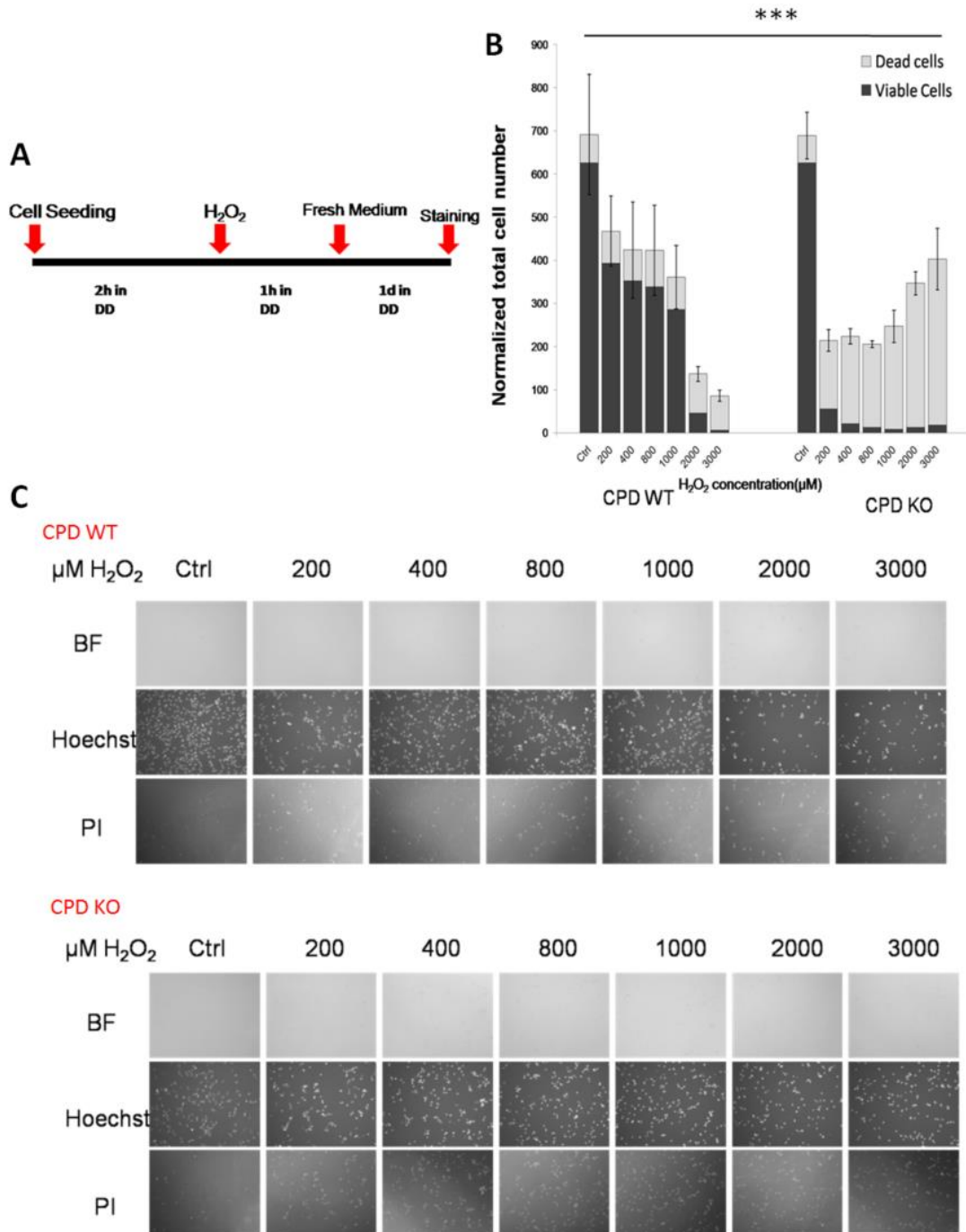


Figure 3.5 Automated microscopy assay of cell survival in medaka WT and photolyase mutant cell lines upon oxidative stress. (A) Schematic representation of experimental design. (B) Medaka wild type (CPD WT) and CPD photolyase mutant (CPD KO) cell lines were exposed to different concentrations of hydrogen peroxide, and then the medium was refreshed and the cells kept in constant darkness. Total cell number of mean \pm SEM (n=8) in relation to untreated cells are indicated on y-axes, while hydrogen peroxide concentrations (from 200 μ M to 3000 μ M) are indicated on the x-axes. This experiment was repeated independently at least 3 times. Cell survival was compared between WT and CPD photolyase mutant groups by using Two-way ANOVA followed by Sidak's multiple comparisons tests and statistical differences of $p < 0.05$,

$p < 0.01$, $p < 0.001$ are represented by *, ** or ***, respectively. (C) Representative images from the automated high-throughput microscopy (AHM) assay following exposure of medaka cell lines to various concentrations of hydrogen peroxide. Bright field (BF) channel, Hoechst staining, and Propidium Iodide (PI) staining are represented.

3.2 Gain of CPD photolyase function in mammalian cells

3.2.1 Establishing a 3T3 cell line ectopically expressing CPD

photolyase

It has been well established that no photolyase genes are present in the genome of placental mammals and that there is no evidence for the presence of photoreactivation DNA repair in these species. Therefore, mammalian cell lines represent useful models to study CPD photolyase DNA repair functionality in gain of function experiments. Specifically, as well as conferring photoreactivation DNA repair functionality on mammalian cells, would ectopic expression of zebrafish CPD photolyase influence the resistance of these cells to oxidative stress-induced DNA damage? Therefore, I next aimed to stably transfect 3T3 mouse cell lines with an expression vector stably expressing zebrafish CPD photolyase.

Initially, I cloned the cDNA encoding zebrafish CPD photolyase into the eukaryotic expression vector, pCS2-MTK. This vector has been routinely used in the Foulkes lab to ectopically express a range of different proteins in fish cell lines. I then seeded 3T3 cells in a 6-well plate and the next day I transfected them with the zebrafish CPD photolyase expression vector mixed with an empty pcDNA vector carrying a neomycin resistance cassette. After 2 days, I replaced the medium with fresh medium supplemented with neomycin to select for stably transfected cells and incubated the cells for about 1 week until all mock-transfected cells were dead and so no longer attached to the culture surface. I then detached the remaining viable cells from the culture plate in the stably transfected samples by trypsinization, counted the cell number and concomitantly aliquoted the cell suspension into individual wells of a 96 well plate to ensure that

each well of 96-well plate carried only 1 cell. I then maintained the culture for several weeks until the single cells had proliferated and each well had a confluent cell layer. I passaged cells into larger plates and prepared whole protein extracts from aliquots of the cells for each original clone. I assessed photolyase expression by Western Blot assay using an anti-Myc epitope tag antibody (Figure 3.6 A). My results revealed that multiple clones displayed expression of an immunoreactive band of the predicted molecular weight. Interestingly, there was a broad range of expression levels. I selected one of these clones (CPD single clone 8) for further analysis and cryopreserved aliquots to secure the line. I next performed a functional analysis of DNA damage repair in these 3T3 cell lines. Specifically, I tested whether the stable cell line ectopically expressing CPD photolyase had also acquired photoreactivation of UV-induced DNA damage.

3.2.2 Cell viability response to UV-C exposure in 3T3 cell lines.

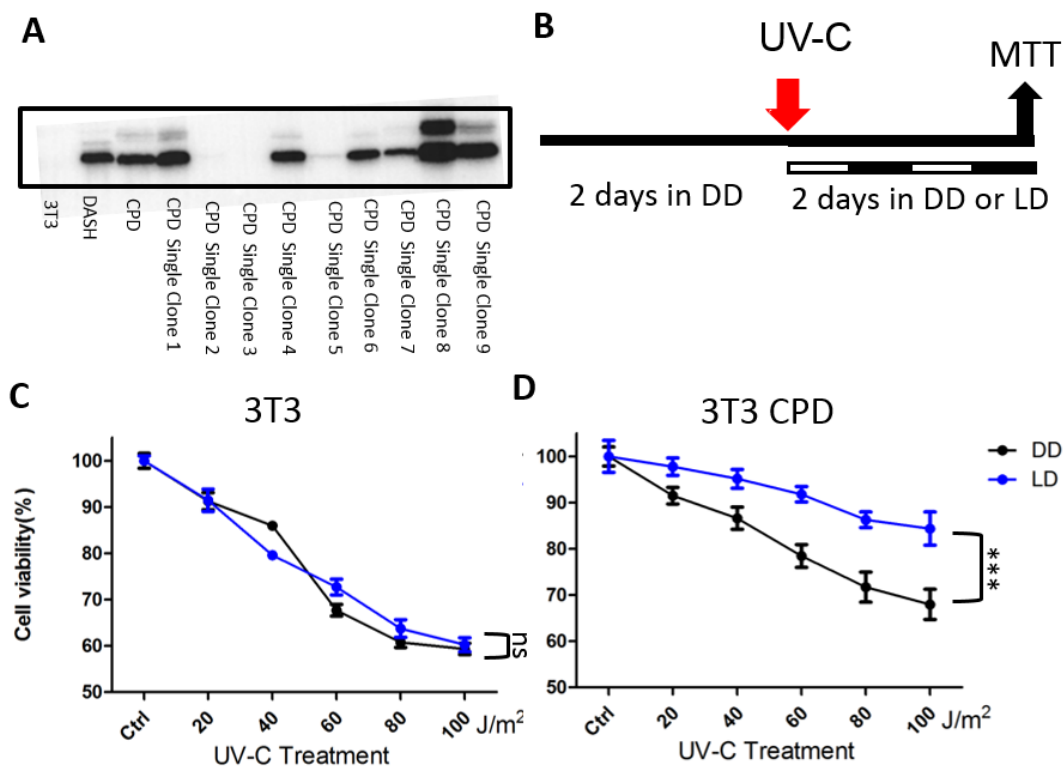


Figure 3.6 Zebrafish CPD photolyase single clone cell line establishment, expression and verification. (A) The expression of a myc tagged zebrafish CPD photolyase in mammalian cells by Western Blot. An expression vector for zebrafish CPD photolyase

was stably transfected into mammalian cells which were then selected for Neomycin resistance. Non-transfected 3T3 cells were employed as a negative control. (B) Schematic representation of the experimental design for testing photoreactivation function in the mammalian cell lines. (C-D) Cell viability assay to test whether ectopic-expression of CPD photolyase in mammalian cells confers photoreactivation upon UV-C exposure. 3T3 cells and 3T3-derived cell lines ectopically expressing CPD photolyase (3T3 CPD) were exposed to various doses of UV-C light and then transferred to constant darkness or light-dark cycle conditions. Percentage of mean \pm SEM (n=8) in cell viability with respect to untreated cells are indicated on the y-axes, while UV-C light doses (from 20 J/m² to 100J/m²) are indicated on the x-axes. This assay of each cell line was repeated independently at least 3 times. Cell viability was compared between LD and DD groups by using Two-way ANOVA followed by Sidak's multiple comparisons tests and statistical differences of $p > 0.05$, $p < 0.05$, $p < 0.01$, $p < 0.001$ are represented by ns, *, **, or ***, respectively.

To test for photoreactivation upon UV-C exposure, I incubated the CPD 3T3 cells as well as nontransfected 3T3 cells in constant darkness for 2 days. After exposure to various doses of UV-C light, I returned the cells to darkness (DD) or light-dark (LD) cycle conditions for 2 days before adding MTT solution to assay for cell viability. Upon recovery in LD conditions, 3T3 CPD cells showed a notable increase in cell viability compared with cells maintained in constant darkness. In contrast, in 3T3 cells, the lighting conditions after UV exposure had no significant effect on the levels of cell survival. My results are consistent with ectopic-expression of CPD photolyase in mammalian cells conferring photoreactivation upon UV-C exposure (Figure 3.6 B-D).

3.2.3 Cellular DNA damage upon oxidative stress in 3T3 cells

I next explored the consequence of ectopic CPD photolyase expression on the DNA repair response of 3T3 cells to oxidative stress. I initially performed a H2A.X assay in these 2 cell lines to more directly test the levels of DNA damage in 3T3 CPD cells upon oxidative stress. I seeded both 3T3 CPD cells and 3T3 control cells in 24-well plates and incubated them in darkness for 2 days. Before fixation, I exposed cells to various concentrations of H₂O₂ for 1 hour and then allowed them to recover by refreshing the medium and exposing the cells for 1 hour to constant darkness conditions (DD). Compared with 3T3 cells, 3T3 CPD cells showed lower H2A.X staining levels when

exposed to a range of hydrogen peroxide concentrations (Figure 3.7).

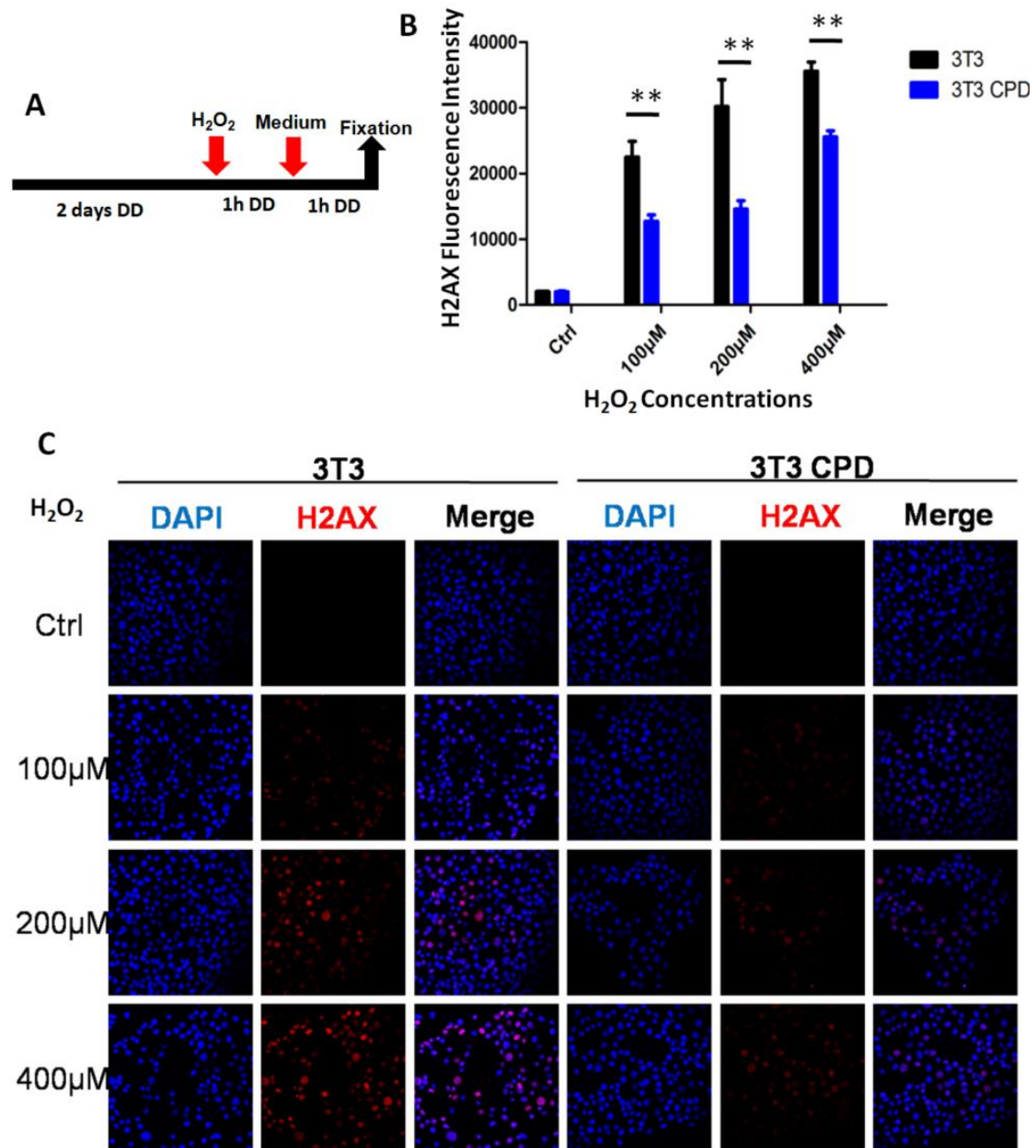


Figure 3.7 Ectopic expression of CPD photolyase reduces H2A.X levels in ROS-treated mammalian cells. (A) Schematic representation of experimental design. (B) 3T3 control cells and 3T3 cells ectopically expressing CPD photolyase (3T3 CPD) were treated with various concentrations of hydrogen peroxide indicated on the x-axis, and then incubated under dark conditions. H2A.X fluorescence intensity is plotted on the y-axis. Data represents the mean \pm SEM (n=6) and this experiment was repeated independently at least 3 times. Fluorescence intensity was compared between 3T3 and 3T3 CPD groups by using Student's t-test (unpaired, two tailed) and statistical differences of $p < 0.05$, $p < 0.01$, $p < 0.001$ are represented by *, ** or ***, respectively. (C) Representative images from immunofluorescence assay of H2A.X upon exposure of 3T3 and 3T3 CPD cell lines to different concentrations of hydrogen peroxide. Nuclear

staining (DAPI, Blue), H2A.X staining (Red) and the merged images of DAPI and H2A.X staining are indicated.

3.2.4 3T3 CPD cell viability response to oxidative stress

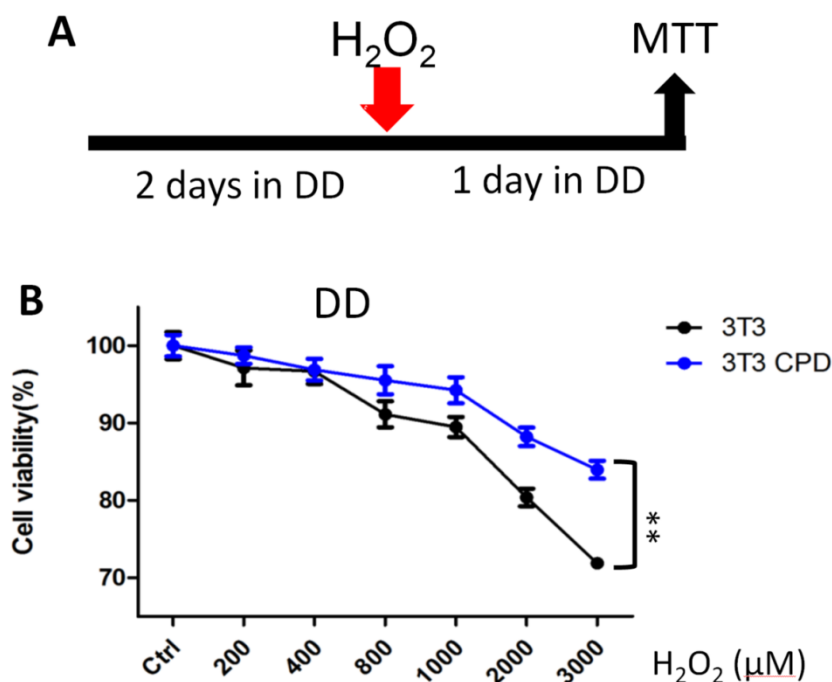


Figure 3.8 Ectopic-expression of CPD photolyase in mammalian cells increases viability upon oxidative stress. (A) Schematic representation of experimental design for cell lines shown in panel B. (B) 3T3 cells and 3T3 cells ectopically expressing CPD photolyase (3T3 CPD) were exposed to different concentrations of hydrogen peroxide, and the medium was refreshed and then the cells were transferred to darkness. Percentage of mean \pm SEM (n=8) in cell viability with respect to untreated cells are indicated on the y-axes, while hydrogen peroxide concentrations (from 200 μ M to 3000 μ M) are indicated on the x-axes. This experiment was repeated independently 3 times. Cell viability was compared between 3T3 and 3T3 CPD groups by using Two-way ANOVA followed by Sidak's multiple comparisons tests and statistical differences of $p < 0.05$, $p < 0.01$, $p < 0.001$ are represented by *, ** or ***, respectively.

I then explored the effect of ectopic expression of CPD photolyase in 3T3 cells upon oxidative stress by cell viability assay. I exposed 3T3 and 3T3 CPD cells to a range of H₂O₂ concentrations, then, after changing the culture medium with fresh medium, I exposed the cell lines to constant darkness (DD) conditions for 1 day. My results indicate that ectopic expression of CPD photolyase in mammalian cells enhances cell

survival following oxidative stress (Figure 3.8).

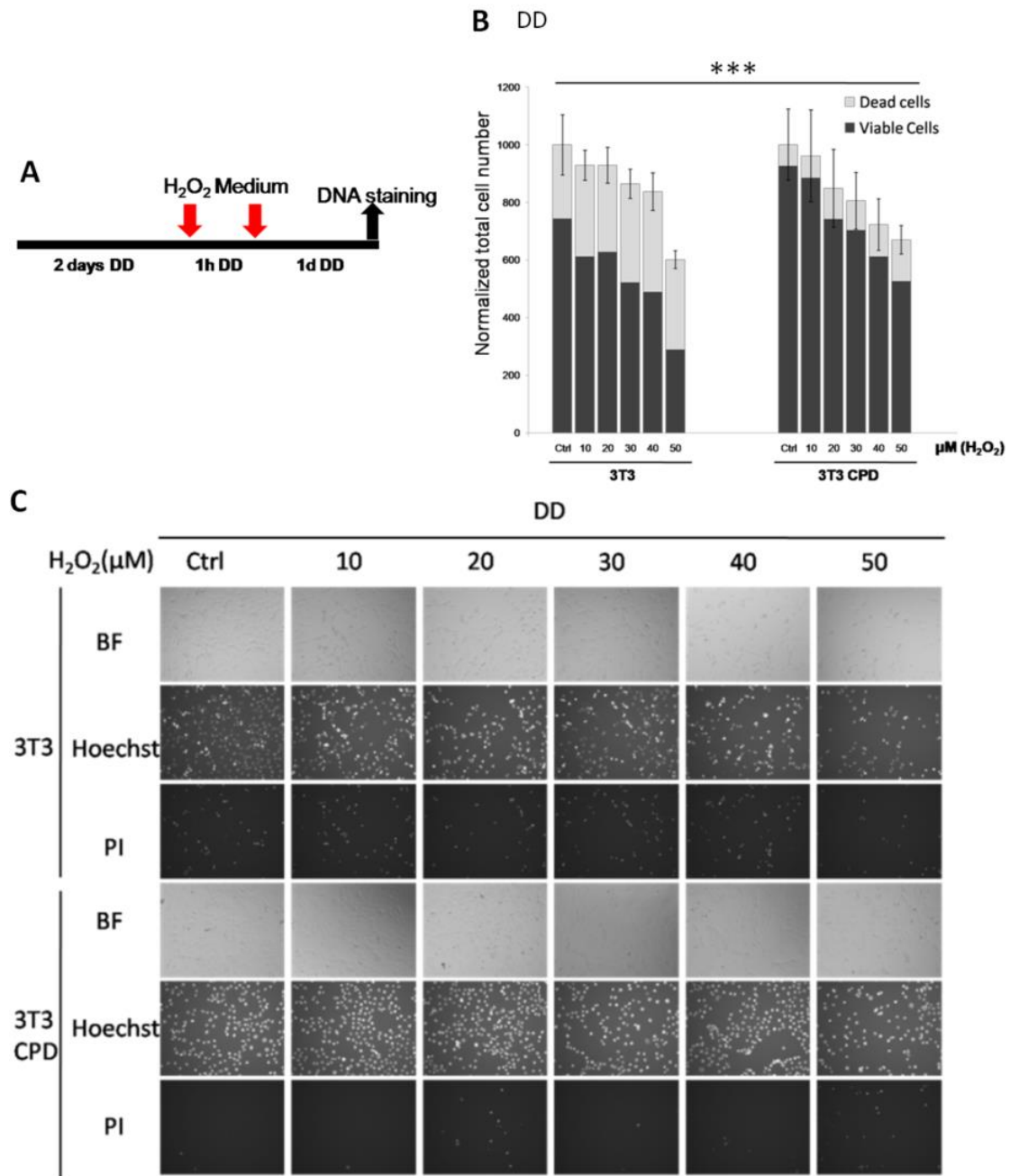


Figure 3.9 Ectopic expression of CPD photolyase increases cell viability following H₂O₂ treatment. (A) Schematic representation of experimental design (B) 3T3 cells and 3T3 cells ectopically expressing CPD photolyase (3T3 CPD) were exposed to lower levels of hydrogen peroxide than those employed for the MTT assay, at various concentrations, and then the medium was refreshed and the cells incubated in constant darkness. Total cell number of mean \pm SEM (n=8) in relation to untreated cells are indicated on the y-axis, while hydrogen peroxide concentrations (from 10 μ M to 50 μ M) are denoted on the x-axis. This experiment was repeated independently at least 3 times. Cell survival was compared between 3T3 control cells and 3T3 cells ectopically expressing CPD photolyase by using Two-way ANOVA followed by Sidak's

multiple comparisons tests and statistical differences of $p < 0.05$, $p < 0.01$, $p < 0.001$ are represented by *, ** or ***, respectively. (C) Representative images from the automated high-throughput microscopy (AHM) assay following exposure of 3T3 and 3T3 CPD cell lines to different concentrations of hydrogen peroxide. Bright field (BF) channel, Hoechst staining, and Propidium Iodide (PI) staining are represented.

I next validated these results by comparing survival of 3T3 and 3T3 CPD cells under constant darkness by our automated microscopy assay following H_2O_2 treatment. Specifically, I plated 3T3 and 3T3 CPD cells in 96-well plates and kept them in constant darkness for 2 days. Subsequently, I treated these cells with lower concentrations of H_2O_2 than for the previous MTT assay for 1 hour and exchanged the medium with fresh medium followed by recovery for 1 day in constant darkness. Then I stained the cells with Hoechst and PI staining dyes and after half hour incubation, scanned images of the plates by automated Olympus IX81 fluorescence microscopy which I analyzed by Scan^R analysis software. My results confirm that ectopic expression of CPD photolyase in mammalian cells enhances viability following H_2O_2 treatment and that cell survival is H_2O_2 dose-dependent (Figure 3.9).

3.3 Impact of light on ROS-induced DNA damage repair

The structure and function of photolyases are very much centered on the harvesting of photons and light energy and then relaying this to enhance the catalysis of DNA repair. Indeed, this represents the mechanistic basis of photoreactivation DNA repair. Given my results which implicate CPD photolyase in the cellular response to oxidative stress, it is therefore relevant to consider whether light might also influence the observed DNA damage repair and cell survival following exposure to oxidative stress. Indeed, by exploring this question in more detail, I may gain more insight into the mechanisms that are involved in this potentially novel property of CPD photolyase.

3.3.1 Impact of light on cellular DNA damage repair upon oxidative stress

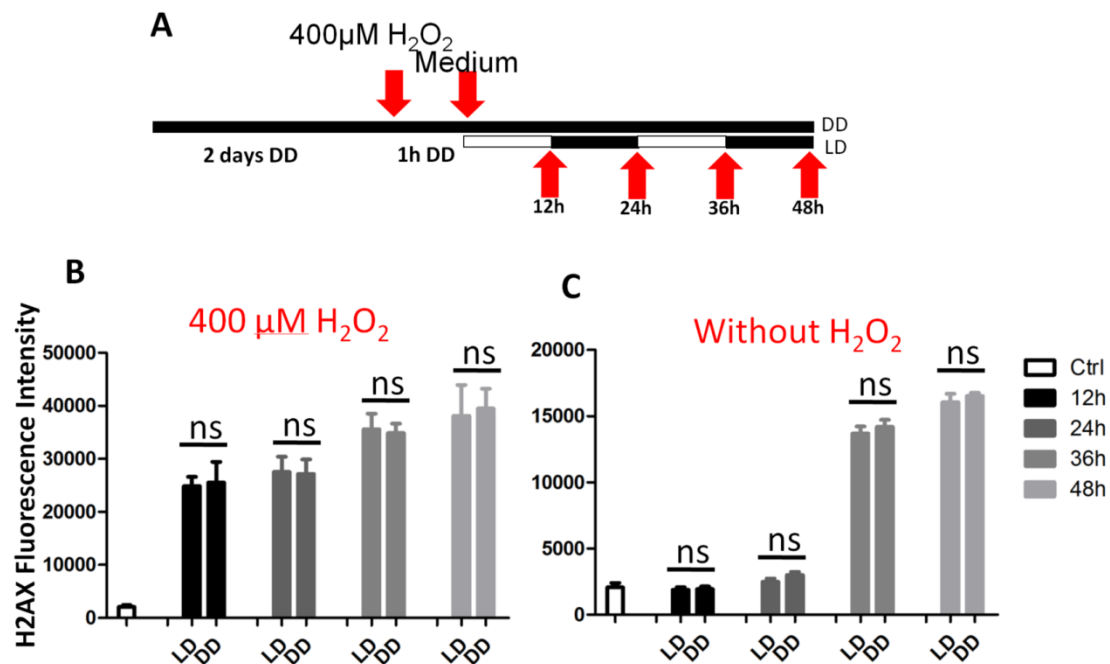


Figure 3.10 Light has no significant effect on the repair of ROS-induced DNA damage in medaka WT cells. (A) Schematic representation of experimental design. (B-C) Medaka WT cells were exposed to 400 µ M H₂O₂ (together with non-treated controls: Without H₂O₂) and later the medium was replaced with fresh medium for recovery. The recovery conditions under a light-dark cycle or constant darkness are indicated on the x-axis and cells were fixed at various timepoints as indicated by the shading of the bars. H2A.X fluorescence intensity is plotted on the y-axis. Data represents the mean

± SEM (n=4) and this experiment was repeated independently at least 3 times. Fluorescence intensity was compared between LD and DD groups at the identical timepoint by using Student's t-test (unpaired, two tailed) and statistical differences of $p > 0.05$, $p < 0.05$, $p < 0.01$, $p < 0.001$ are represented by ns, *, ** or ***, respectively.

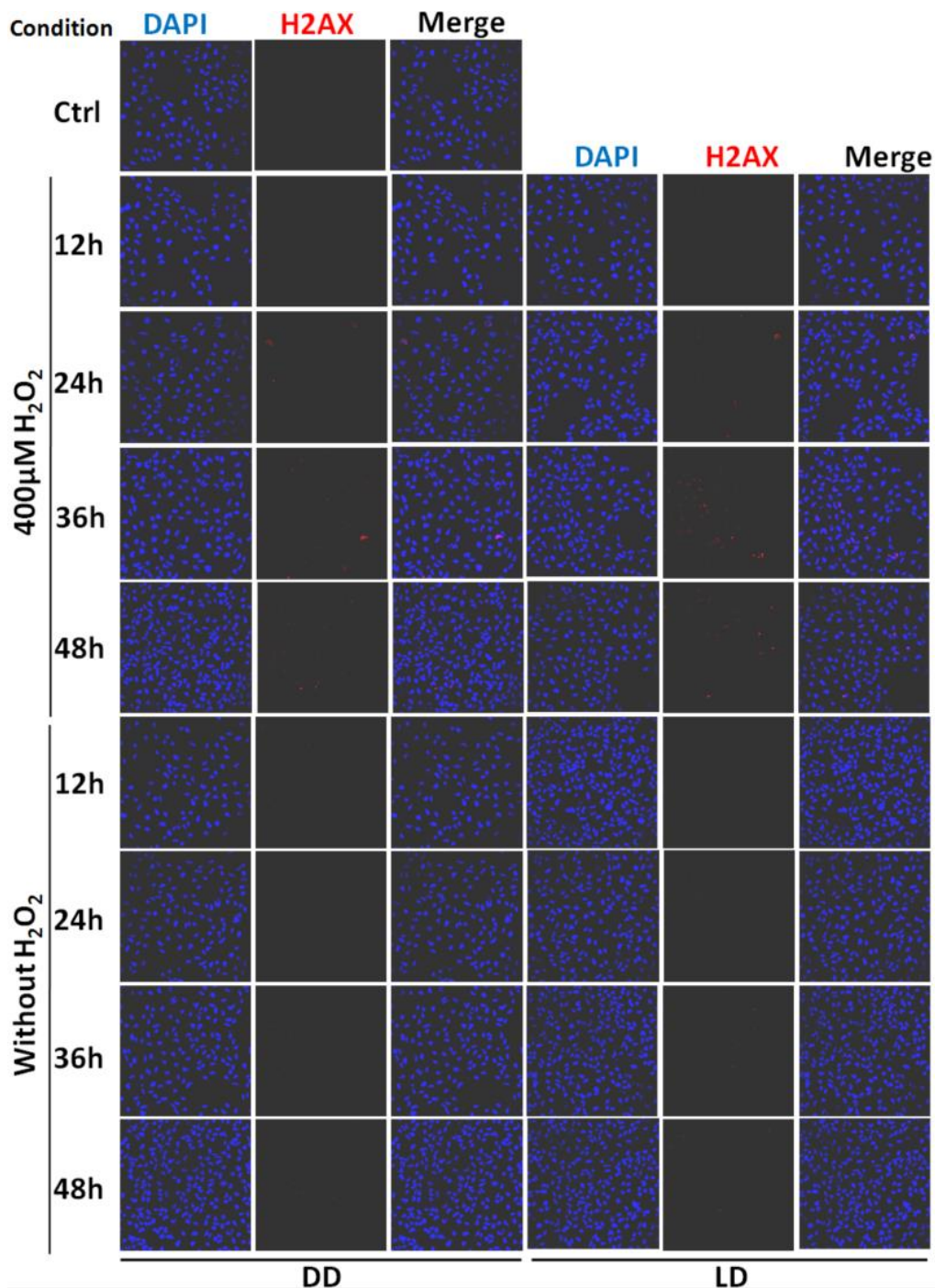


Figure 3.11 Representative images from immunofluorescence assay of H2A.X upon exposure of the medaka WT cell line to 400 μ M hydrogen peroxide (with non-treated controls) and recovery was under DD or LD conditions with cells being sampled at different timepoints as indicated on the left hand side adjacent to each set of images. Nuclear staining (DAPI, Blue), H2A.X staining (Red) and the merged images of DAPI and

H2A.X staining are shown.

To investigate the effects of visible light on the DNA repair which follows oxidative stress exposure, I next performed a H2A.X assay to study the changes in histone phosphorylation following oxidative stress under different lighting conditions in wild type medaka cell lines. Specifically, I treated WT medaka cells with 400 μ M H₂O₂ for 1 hour, then replaced the medium with fresh medium and left the cells to recover under either DD or LD conditions before fixation at various timepoints. A control group of WT medaka cells without hydrogen peroxide treatment still exposed to DD or LD conditions and sampling at the identical timepoints, I compared with the treated group. Following staining with the H2A.X antibody and then confocal microscopy, my results revealed that upon treatment with H₂O₂, H2A.X staining levels increase in a time-dependent manner, however, there were no significant differences between the cells exposed to DD and LD conditions at the various timepoints (Figure 3.10 and 3.11). Interestingly, there is also a modest increase in H2A.X staining in the untreated group at later time points possibly connected with the effects of handling the cells and the medium change however, there was no difference in staining between the DD and LD treated groups (Figure 3.10). Therefore, my results are consistent with light having no significant effect on ROS-induced DNA repair (Figure 3.10).

3.3.2 Impact of light on cell viability upon oxidative stress in medaka cells

I next explored whether light has an impact on cell viability following ROS exposure. I performed a MTT cell viability assay in medaka WT cells following exposure to ROS and recovery under either DD or LD conditions. As previously documented, exposure to increasing levels of H₂O₂ resulted in a dose-dependent decrease in cell viability. However, no significant difference of cell viability was observed between the cells recovering under DD and LD conditions following exposure to oxidative stress. My findings are consistent with light having no significant effect on cell survival upon ROS-

induced cellular damage (Figure 3.12 B).

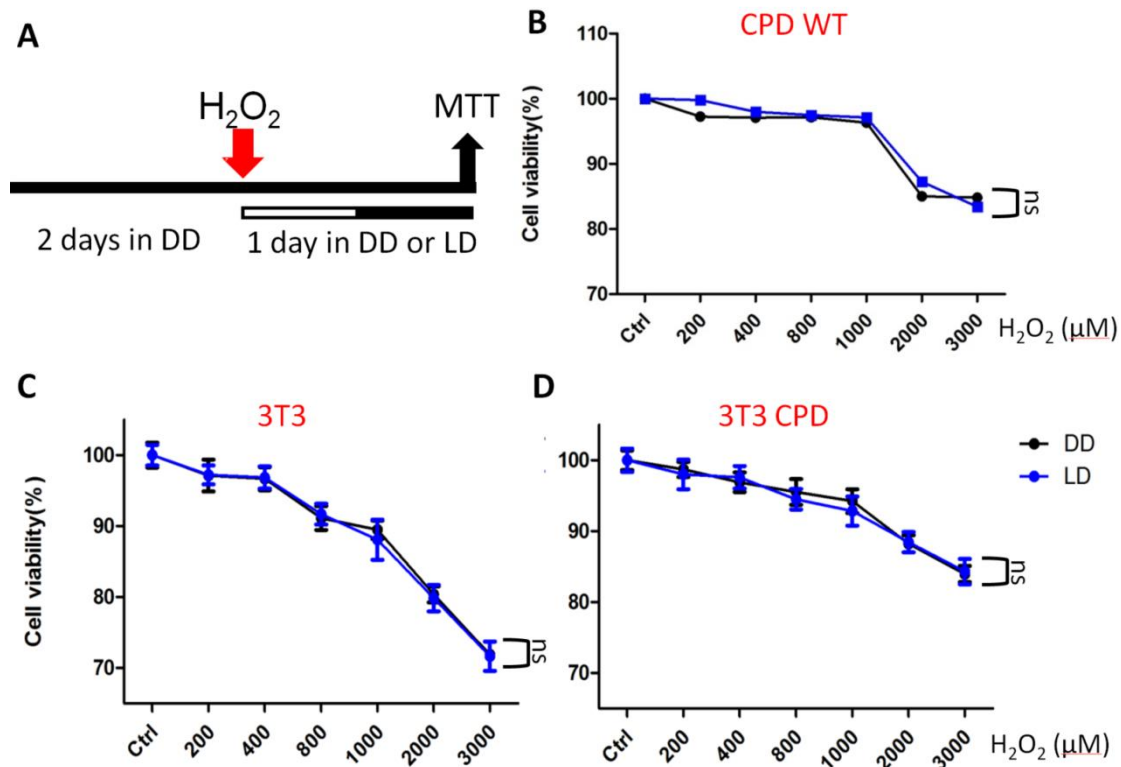


Figure 3.12 No significant effect of light on CPD photolyase-induced protection against ROS-induced mortality in medaka and mammalian cells. (A) Schematic representation of experimental design (B-D) Medaka wild type (WT) cells, 3T3 cells and 3T3 cells ectopically expressing CPD photolyase (3T3 CPD) were exposed to various concentrations of hydrogen peroxide, then the culture medium was refreshed to remove the hydrogen peroxide and the cells recovered under DD or LD conditions. Cell viability was then assayed using MTT assays. Percentage of mean \pm SEM (n=8) in cell viability with respect to untreated cells are showed on the y-axes, while hydrogen peroxide concentrations (from 200 μM to 3000 μM) are shown on the x-axes. This experiment was repeated independently 3 times. Cell viability was compared between LD and DD groups of multiple cell lines by using Two-way ANOVA followed by Sidak's multiple comparisons tests and statistical differences of $p > 0.05$, $p < 0.05$, $p < 0.01$, $p < 0.001$ are represented by ns, *, ** or ***, respectively.

I next investigated whether light has any impact on the survival of mammalian cells ectopically expressing CPD photolyase following exposure to hydrogen peroxide. Therefore, I grew 3T3 CPD cells together with non-transfected 3T3 cells in 96-well plates. After treatment with a range of H_2O_2 concentrations, the cells recovered under either DD or LD conditions following removal of the H_2O_2 by replacement with fresh medium. I tested cell viability as described previously using an MTT assay. For all the

cell lines I tested, light had no significant effect on the levels of ROS-induced mortality (Figure 3.12 C-D).

I also performed our automated high throughput microscopy assay to measure the effects of light upon cell viability in 3T3 and 3T3 CPD cells following H₂O₂ treatment. Cells were exposed to lower concentrations of H₂O₂ compared with the MTT assay and allowed to recover in DD or LD conditions for 1 day. My results revealed that cell survival decreases in a H₂O₂ dose-dependent fashion but that light has no significant effect on survival following oxidative stress in 3T3 or 3T3 CPD cells (Figure 3.13 and 3.14). Therefore, these AHM-derived findings are consistent with my MTT assay results and point to the conclusion that light has no apparent protective effect on the survival of cells exposed to oxidative stress.

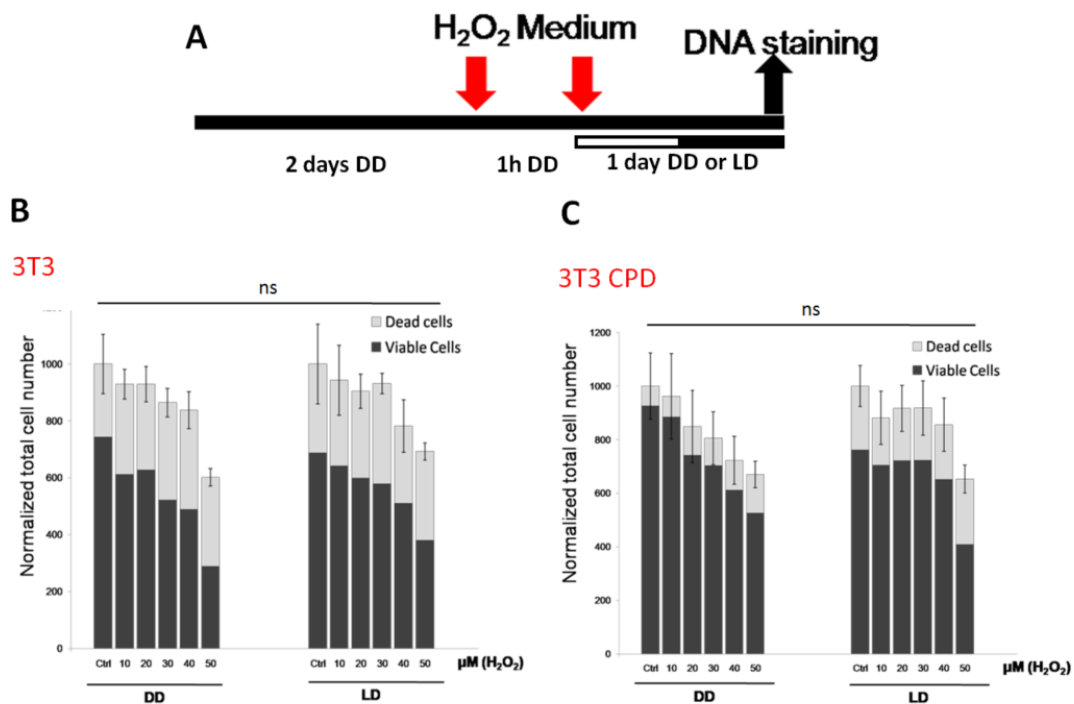


Figure 3.13 Light has no effect on cell viability following oxidative stress in 3T3 cells and 3T3 cells ectopically expressing CPD photolyase. (A) Schematic representation of experimental design. (B) 3T3 cells and 3T3 CPD cells were exposed to various concentrations of hydrogen peroxide, and then allowed to recover by refreshing the medium and subsequently incubation in constant darkness or a light-dark cycle. Mean of the total cell number \pm SEM (n=8) in relation to untreated cells are indicated on the y-axes, while hydrogen peroxide concentrations (from 10 μ M to 50 μ M) are denoted on the x-axis. This experiment was repeated independently at least 3 times. Cell survival was compared between DD and LD groups of each cell line by using Two-

way ANOVA followed by Sidak's multiple comparisons tests and statistical differences of $p > 0.05$, $p < 0.05$, $p < 0.01$, $p < 0.001$ are represented by ns, *, ** or ***, respectively.

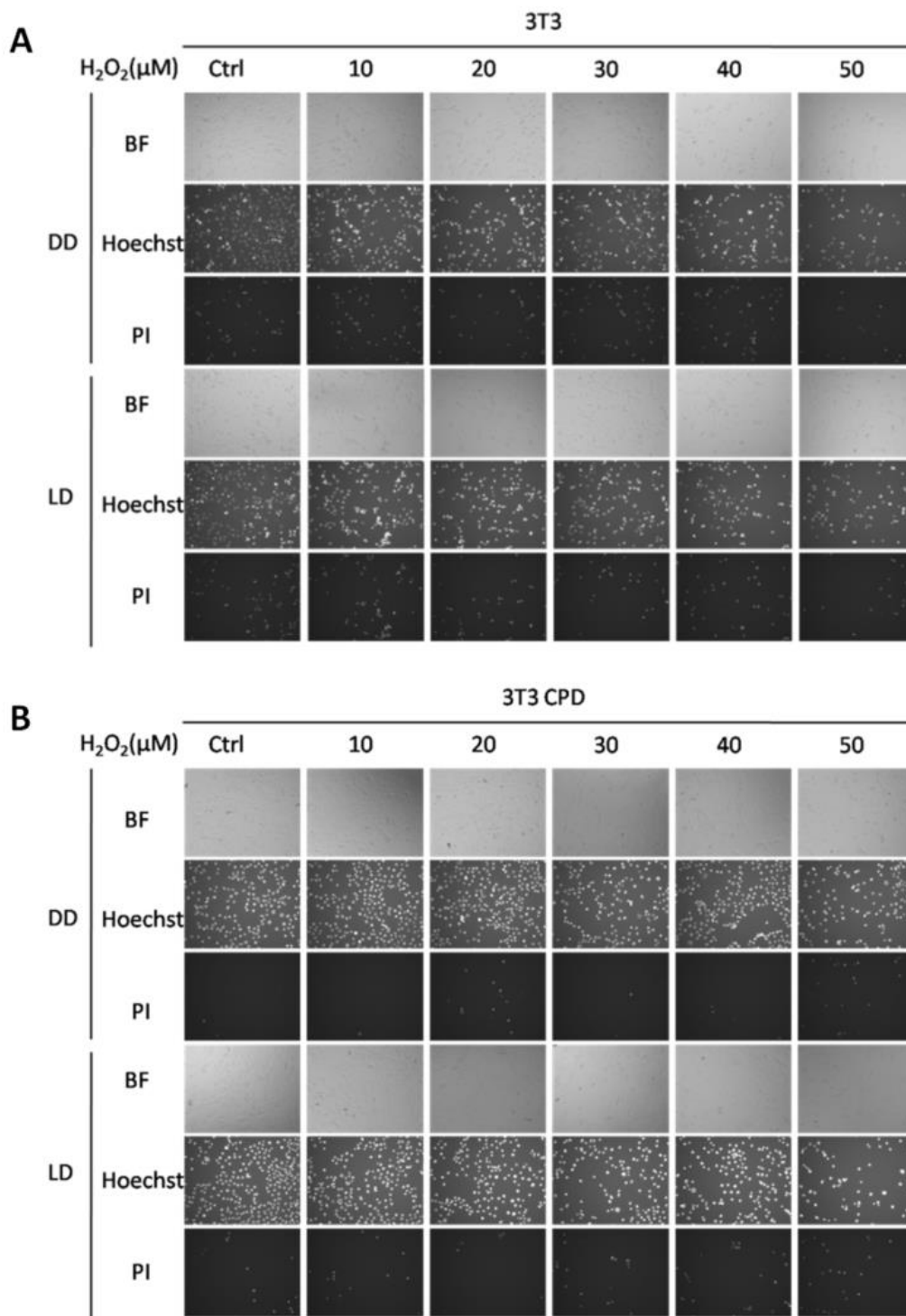


Figure 3.14 Representative images from automated high-throughput microscopy (AHM) assay following exposure of 3T3 and 3T3 CPD cell lines to different concentrations of hydrogen peroxide and then recovery under constant darkness or light-dark cycle. Bright field (BF) channel, Hoechst staining, and Propidium Iodide (PI) staining are represented.

My results reported so far point to CPD photolyase playing a role in DNA damage repair that is induced following oxidative stress. Consequently, loss of CPD photolyase function is associated with increased levels of DNA damage following ROS exposure as visualized by phosphorylated H2A.X assay. Consistently, CPD Photolyase seems to play a role of enhancing survival following exposure to oxidative stress, as shown by MTT assays and AHM assays. Therefore, loss of CPD photolyase function results in elevated levels of cell mortality following oxidative stress while gain of CPD photolyase function reduces cell mortality upon oxidative stress. Importantly, in contrast to the role played by CPD photolyase in the repair of UV damaged DNA in photoreactivation, these functions of CPD photolyase are independent of visible light. These results are difficult to rationalize within the context of the classical view of CPD photolyase serving as a light-dependent enzyme catalyzing the repair of UV damaged DNA. Interestingly, it has been reported that photolyases can bind to sites of DNA damage and thereby recruit other DNA repair pathways elements to target DNA repair capacity. Interestingly, the latter system does not require light but the underlying repair mechanism remains completely unclear⁶.

Consequently, regarding my observations linking CPD photolyase with oxidative stress responses, I propose 2 alternative hypotheses to explain these results.

1) It has been reported that CPD photoproducts can be formed hours after UV exposure⁷⁸, in complete darkness and so have been termed “dark CPD” (see section 1.2.9). Since UV exposure also can induce ROS production, this implicates ROS itself in CPD formation in the absence of light. Furthermore, I hypothesize that ROS might reduce the CPD photolyase FAD domain to a reduced state which in the absence of light might enable the normal catalytic function of this enzyme. Thereby, the activated CPD photolyase would bind to the dark CPD damage sites and repair them.

2) ROS exposure gives rise to several types of oxidative DNA damage, a notable example being 8-OHdG. Previous studies have revealed that prokaryotic photolyase proteins have the capacity to bind to DNA damage sites. Hence, CPD photolyase may be able to recognize and bind to this non-CPD DNA damage, thereby acting as a tag to

recruit other factors of other DNA repair systems, such as NER or BER pathway proteins, to repair these types of damage.

Both hypotheses would account for why CPD photolyase has been highly conserved in the Somalian cavefish despite experiencing a complete lack of sunlight for millions of years.

In order to test these alternative hypotheses, I have focused on exploring the types and dynamics of DNA damage formation associated with CPD photolyase function as well as the mechanism of CPD photolyase action in the absence of light.

3.4 Kinetics of DNA damage and repair

Inhabiting the dark cave environment can result in the production of multiple types of DNA damage, such as dark CPD and 8-oxoG, both potentially connected with elevated levels of ROS. Hence, I explored the dynamics of oxidative DNA damage formation and repair in the context of CPD photolyase function in constant dark conditions.

3.4.1 Kinetics of UV-induced DNA damage and repair

As a control for the efficiency of our ELISA kit to assay the production and repair of CPD photoproducts, I initially performed control experiments using UV radiation to induce DNA damage in these fish cell lines. Specifically, I tested the kinetics of UV-induced DNA damage and repair in zebrafish and medaka cell lines using an ELISA assay to quantify UV-induced CPD photoproduct production in genomic DNA extracts. It has been demonstrated that CPD photoproducts can be produced in picoseconds following UV exposure, thus the content of CPD photoproducts can be used to quantify DNA damage caused by UV-C light and the kinetics of photoreactivation. Specifically, I exposed zebrafish and medaka WT and CPD photolyase mutant medaka cell lines to 20 J/m² UV-C light and then transferred them to darkness or blue light for recovery and extracted genomic DNA at different timepoints. In addition, I pre-illuminated the blue light exposure samples of the WT and CPD mutant medaka cell lines, with blue

light for 12 hours before UV-C exposure in order to accumulate sufficient photolyase for photoreactivation. The timepoints I chose were Control (untreated sample), 0h, which denotes the timing for sampling immediately after the completion of UV-C exposure and 3h, 9h, 12h, which represent increasing recovery times following UV-C exposure. My results demonstrate that in zebrafish and medaka cells, compared with DD conditions, the cells recovered under blue light have substantially decreased CPD photoproduct remaining after UV-C light exposure. In contrast, and consistent with the enabling role of CPD photolyase in the photoreactivation process, blue light had no significant effect on the levels of CPD in medaka CPD mutant cells (Figure 3.15).

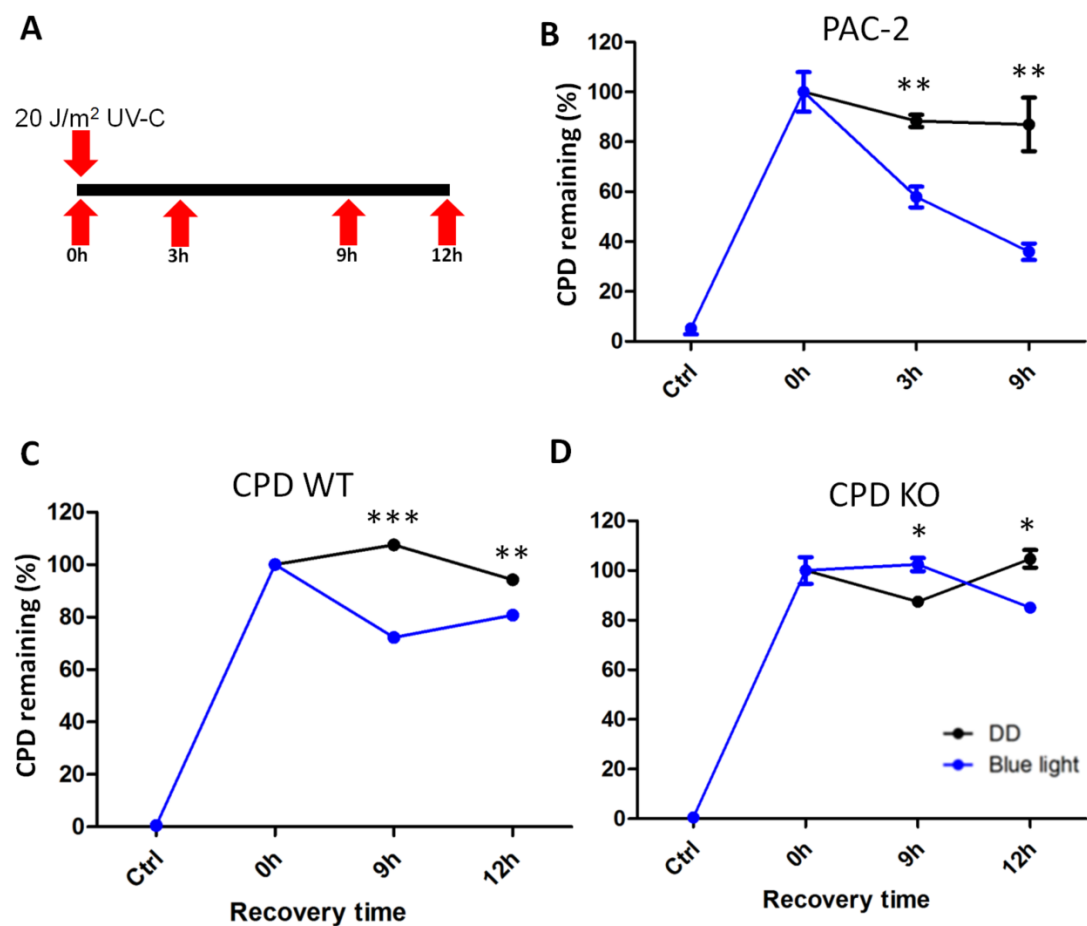


Figure 3.15 Visible light confers photoreactivation in zebrafish and medaka cell lines, but not in medaka CPD photolyase mutants upon UV-C light exposure. (A) Schematic representation of experimental design. (B-D) Wild type zebrafish (PAC-2) and medaka (CPD WT) cell lines as well as CPD photolyase mutant (CPD KO) cell lines were exposed to 20 J/m² UV-C light and then transferred to constant darkness or blue light conditions. Specifically, for blue light exposure of the medaka wild type (WT) and CPD mutant (KO) cell lines, they were pre-illuminated with blue light for 12 hours before UV-C exposure

to accumulate sufficient photolyase for photoreactivation. The percentage of CPD photoproduct remaining calculated from the mean values \pm SEM (n=3) is plotted on the y-axis against recovery time on the x-axis. This assay was repeated independently 3 times. The quantity of CPD photoproduct remaining was compared between DD and blue light exposure groups of each cell line at identical recovery timepoints by using Student's t-test (unpaired, two tailed) and statistical differences of $p > 0.05$, $p < 0.05$, $p < 0.01$, $p < 0.001$ are represented by ns, *, ** or ***, respectively.

3.4.2 Kinetics of ROS-induced DNA damage and repair

Can ROS exposure induce CPD photoproduct production in the CPD photolyase mutant medaka cell line under constant darkness and subsequently, what is the effect of exposure to blue light or constant darkness on levels of this ROS-induced CPD? To address these questions, I used the ELISA CPD assay to quantify the CPD photoproduct induced by ROS. Previous work from the Foulkes lab (Cristina Pagano's PhD thesis) revealed that when zebrafish PAC-2 cells were exposed to white light for 2 hours, there was a clear increase in ROS levels. In addition, in melanocytes, CPDs continue to be produced after UV exposure, reaching a peak at 3h post UV exposure, and then levels decrease to basal levels at 5h after UV exposure, probably the result of DNA repair⁷⁸. Hence, I chose the sampling timepoints of this ELISA assay as Ctrl, Te 3h (H₂O₂ treatment for 3 hours), Re 3h Re 6h and Re 9h (3, 6 and 9 hours recovery with fresh medium respectively).

Specifically, I seeded wild type medaka and CPD mutant cell lines in a 6-well plate and grew them to confluence under darkness. Following treatment with 1mM H₂O₂ for 3 hours, I replaced the medium with fresh medium and then maintained the cells either in constant darkness or illuminated using blue light, with sampling at various timepoints for the extraction of genomic DNA. In addition, before incubation with 1mM hydrogen peroxide, the cells that would ultimately be exposed to blue light, I pre-illuminated with blue light for 12 hours to accumulate sufficient photolyase protein.

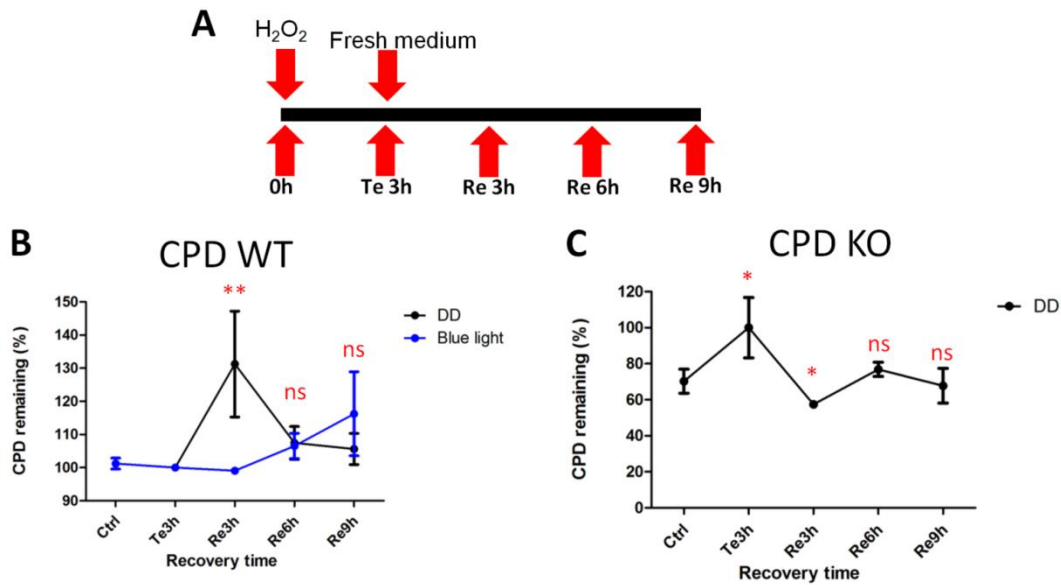


Figure 3.16 CPD production following H₂O₂ treatment in medaka WT and CPD photolyase mutant cell lines. (A) Schematic representation of experimental design. (B-C) Wild type medaka (CPD WT) and CPD photolyase mutant cell lines (CPD KO) were exposed to 1mM hydrogen peroxide and then recovered under constant darkness (DD) or blue light illumination (Blue light). The cells that were exposed to blue light were pre-illuminated with blue light for 12 hours before hydrogen peroxide treatment to ensure the expression of sufficient photolyase protein. The percentage of CPD photoproduct remaining calculated from the mean values \pm SEM (n=3) is plotted on the y-axes against recovery time on the x-axes. This assay was repeated independently 3 times. The CPD photoproduct remaining was compared between the DD and Blue light groups of the CPD WT cell line at identical recovery timepoints by using Student's t-test (unpaired, two tailed), while the amount of remaining CPD photoproduct was compared between Control and various recovery timepoints by using Student's t-test (unpaired, two tailed) as well. Statistical differences of $p > 0.05$, $p < 0.05$, $p < 0.01$, $p < 0.001$ are represented by ns, *, ** or ***, respectively.

My ELISA assay results imply that after treating with H₂O₂ for 3 hours, CPD content does increase significantly, suggesting that despite a complete lack of UV exposure, ROS exposure is able to induce CPD photoproduct production, although clearly at significantly lower levels than are observed following UV exposure. Consistent with the expression of light-inducible CPD photolyase activity in the wild type medaka cells, exposure to blue light following the treatment with hydrogen peroxide results in no increase in CPD levels, presumably the result of photoreactivation DNA repair in these cells efficiently removing the ROS-induced CPD (Figure 3.16). Interestingly, the peak of

CPD levels observed in the constant dark wild type medaka cells is not observed immediately at the end of the hydrogen peroxide incubation step, but actually appears later, at a time point 3 hours after the hydrogen peroxide has been removed from the culture medium. These results potentially reveal complexity in the biochemical mechanism that generates CPD in the absence of UV exposure. A significant increase in CPD levels is also observed in the CPD photolyase mutant cells, although the amplitude of this increase is lower than for the wild type cells. In the context of the absence of functional CPD photolyase in these cells, this is an unexpected result. Furthermore, the peak of CPD levels occurs immediately after hydrogen peroxide treatment in this mutant cell line.

3.4.3 ROS-induced 8-OHdG DNA damage and repair

Besides CPD photoproducts, ROS exposure can also elicit other types of oxidative DNA damage, one example is the formation of 8-hydroxydeoxy-guanosine (8-OHdG), a commonly used marker of oxidative stress. I employed an ELISA assay to quantify 8-OHdG levels in genomic DNA extracts of hydrogen peroxide-treated cells. Specifically, I seeded wild type and CPD mutant medaka cells on 10 cm petri dishes in darkness for 2 days, then treated with 1mM hydrogen peroxide for 3 hours, the medium was exchanged for fresh medium and finally I harvested the cells and extracted genomic DNA at various timepoints to perform an ELISA assay. The timepoints I chose were 0h, which represents the time immediately before the 1mM hydrogen peroxide was added to the cells, 3 hours after the onset of hydrogen peroxide treatment and then 3 hours, 6 hours and 12 hours after adding fresh medium for recovery. My results demonstrate that loss of CPD photolyase function cells have higher basal and induced 8-OHdG levels (Figure 3.17).

Therefore, in summary it appears that the loss of CPD (but not 6-4 or DASH) photolyase results in an increase of ROS-induced DNA damage and reduced cell survival following oxidative stress.

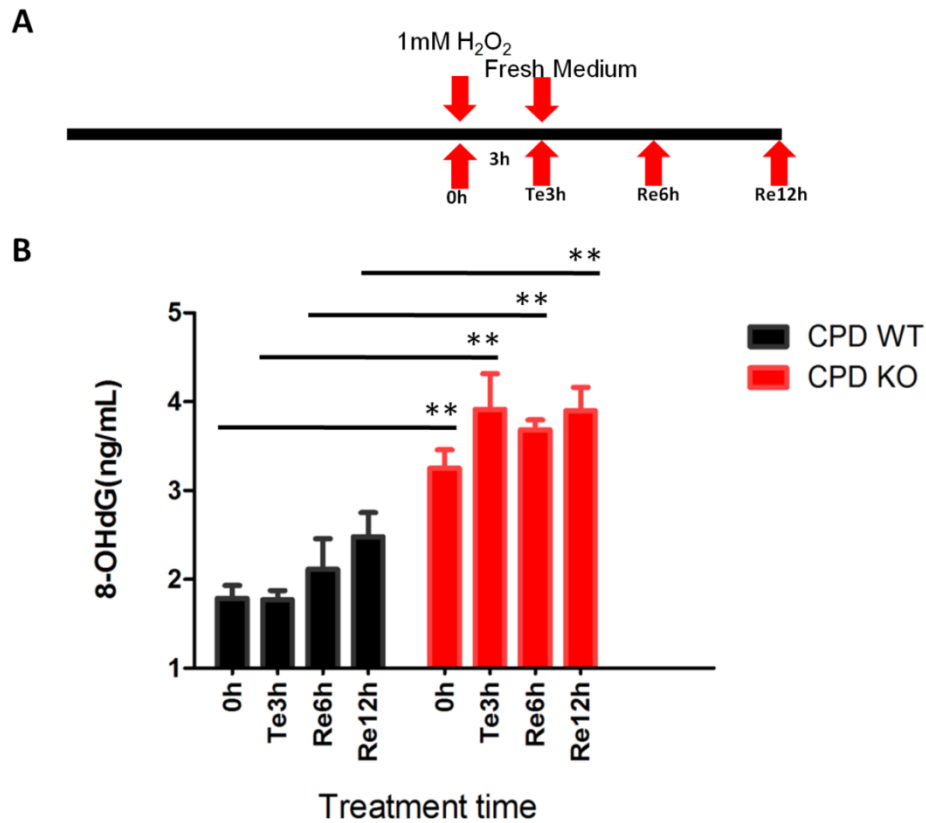


Figure 3.17 8-OHdG accumulation following H₂O₂ treatment in medaka WT and CPD photolyase mutant cells. (A) Schematic representation of experimental design. (B) Medaka WT and CPD photolyase mutant cell lines were exposed to 1mM hydrogen peroxide and then left to recover under constant darkness. The content of 8-OHdG calculated as mean \pm SEM (n=3) is plotted on the y-axis against recovery time on the x-axis. This assay was repeated independently 3 times. 8-OHdG content was compared between WT and CPD KO groups at identical recovery timepoints by using Student's t-test (unpaired, two tailed) and statistical differences of $p > 0.05$, $p < 0.05$, $p < 0.01$, $p < 0.001$ are represented by ns, *, **, or ***, respectively.

3.5 Gain of function with CPD photolyase mutants

I next chose to investigate the role of the CPD photolyase photoreactivation enzymatic mechanism in ROS-induced DNA damage repair. There is a considerable amount of knowledge about the mechanism whereby photolyases catalyse photoreactivation DNA repair. Does the same mechanism contribute to how CPD photolyase enhances DNA repair and survival during oxidative stress under complete darkness? To address this question, I generated mutations in the zebrafish CPD photolyase by site-directed mutagenesis to inactivate photoreactivation. Specifically, I substituted 2 of the key Tryptophan residues of the Three Tryptophan Electron Transfer Chain involved in harvesting photons from sunlight and then transferring an electron from the protein surface to the FAD domain, which plays a crucial role in photorepair. The 2 Tryptophan residues were substituted for Phenylalanines, one at a position proximal to the FAD binding site (W310F) and the other one on the surface of CPD photolyase protein (W400F) as indicated on Figure 3.18.

> Zebrafish CPD photolyase

```
1   MSANKNNLKR QMKSTISAGG KQPKLTGEKG KESGWLLKEV
41  AELRRAAQGC EFNKKRLRYL SDTQKVKQSS QGVLYWMSRD
81  QRIQDNWALI YSQQLALAEK LPLHICFCLV PKFLDATYRQ
121 YAFMLKGLQE VVKECKSLDI EFHLLSGEPV HNLPAFVKSW
161 NIGAVVTDFN PLRISLQWID TVKKHLPSDI PFIQVDAHNV
201 VPCWEASTKL EYGARTIRGK ITKHLQEFLT DMPLVDTHPY
241 CASRAAKIID WEEVLSSLEV DHNVCEVEWA QPGTTGGMFM
281 LESFIDQRLH IFATHRNNPN SDAVSHLSEW IHAGQLSAQR
321 VVMQVKRKKK ASESVASFIE EIVVRRELAD NFCFYNQNYD
361 NISGAYDWAK KTLQEHAADR RQYLYTKKEL ESAETHDQIW
401 NAAQRQLLE  GKMHGFLRMY WAKKILEWTA SPEEALSI AI
441 YLNDRLSLDG CDPNGYVGCM WSICGIHDQG WAERPFI FGKI
481 RYMNYAGCKR KFDVEQFERK YAAIKKNPNL NAKISV
```

Figure 3.18 Zebrafish CPD photolyase protein sequence. The red rectangles indicate the Tryptophan amino acids that were mutated by site-directed mutagenesis for investigating the underlying molecular mechanism of "dark" DNA repair functionality of CPD photolyase.

3.5.1 Construction of mammalian cell lines expressing CPD

photolyase mutants

Again profiting from the lack of photoreactivation repair in mammalian cell lines, I generated stable 3T3 cell lines (mouse cells) ectopically expressing zebrafish CPD photolyase carrying the W310 or W400 mutations. I performed mutagenesis using the Q5 Site-Directed Mutagenesis Kit (New England Biolabs). Next, I seeded 3T3 cells on a 6-well plate as previously described, and the following day co-transfected with a pcDNA-based expression vector for zebrafish CPD photolyase containing the W310 or W400 mutation as well as an empty pcDNA vector carrying a neomycin resistance cassette. After 2 days incubation, I replaced the medium with fresh medium that included neomycin to select for cells that had been successfully transfected. Afterwards, I seeded single surviving cells in individual wells of a 96-well plate. After expanding the single clones, I tested ectopic photolyase expression in each clone by western blotting using an anti-myc antibody to detect the epitope-tagged zebrafish protein (Figure 3.19 A).

3.5.2 Validating loss of photoreactivation of UV-damaged DNA

Initially, as a control, I validated that the Tryptophan mutants had lost photoreactivation function following exposure to UV light by using a cell viability assay. Specifically, I exposed cells to a range of UV-C pulses and then allowed them to recover under either DD or LD conditions for 2 days. In contrast to my previous results obtained with 3T3 CPD cells which express the wild type CPD photolyase protein (Figure 3.6), my two 3T3 CPD mutants did not exhibit an increase in cell survival when recovering under LD conditions, which is consistent with the loss of the three Tryptophan Electron Transfer Chain in CPD photolyase, resulting in the absence of photoreactivation (Figure 3.19 C-E).

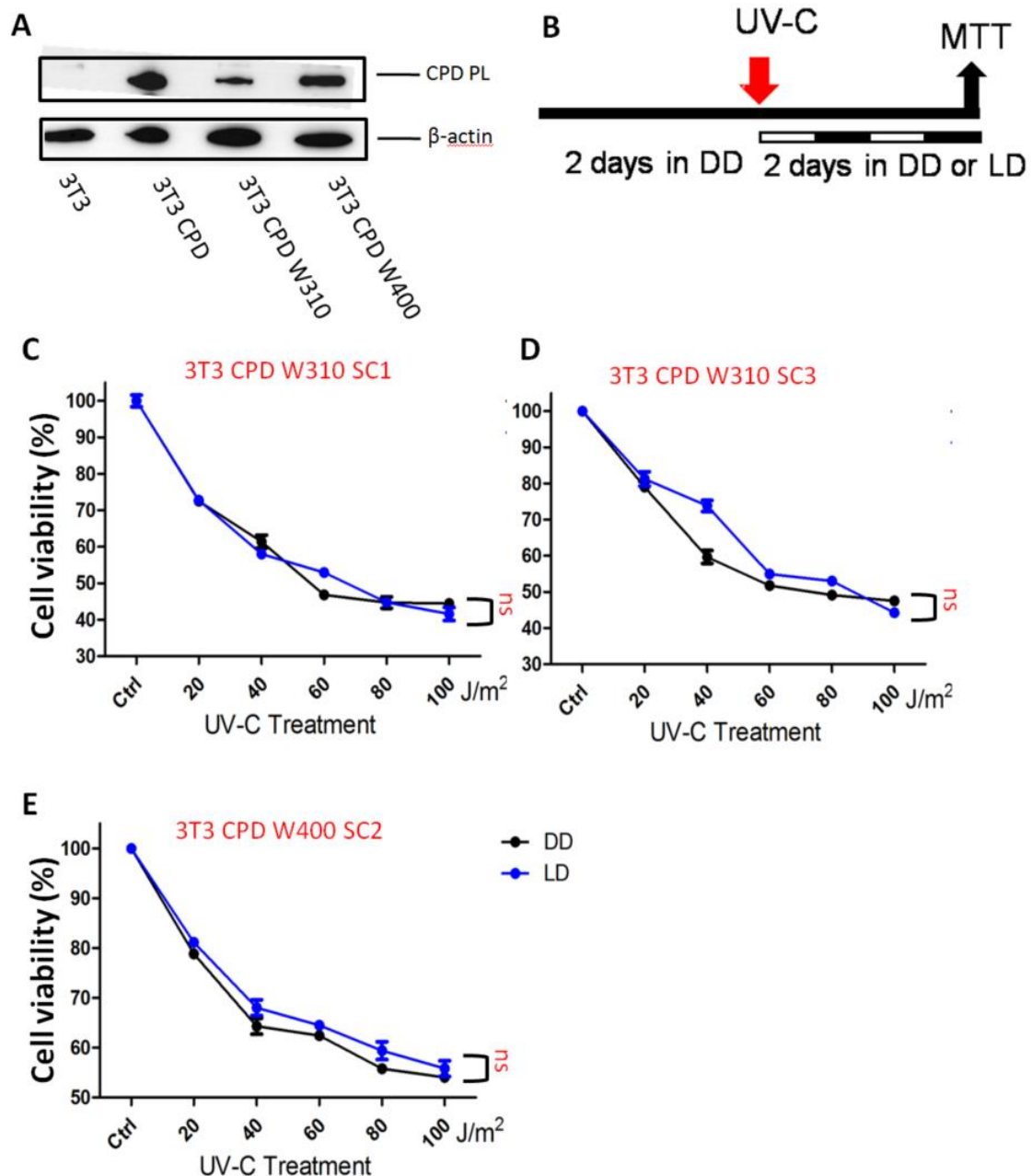


Figure 3.19 Establishing 3T3 stable clones expressing mutated versions of zebrafish CPD photolyase. (A) Expression of myc eptope-tagged, wild type (3T3 CPD) and mutant (3T3 CPD W310 and 3T3 CPD W400) zebrafish CPD photolyase protein detected by Western Blot assay. The zebrafish CPD photolyase gene was mutated by site-directed mutagenesis in the context of a pcDNA-based expression vector and then stably transfected into mammalian cells. Non-transfected 3T3 cell extracts (3T3) were analysed as a negative control and zebrafish β -actin was detected as a loading control. (B) Schematic representation of experimental design for the cell viability assays represented in panels C-E. (C-E) MTT cell viability assay of the 3T3 cell lines exposed to a range of UV-C light levels and then transferred to constant darkness (DD) or light-dark cycles (LD). Percentage calculated from means \pm SEM (n=8) in cell viability with respect to untreated cells is indicated on the y-axes, while UV-C light doses (from 20

J/m² to 100J/m²) are indicated on the x-axes. Each cell line was analysed independently at least 3 times. Cell viability was compared between DD and LD groups by using Two-way ANOVA followed by Sidak's multiple comparisons tests and statistical differences of $p > 0.05$, $p < 0.05$, $p < 0.01$, $p < 0.001$ are represented by ns, *, ** or ***, respectively.

3.5.3 Cell viability response to oxidative stress

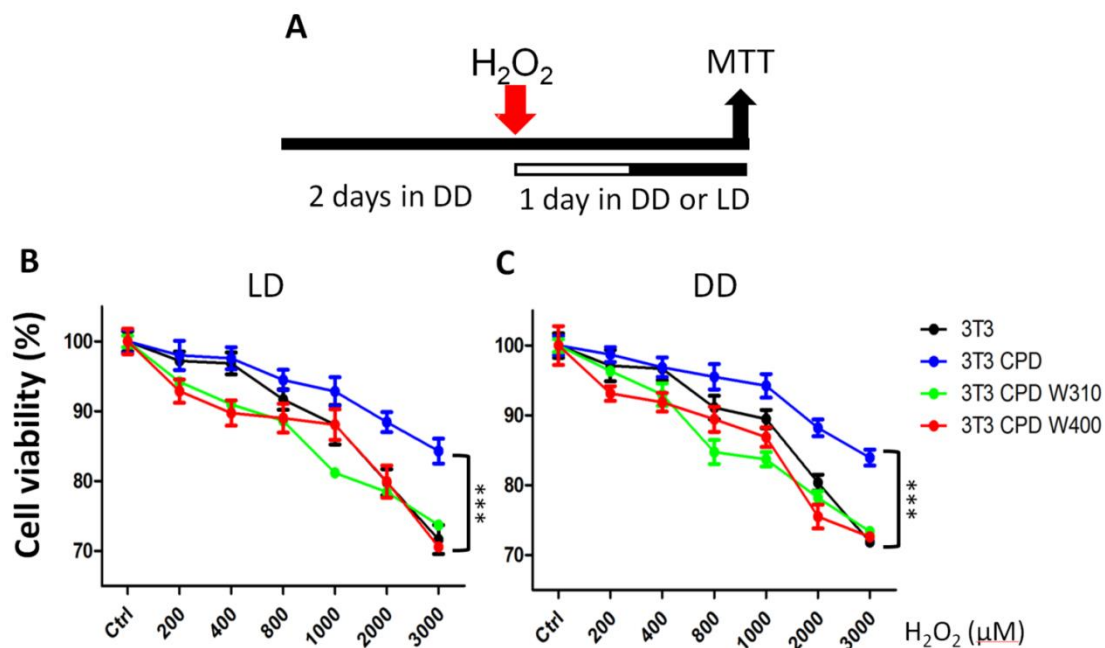


Figure 3.20 Loss of Three Tryptophan Electron Transfer Chain in CPD photolyase results in loss of protection against ROS-induced mortality in mammalian cells. (A) Schematic representation of experimental design for the analysis shown in panels B-C. (B) The various 3T3 cell clones (see Figure 3.19) were exposed to a range of hydrogen peroxide concentrations, allowed to recover with fresh medium and then transferred to darkness (DD) or light dark cycle conditions (LD) before performing a MTT cell viability assay. Percentage calculated from the mean \pm SEM (n=8) in cell viability with respect to untreated cells are indicated on the y-axes, while hydrogen peroxide concentrations (from 200 μ M to 3000 μ M) are indicated on the x-axes. This experiment was repeated independently 3 times. Cell viability was compared between 3T3 CPD and 3T3 CPD mutant groups by using Two-way ANOVA followed by Sidak's multiple comparisons tests and statistical differences of $p < 0.05$, $p < 0.01$, $p < 0.001$ are represented by *, ** or ***, respectively.

I next investigated whether ectopic expression of the Tryptophan mutant CPD photolyases influenced the survival of mammalian cells upon exposure to oxidative stress compared with cells expressing wild type CPD photolyase. Furthermore, I also wished to test whether light exposure influenced survival of the various 3T3 cell clones. I exposed the 3T3 cell lines to various doses of H₂O₂ and then allowed them to recover with fresh medium under DD or LD conditions for 1 day before performing an MTT cell viability assay. My results revealed that, compared with 3T3 CPD cells, the CPD mutants showed reduced viability under both DD and LD conditions, indicating that loss of the Three Tryptophan Electron Transfer Chain function in CPD photolyase results in reduced protection against ROS-induced cell mortality (Figure 3.20).

To confirm these MTT assay results, I next tested the effects of hydrogen peroxide exposure on cell viability using the AHM automated microscopy assay. I again exposed the 3T3, 3T3 CPD WT and 3T3 CPD mutant cell lines to a range of hydrogen peroxide concentrations and then refreshed the medium and transferred the cells to constant darkness for 1 day. Following staining with Hoechst and PI, I assessed cell viability by automated microscopy. Cells were scanned and imaged using an automated Olympus IX81 fluorescence microscope. Consistent with my previous results and compared with 3T3 cells, 3T3 CPD cells displayed increased cell survival following oxidative stress (Figure 3.21 and 3.22). However, contrary to the results of the previous MTT cell viability assay, my results with the 3T3 CPD mutant clones revealed that compared with 3T3 CPD cells, both CPD mutant cell lines did not exhibit a significant reduction in cell survival upon oxidative stress. However, the lower concentrations of hydrogen peroxide used in the AHM assay may explain this discrepancy, since under similar conditions in the MTT assay, there were no significant differences in cell survival between the 3T3 CPD and 3T3 CPD mutant clones.

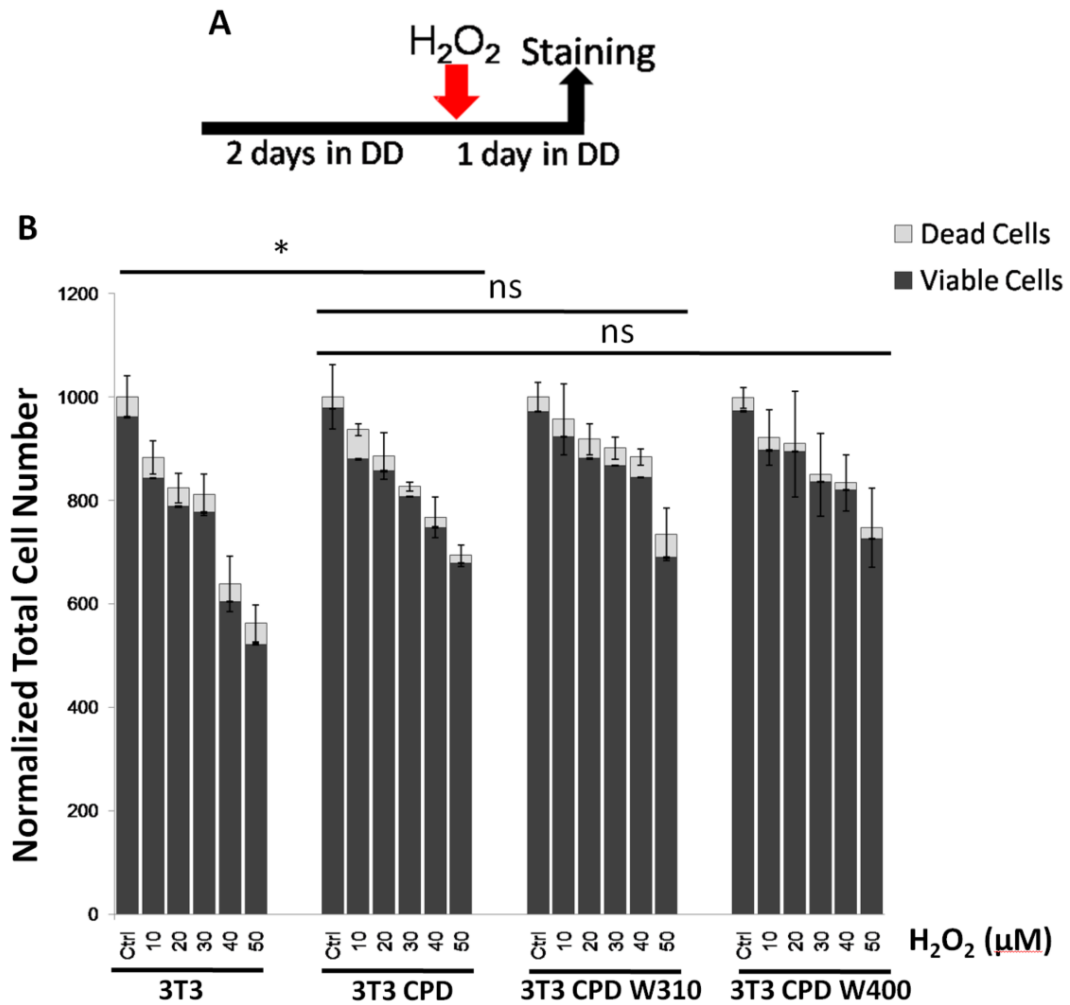


Figure 3.21 Effects of loss of the Three Tryptophan Electron Transfer Chain in CPD photolyase on cell viability using AHM assay. (A) Schematic representation of experimental design for the experiments shown in panel B. (B) The various 3T3 cell clones (see Figure 3.19) were exposed to lower concentrations of hydrogen peroxide than those used in Figure 3.20, and then the culture medium was refreshed and the cells were transferred to constant darkness before staining and automated microscopy analysis. Total cell number calculated as mean \pm SEM (n=8) in relation to untreated cells are indicated on the y-axes, while hydrogen peroxide concentrations (from 10 μ M to 50 μ M) are showed on the x-axis. Viable cell number was compared between 3T3 CPD and 3T3 CPD mutant groups by using Two-way ANOVA followed by Sidak's multiple comparisons tests and statistical differences of $p > 0.05$, $p < 0.05$, $p < 0.01$, $p < 0.001$ are represented by ns, *, **, or ***, respectively.

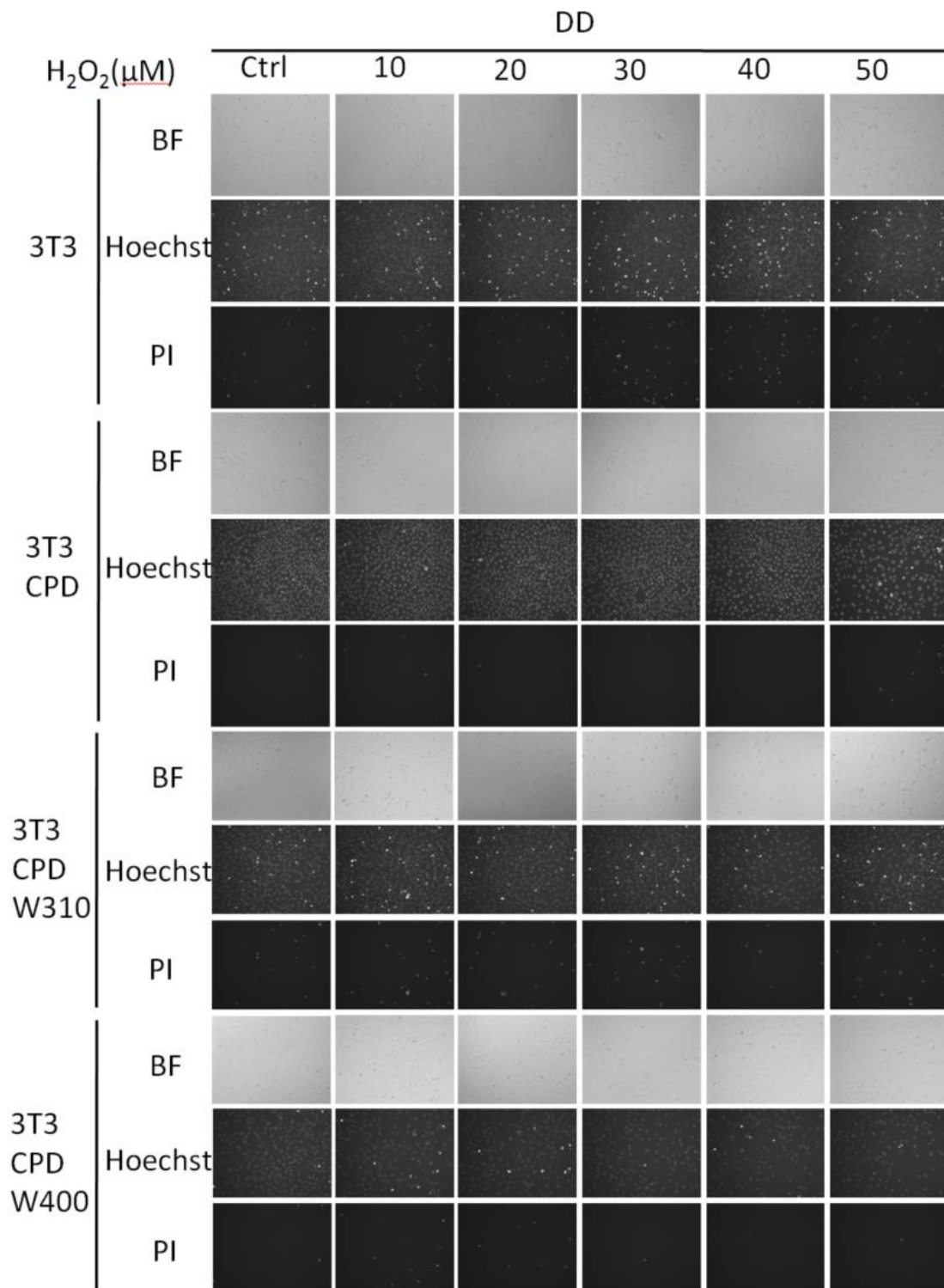


Figure 3.22 Representative images from automated high-throughput microscopy (AHM) assay following exposure of 3T3 and 3T3 CPD and 3T3 CPD mutant cell lines to various concentrations of hydrogen peroxide and then recovery under constant darkness. Bright field (BF) channel, Hoechst staining, and Propidium Iodide (PI) staining are represented.

3.6 Circadian clock gene expression upon loss of photolyase function

The cryptochrome/photolyase superfamily constitutes a group of highly conserved, homologous proteins involved in DNA repair as well as circadian clock-related functions. Cryptochromes represent circadian clock components while classically, the photolyases are dedicated to DNA repair. However, all share a FAD chromophore which is central for the harvesting of blue light and both the DNA photolyase domain and the FAD binding domain are quite conserved in cryptochromes and are essential for photolyase function. This raises a potentially important question concerning potential overlap between the functions of cryptochromes and photolyases and more specifically, can photolyases also contribute to circadian clock function? Previous published results have reported that marsupial CPD photolyase can rescue loss of CRY function and that rhythmically expressed *Potorous* CPD photolyase can functionally substitute for CRY proteins in the mammalian circadian oscillator. Might this functionality be restricted to marsupial photolyase or could it reflect a more general photolyase property? To address this question, I chose to explore whether there was any evidence for abnormalities of clock function in the loss-of-function medaka cell lines.

3.6.1 Circadian clock gene expression in loss of photolyase function cell lines.

To identify whether photolyase may act as a circadian clock component by regulating circadian clock gene expression, I examined rhythmic clock gene expression in the CRISPR-Cas9 generated KO medaka cell lines. I placed all three photolyase mutant cells (6-4, CPD and DASH photolyase) together with the corresponding wild type control lines under LD conditions for 4 days to entrain their circadian clock function and then extracted RNA at different timepoints through a complete light dark cycle and the start

of the subsequent cycle and reverse transcribed this into cDNA. Afterwards, I performed qPCR to quantify the expression levels of a set of representative circadian clock genes. I employed medaka mitochondrial ribosomal protein S18B as an internal control for normalization.

In both CPD and DASH photolyase mutant cells, robust rhythms in the expression of 5 clock genes were detected which closely matched the expression patterns observed in the wild type controls. *per2*, *cry1a* and *cry5* are predominantly light-driven clock genes, with their transcription being activated by light exposure via the effects of D-box enhancer elements. Consequently, highest levels of expression are observed during the light period. Similarly, *per1b* and *per3* expression also peaks early during the light period, however both genes are clock regulated via E-box enhancer promoter elements. My results from the loss of photolyase function mutants indicate that CPD and DASH photolyase function is dispensable for normal clock function under LD cycles (Figure 3.23).

I also analysed expression of these same 5 clock genes in 6-4 WT and mutant cells. While a rhythmic expression pattern of the two cry genes (*cry1a* and *cry5*) was observed in both wild type and mutant cell lines, there was a notable disruption of rhythmic expression for the per clock genes (*per1b*, *per2* and *per3*). While in 6-4 WT cells, the *per* genes showed a normal clock or light-driven expression pattern, in the mutant cells, basal expression levels were relatively low and the only shallow rhythms of expression were visible. These qPCR results demonstrate that the loss of 6-4 photolyase function in the medaka cell line disrupts clock- and potentially light-regulated *per* clock gene expression in cell lines (Figure 3.23).

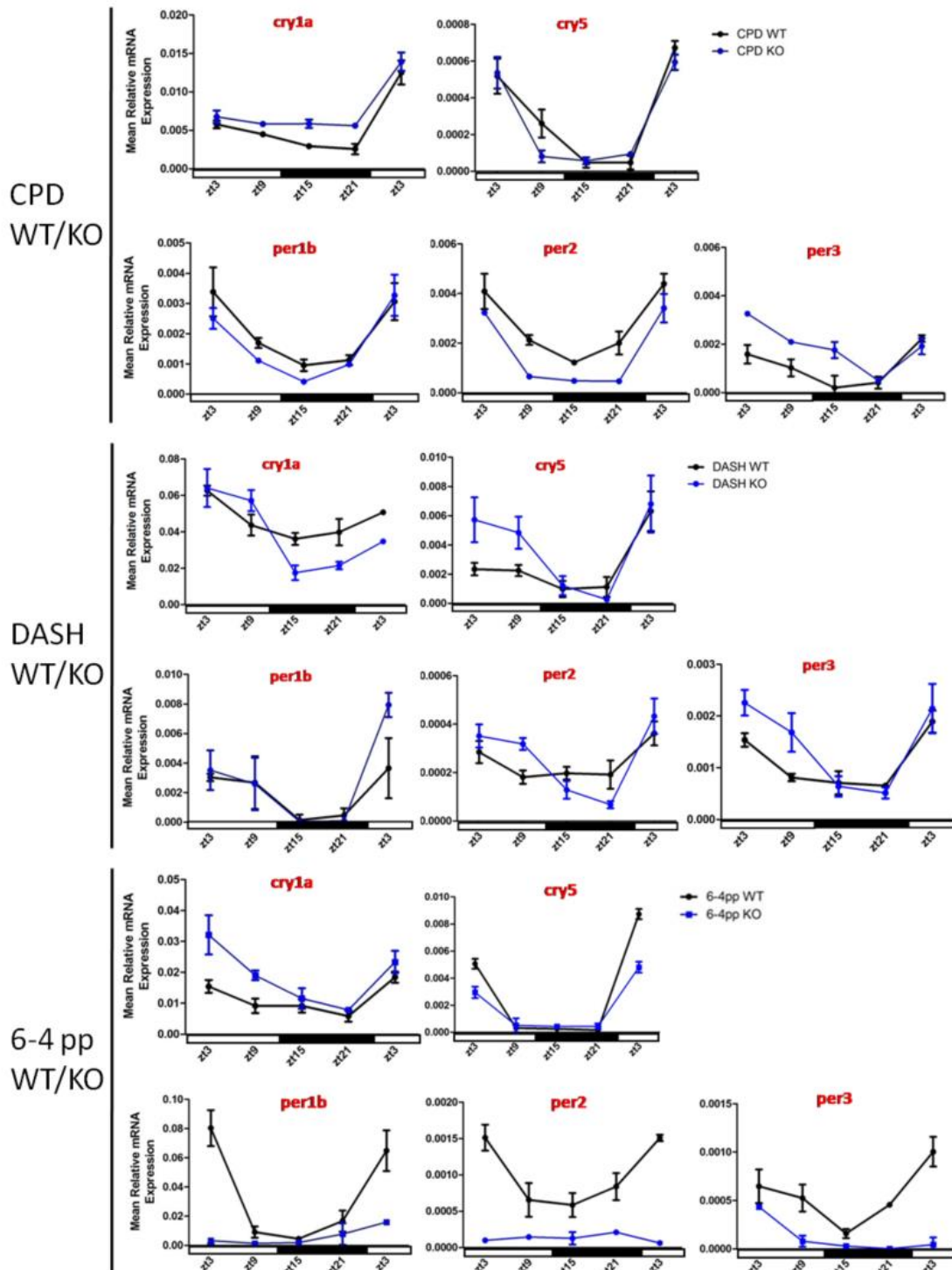


Figure 3.23 Light-driven and clock-regulated clock gene expression in medaka wild type and mutant cell lines. Medaka WT and photolyase mutant cell lines were incubated under LD conditions (12 hours light and 12 hours dark) for 4 days to entrain their circadian clocks and then sampled at regular timepoints through a complete light-dark cycle. The mRNA expression levels of light-driven genes *cry1a*, *cry5* and *per2* as well as the clock-regulated genes *per1b*, and *per3* were analysed by qPCR. Relative mRNA expression calculated as mean \pm SEM (n=3) is plotted on the y-axes, while Zeitgeber (zt) sampling time is plotted on the x-axes. The analysis of each clock gene

in each cell line was repeated independently at least 3 times. White and black bars below each panel indicate the light and dark periods, respectively.

3.6.2 Circadian clock gene expression in loss of photolyase function mutant fish.

I next wished to determine whether these cell line results were representative of clock gene expression patterns in various tissues *in vivo*. I therefore raised medaka in breeding tanks in the IBCS-BIP fish facility where they were exposed to LD conditions (14 hours light and 10 hours dark) for several months. I then sacrificed adult fish at regular time points through a complete light dark cycle and the start of the subsequent cycle and then dissected eye, brain, heart, liver, muscle, skin and fins for RNA extraction and qPCR analysis. The same set of clock genes that was analyzed in the cell lines, I then studied in the various tissue extracts. I used medaka mitochondrial ribosomal protein S18B was used as an internal control to normalize expression levels.

Interestingly, my results revealed tissue and gene-specific differences in rhythmic clock gene expression between the wild type and 6-4 mutant fish. For example, in the case of the eye and brain, *cry1a* showed a lower amplitude of rhythmic expression while in the muscle, a phase shift was observed in the 6-4 mutant compared with the wild type fish. In the case of *per3*, low amplitude expression was observed in the brain, heart and fin in the mutant compared with wild type tissues. Furthermore, *cry5* showed lower amplitude rhythms in the mutant in the heart, muscle, skin and fin of the mutant fish compared with wild type controls (Figure 3.24 and Figure 3.25). Combined with my results obtained from the cell lines, these findings point to a tissue-specific role for 6-4 photolyase in circadian clock function under light-dark cycle conditions.

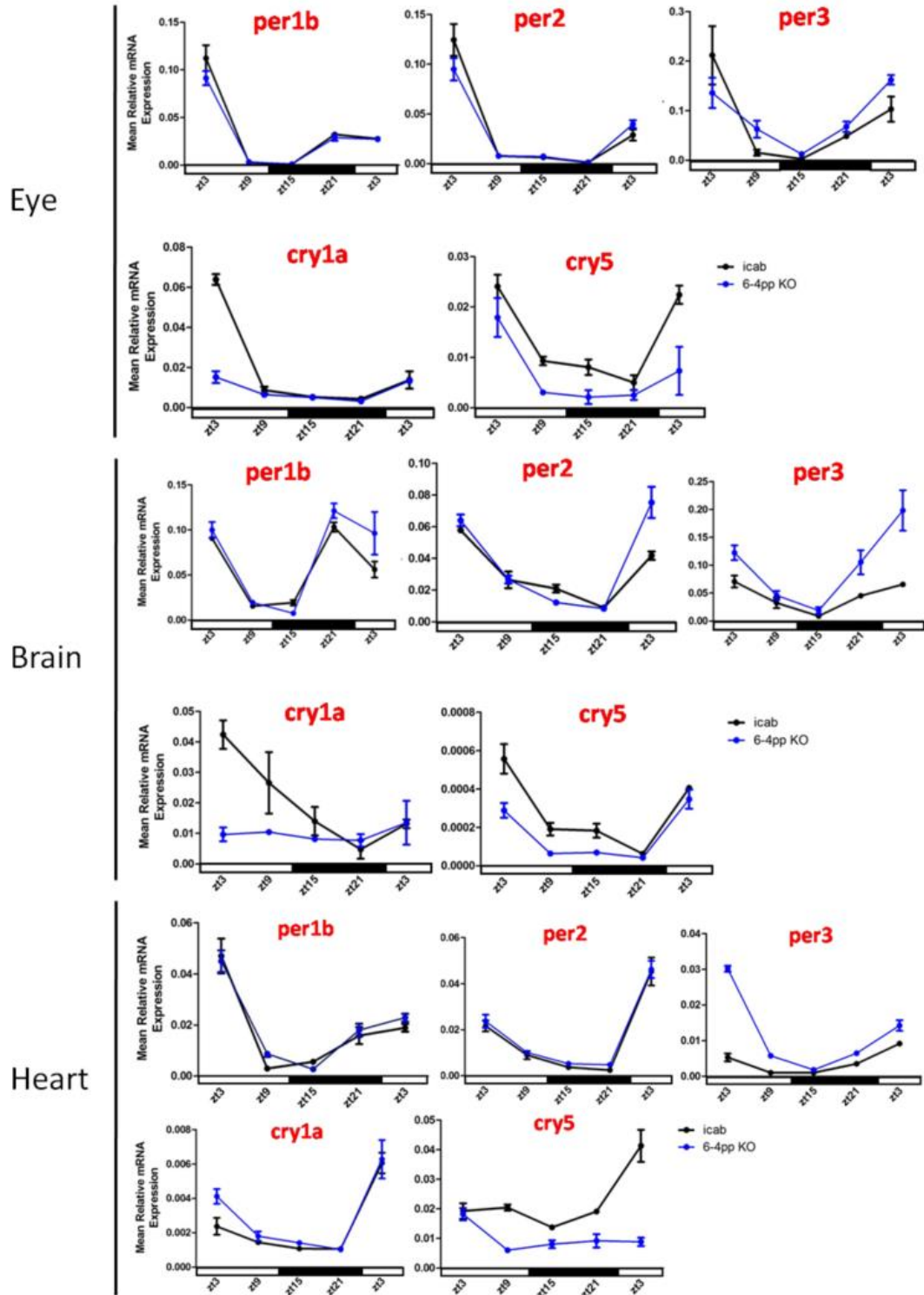


Figure 3.24 Clock gene expression in eye, brain and heart tissues of medaka WT and 6-4 photolyase mutant fish. Medaka WT and 6-4 photolyase mutant fish were maintained under LD conditions (14 hours light and 10 hours dark) to entrain the circadian clock and then were sacrificed at regular time points and various tissues were dissected for RNA extraction followed by qPCR analysis. Relative mRNA expression calculated as the mean \pm SEM (n=3) is plotted on the y-axes, while dissection time (as zeitgeber time, ZT) is plotted on the x-axes. The qPCR analysis of each clock gene

in each tissue was repeated independently at least 3 times. White and black bars below each panel indicate the light and dark periods, respectively.

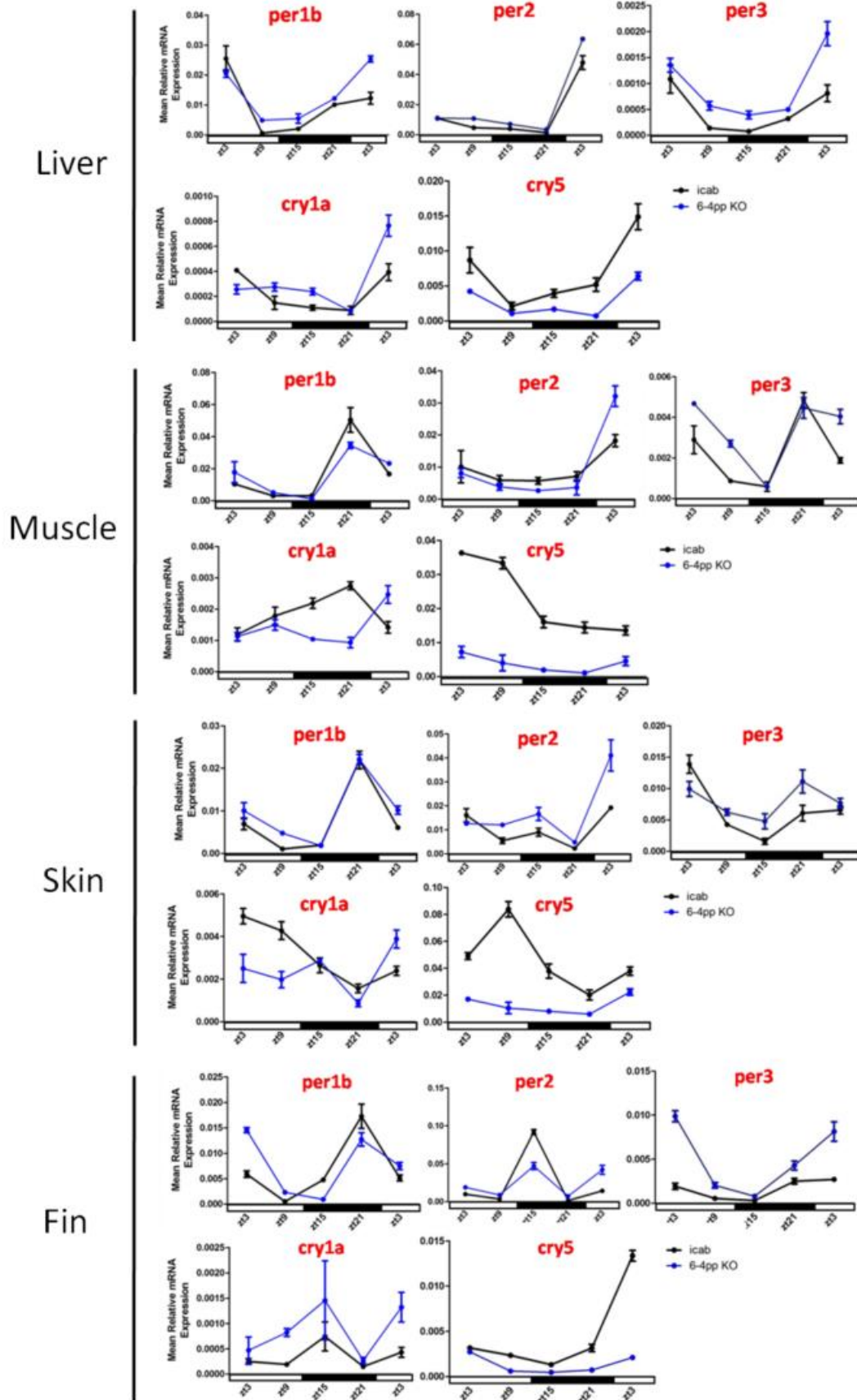


Figure 3.25 Clock gene expression in liver, muscle, skin, fin tissues of medaka WT and 6-4 photolyase mutant fish. Medaka WT and 6-4 photolyase mutant fish were kept under LD conditions (14 hours light and 10 hours dark) to entrain the circadian clock and then were sacrificed at regular timepoints, and various tissues were dissected for RNA extraction followed by qPCR analysis. Relative mRNA expression calculated as the mean \pm SEM (n=3) is plotted on the y-axes, while dissection time (as zeitgeber time, ZT) is plotted on the x-axes. Each clock gene in each tissue was repeated independently at least 3 times. White and black bars below each panel indicate the light and dark periods, respectively.

3.7 Circadian clock gene regulation by 6-4 photolyase

3.7.1 Circadian oscillation of *per1b* upon loss of 6-4 photolyase function.

The above qPCR results suggest that 6-4 photolyase may indeed be involved in core clock function. To explore further the potential role of 6-4 photolyase in core circadian clock function, I next wished to test the contribution of 6-4 photolyase to the circadian clock-regulated, rhythmic transcription of *per1b*. I transfected medaka 6-4 photolyase mutant cells and wild type control cells with a luciferase reporter driven by the zebrafish *per1b* promoter. After adding luciferin to the culture medium, I placed the cultures on a bioluminescence detector and exposed them to LD conditions to entrain the circadian clock for 3 days followed by incubation under constant darkness in free-running conditions for 2 days. Consistent with my results documenting endogenous *per1b* mRNA expression in wild type and 6-4 mutant medaka cell lines, there was a remarkable attenuation of clock-regulated rhythmic gene expression. This supports a conclusion that 6-4 photolyase plays a role in core circadian clock function in the medaka cell lines which regulates *per1b* transcription (Figure 3.26 A).

3.7.2 Light impact on D-box in loss of 6-4 photolyase mutants

Light-driven transcription of a subset of *cry* and *per* clock genes, mediated via the D-box enhancer is a key element in the entrainment of the clock mechanism in response to lighting conditions. Abnormal expression patterns of light-regulated clock genes were also observed in the 6-4 photolyase mutant cell lines and certain tissues (Figures. 23-25). I therefore also wished to investigate how 6-4 photolyase influences the response of the D-box enhancer to induce clock gene transcription in response to light. I transfected our medaka mutant and wild type cell lines with a luciferase reporter containing 15 tandemly repeated copies of the D-box enhancer derived from the zebrafish *cry1a* promoter. I exposed the transfected cells to visible light for 15 hours

and maintained a control set of cells in constant darkness. I then lysed the cells, prepared extracts and employed a β -galactosidase assay to normalize luciferase assay values. Comparing the bioluminescence levels of 6-4 photolyase mutant cells with wild type cells upon light exposure, revealed a considerably stronger induction of D-box-driven luciferase reporter gene expression in the wild type cells following light exposure, indicating that 6-4 photolyase may also be involved in the mechanism responsible for D-box-regulated clock gene transcription (Figure 3.26 B).

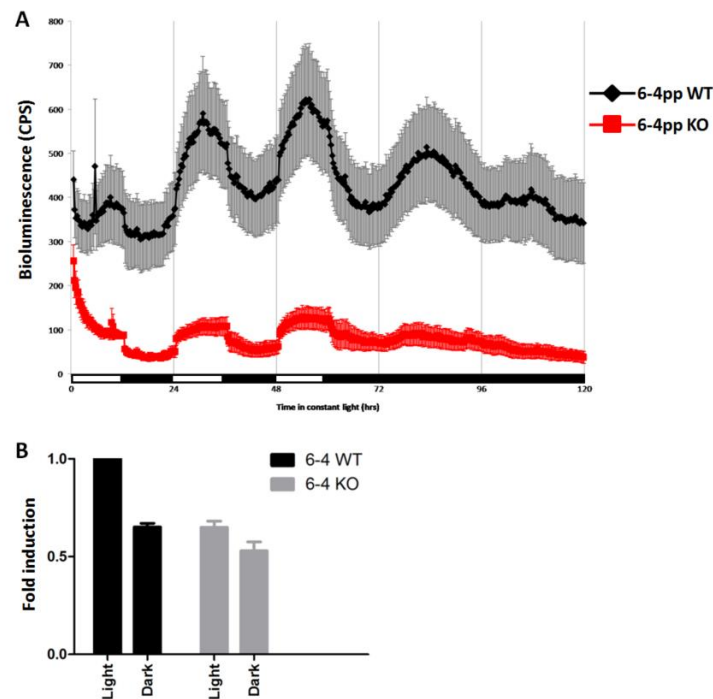


Figure 3.26 Abnormal circadian clock gene regulation in loss of 6-4 photolyase function medaka cells. (A) *In vivo* luciferase assay of medaka 6-4 wild type (black trace) and mutant (red trace) cell lines transfected with a luciferase reporter carrying the zebrafish clock-regulated *per1b* promoter. This assay was repeated independently at least 3 times. Bioluminescence (cps) values are plotted on the y-axis against time (hrs) on the x-axis. Each timepoint represents the mean of at least eight independently transfected wells \pm SEM. White and black horizontal bars along the x-axis indicate the light and dark periods, respectively. (B) *In vitro* luciferase assay of medaka 6-4 wild type (black) and mutant (grey) cells transfected with a luciferase reporter construct containing 15 tandemly repeated copies of the D-box sequence derived from the zebrafish *cry1a* gene promoter and exposed to visible light or maintained in constant darkness. The fold induction of relative bioluminescence values is plotted on the y-axis against exposure conditions on the x-axis. The results are presented as mean \pm SEM (n=3) and repeated 3 times. A β -galactosidase assay was employed to standardize for transfection efficiency.

3.8 Regulation of the E-box enhancer by 6-4 photolyase.

The Foulkes group has previously demonstrated that *per1b* in zebrafish is rhythmically expressed as the result of CLOCK and BMAL heterodimers binding to multiple E-box enhancers located in the *per1b* gene promoter which activate clock gene transcription¹⁴⁴. In turn, PER and CRY proteins interact physically with the CLOCK-BMAL heterodimer and repress the transactivation of CLOCK-BMAL as part of the core transcription-translation feedback loop in the clock mechanism. Since photolyases and cryptochromes are close relatives, I wondered whether photolyase can also act as a negative regulator of CLOCK-BMAL-mediated transactivation.

To test whether 6-4 photolyase can down-regulate transactivation mediated by the CLOCK-BMAL heterodimer, I transfected the zebrafish PAC-2 cell line with a luciferase reporter under the transcriptional control of a minimal promoter carrying 4 tandemly repeated copies of a canonical E-box element originating from the zebrafish *per1b* promoter. I also cotransfected the cells with expression vectors for zebrafish CLOCK1 and BMAL1 as well as zebrafish 6-4 photolyase, CPD photolyase or CRY1a. CRY1a has already been demonstrated to prevent the formation of CLOCK-BMAL heterodimers and so repress E-box driven clock gene transcription^{106,107}, and so serves as a negative control in this experiment. The results of this *in vitro* luciferase assay confirm that CRY1a indeed serves as a potent repressor of the transactivating function of CLOCK-BMAL on the E-box (Figure 3.27). Interestingly, coexpression of CPD photolyase does not result in any significant repression of the CLOCK-BMAL transactivation, however in contrast, coexpression of 6-4 photolyase results in a clear, dose-dependent repression of CLOCK-BMAL activity (Figure 3.27 A). Comparable results were obtained by transfecting the same expression constructs into the murine 3T3 cell line. These findings are consistent with 6-4 photolyase, but not CPD photolyase, sharing a CLOCK-BMAL repression function with cryptochromes (Figure 3.27 A and B).

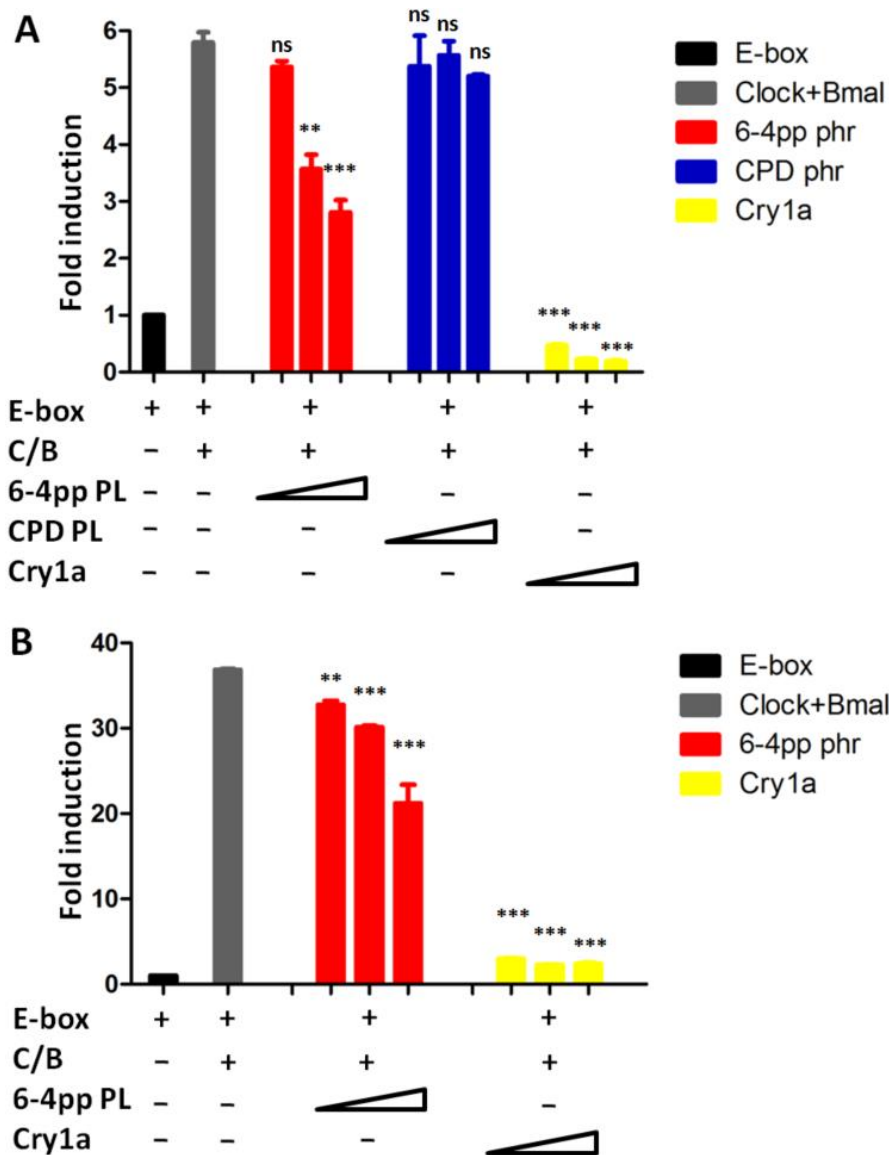


Figure 3.27 6-4 photolyase acts as a repressor of CLOCK-BMAL-mediated transactivation in fish and mammalian cells. *In vitro* luciferase assay of zebrafish PAC-2 (A) and mammalian 3T3 (B) cells co-transfected with an E-box luciferase reporter construct containing 4 tandemly multimerized copies of the E-box sequence derived from the zebrafish *per1b* gene promoter and expression vectors for zebrafish CLOCK1 and BMAL1, 6-4 photolyase, CPD photolyase and CRY1a expression constructs (from 50 ng to 150 ng). The expression plasmids included in each transfection are indicated below each graph. Fold induction of relative bioluminescence values is plotted on the y-axis. The result is reported as the mean \pm SEM (n=3) and performed at least 3 times. A β -galactosidase assay was employed to standardize for transfection efficiency.

3.9 Regulation of the D-box enhancer by 6-4 photolyase.

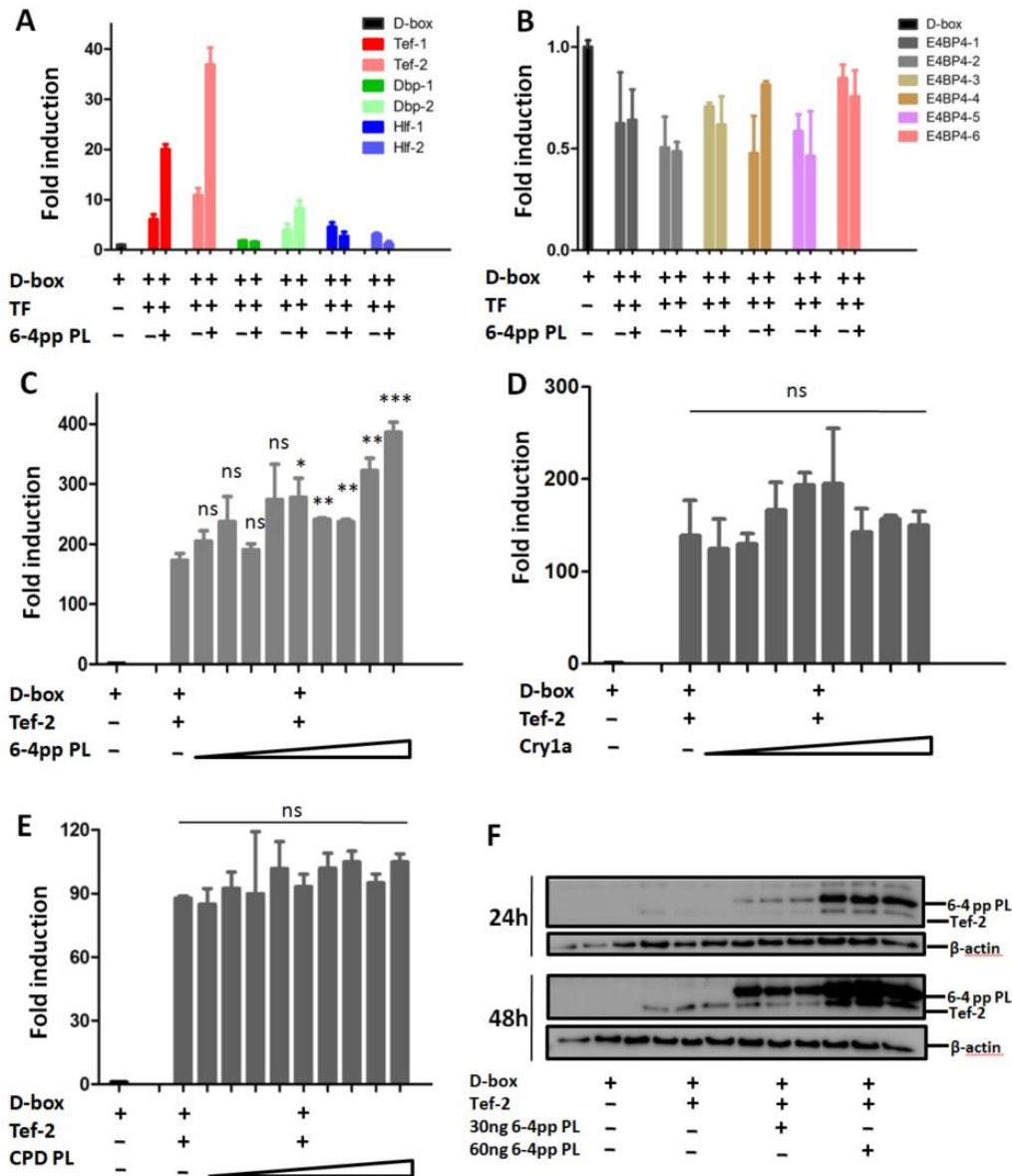


Figure 3.28 6-4 photolyase acts as an activator of TEF-2-regulated transactivation in zebrafish cells. (A-B) *In vitro* luciferase assay of zebrafish PAC-2 cells co-transfected with a D-box reporter construct containing 15 tandemly multimerized copies of the D-box sequence derived from the zebrafish *cry1a* gene promoter together with expression vectors for the 6 PAR factors and 6 E4BP4 factors (25 ng) as well as zebrafish 6-4 photolyase (30 ng). (C-E) *In vitro* luciferase assay of zebrafish PAC-2 cells co-transfected with the D-box reporter construct and expression vectors for zebrafish *tef-2* (25 ng) together with increasing amounts of expression vectors for 6-4 photolyase, *cry1a* or CPD photolyase (from 1 ng to 40 ng). The fold induction of relative bioluminescence values is plotted on the y-axis. The result is indicated as mean \pm SEM (n=3) and performed at least 3 times. The β -galactosidase assay was used to standardize for transfection efficiency. (F) Western Blot assay of zebrafish PAC-2 cells

co-transfected with the D-box reporter construct and expression constructs for zebrafish *tef-2* (25 ng) together with 6-4 photolyase (30 ng or 60 ng). Zebrafish β -actin was used as a loading control. The plasmids included in each transfection are indicated below each graph.

The similarity between photolyases and cryptochromes and the well-documented role of cryptochromes as negative regulators in the core clock seems to be consistent with the negative regulation of CLOCK-BMAL transactivation by 6-4 photolyase. However, there have been no previous reports of D-box regulatory factors interacting with cryptochrome or photolyase proteins. I therefore wished to explore in more detail the mechanism whereby 6-4 photolyase can influence D-box enhancer-mediated transactivation function. 6 PAR bZip transcription factors (TEF-1, TEF-2, HLF-1, HLF-2, DBP-1 and DBP-2) and 6 E4BP4 family members (E4BP4 1-6) are recognized as D-box binding bZip transcription factors. I therefore tested the possible functional interaction between 6-4 photolyase and these 12 transcription factors by performing *in vitro* luciferase assays in the zebrafish PAC-2 cell line. Specifically, I cotransfected PAC-2 cells with the D-box luciferase reporter construct together with expression vectors for each of these 12 transcription factors as well as 6-4 photolyase and then measured bioluminescence levels in an *in vitro* assay. My results demonstrate that in zebrafish, while all 6 PAR factors activate transcription of the D-box reporter construct, cotransfection of expression vectors for *tef-1*, *tef-2* and *dbp-2* together with 6-4 photolyase led to a significantly elevated activation compared with that observed for cotransfection of the expression vectors for *tef-1*, *tef-2* and *dbp-2* alone. In the case of the co-expressed E4BP4 factors, levels of D-box reporter expression were at a relatively low level and were not significantly affected upon cotransfection with the 6-4 photolyase expression vector.

Given the strong effect of 6-4 photolyase expression on transactivation by TEF-2, I chose to focus more attention on the effects of 6-4 photolyase on this particular D-box binding transcription factor (Figure 3.28 A and B). To validate my initial results, I systematically cotransfected increasing quantities of the 6-4 photolyase expression

vector with a fixed amount of the *tef-2* expression vector and the D-box reporter. My results revealed a dose dependent increase in TEF-2 transactivation with increasing levels of the photolyase expression vector (Figure 3.28 C). I next performed a comparable experiment to test the effect of cotransfecting increasing amounts of CPD photolyase or *cry1a* expression vectors. The results once again confirmed my initial experiments, showing that there was no notable effect of CPD photolyase or *cry1a* on the TEF-2 activation of D-box reporter transcription in zebrafish cells (Figure 3.28 D-E). I next repeated these experiments in mouse 3T3 cells as well as the EPA cell line derived from the Somalian cavefish, *P. andrussii*. In both cell lines, I observed a comparable, dose-dependent increase in TEF-2 – driven activation of D-box reporter transcription with increasing levels of cotransfected 6-4 photolyase expression vector (Figure 3.29).

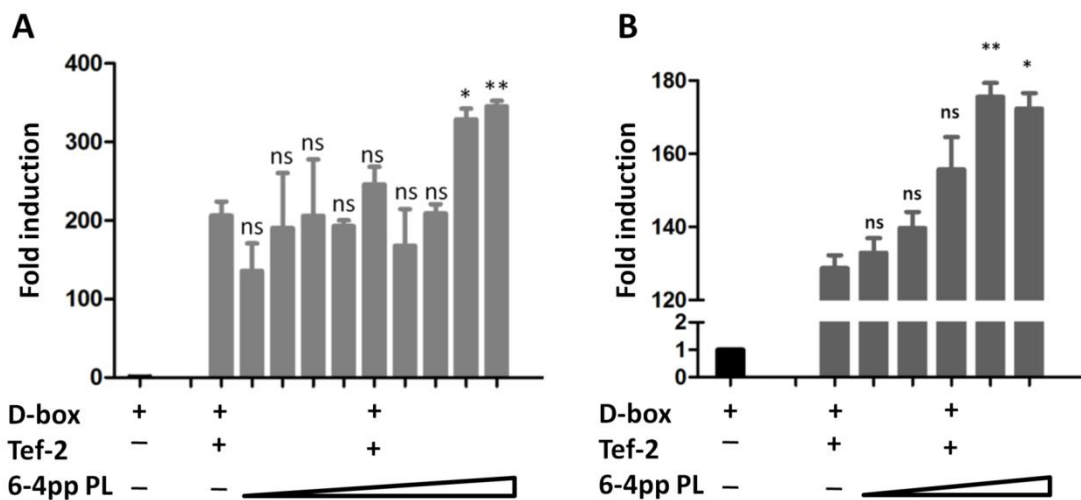


Figure 3.29 6-4 photolyase acts as an activator of TEF-2-regulated transactivation in cavefish *P. andrussii* and mammalian cells. *In vitro* luciferase assay of cavefish EPA (A) and mammalian 3T3 (B) cells co-transfected with reporter construct containing 15 copies of the D-box derived from the zebrafish *cry1a* gene promoter together with an expression vector for zebrafish *tef-2* (25 ng) together with increasing amounts of 6-4 photolyase expression vector (EPA: from 1 ng to 40 ng, 3T3: from 1 ng to 150 ng). Fold induction of relative bioluminescence values is plotted on the y-axis. The result is indicated as mean \pm SEM (n=3) and performed at least 3 times. The expression plasmids employed are showed below each graph. A β -galactosidase assay was employed to standardize for transfection efficiency.

These results could be interpreted in two ways: The coexpression of 6-4 photolyase might result in a decrease in the protein levels of TEF-2 or alternatively this photolyase might alter the function of TEF-2 without affecting the protein levels. To distinguish between these two possibilities, I performed a Western Blot to investigate the levels of 6-4 photolyase and TEF-2 expression in my cotransfection experiment at the protein level. Levels of the TEF-2 and 6-4 photolyase proteins were measured using epitope tag-specific antibodies while Western Blot analysis with a β -actin antibody was used as a loading control. Thus, I cotransfected zebrafish PAC-2 cells with a fixed amount of *tef-2* as performed previously together with 30 ng or 60 ng of 6-4 photolyase expression vector and incubated the cells for 24 hours or 48 hours before protein extraction. My results confirmed that with increasing amounts of cotransfected 6-4 photolyase expression vector, increasing levels of 6-4 photolyase protein were detected. However, increasing levels of TEF-2 protein were also observed for both incubation times, even though identical amounts of *tef-2* expression vector were included in each sample. These results indicate that 6-4 photolyase indeed influences the functionality of TEF-2 by increasing basal levels of the TEF-2 protein, possibly by increasing its stability (Figure 3.28 F).

4. Discussion

My project was initiated based on the observation that while 6-4 and DASH photolyase have accumulated loss of function mutations in the blind cavefish, *P. andruzzii*, CPD photolyase is still highly conserved. This suggests given the complete absence of sunlight in the cavefish environment as well as the essential links between photoreactivation repair and sunlight, that there must be some selective pressure operating in this perpetually dark cave environment specifically maintaining CPD photolyase function. By studying a unique collection of medaka CRISPR-generated mutant lines where each of the three photolyase genes has been targeted by loss-of-function mutations, I have revealed that loss of CPD photolyase function is associated with an increase in DNA damage and a decrease in cell survival upon exposure to elevated levels of ROS. Consistently, heterologous expression of CPD photolyase in cell lines from mice, which characteristically lack photolyase genes and photoreactivation function, confers photoreactivation as well as enhanced cell survival upon oxidative stress and mitigated levels of DNA damage. Moreover, my results demonstrate that light has no prominent impact on the levels of ROS-induced DNA damage or on CPD phr-induced protection against ROS-induced mortality. Interestingly, my data indicate that even in constant darkness, ROS exposure is able to induce CPD photoproduct production. Furthermore, loss of the Three Tryptophan Electron Transfer Chain in ectopically expressed CPD photolyase as well as not conferring photoreactivation DNA repair function, also fails to protect mammalian cells from ROS-induced mortality.

The similarities between cryptochromes and, in particular 6-4 photolyase, have been used as an argument that there may be overlap of function between the two classes of protein. Indeed, according to my qPCR data from WT and photolyase mutant medaka fish cell lines, the loss of 6-4 photolyase function but not that of CPD or DASH photolyase disrupts clock regulated core clock gene expression in a gene- and tissue-specific fashion. Specifically, 6-4 photolyase acts as a repressor of transcriptional transactivation by the E-box enhancer by repressing CLOCK-BMAL heterodimer

activation. Furthermore, I also implicate 6-4 photolyase in the transcriptional regulation of D-box-driven clock genes via enhancing the activation of the PAR transcription factors, notably TEF.

4.1 Activator for CPD photolyase "dark" DNA repair function

Oxidative stress has been well documented to induce DNA damage, notably 8-hydroxydeoxy-guanosine (8-OHdG). A major question resulting from my findings is how CPD photolyase may contribute to repair of this damage. Given the high degree of specificity of CPD photolyase for catalyzing the repair of pyrimidine dimers, it seems unlikely that this photolyase could enzymatically repair 8-OHdG damage. However, there have been reports that photolyases are able to bind to other types of helix distorting DNA damage^{46,219}. By binding to this type of DNA it is tempting to speculate that the photolyase could act to target other DNA repair machinery to the damage site and thereby indirectly enhance repair. However, an alternative explanation could be that the protective effects of CPD photolyase may be related to the formation of CPD photoproducts in the absence of sunlight. For this hypothesis to be relevant, two issues need to be resolved: Can CPD be formed in perpetual darkness in the absence of UV radiation and then how could the photolyase enzyme repair the resulting DNA damage without access to visible light. My results indicate that redox changes resulting from life in the extreme cave environment might substitute for UV in generating CPD photoproducts, although with lower efficiency. This is consistent with the formation of "dark CPD" that continues some hours after UV exposure has been completed. The existing models to explain dark CPD production invoke redox changes occurring in the context of melanin metabolism. However, dark CPD formation has also been documented in cell types that do not metabolize melanin and so this model does not fully explain how this DNA damage can be formed in the absence of sunlight. Elevated levels of reactive oxygen species have been well documented in subterranean animals such as the naked mole rat as well as other cave dwelling species²²⁰⁻²²² and so could serve as a source of oxidative stress driving CPD formation in darkness. As well as

serving as a source of various types of oxidative DNA damage, in fish, ROS also acts as a signal directing gene expression via the ROS responsive enhancer, the D-box. Furthermore, ROS operates as a messenger in intracellular signaling pathways and plays an essential role in modulating biological processes, such as cell growth, proliferation, migration and apoptosis⁸ through altering the intracellular redox status or chemically modifying critical amino acid residues of functional proteins. Based on my observation that the protective effect of CPD photolyase is lost upon mutation of key amino acids within the Three Tryptophan Electron Transfer Chain, I speculate that ROS may activates CPD photolyase catalytic function via redox reactions which reduce the FAD domain of CPD photolyase in perpetual dark conditions and thereby enable the repair reaction to proceed. Furthermore, it has been previously demonstrated that the binding of CPD photolyase to CPD photoproducts does not require light⁶, and so could still operate in the cave environment. Clearly, future biochemical experiments performed with purified recombinant photolyase proteins *in vitro* will be essential to test this hypothesis.

4.2 Molecular mechanism of 6-4 photolyase in light-dependent transcriptional control.

My results in relation to the circadian clock have revealed that 6-4 photolyase inhibits the transactivation of the CLOCK-BMAL heterodimer, thereby repressing the E-box regulated transcription of clock genes. However, the underlying molecular mechanism is still unclear. For example, how does 6-4 photolyase interact physically with the CLOCK-BMAL complex and how does this lead to repression of the CLOCK-BMAL heterodimer? It has been documented that CRY1 binds physically to the C-terminus of BMAL in the CLOCK-BMAL complex^{106,107} and effectively inhibits the activity of the CLOCK-BMAL heterodimer in mammals, while in zebrafish, CRY1a can interact tightly with the PAS B domain of CLOCK and various domains of BMAL, including the bHLH, PAS B and C-terminus domains to potentially suppress the formation of the CLOCK-BMAL complex¹¹⁰. Since 6-4 photolyase and CRY1a both belong to the

cryptochrome/photolyase family, it is worthwhile to investigate the physical interaction between 6-4 photolyase and CLOCK or BMAL proteins based on knowledge of how cryptochromes interact with these proteins. Two hypotheses may explain 6-4 photolyase function: the first is that the photolyase protein may inhibit the transactivation of CLOCK-BMAL heterodimer directly by interaction with CLOCK or BMAL or both. In this scenario, the presence of the physically bound photolyase protein may interfere with the ability of CLOCK and BMAL with other transcriptional co activators or with the RNA polymerase machinery itself^{114,223}. In the second hypothesis, 6-4 photolyase perhaps can competitively interact with particular domains of CLOCK or BMAL protein, where CLOCK and BMAL themselves bind directly to form an active complex, to thereby prevent the formation of the CLOCK-BMAL heterodimer.

Surprisingly, my data have now also implicated 6-4 photolyase in regulating D-box-driven transcription of gene expression via activating the D-box binding transcription factor, TEF-2. There are no previous reports of any members of the CPF family interacting with bZip transcription factors, and so my results raise new questions about whether photolyases interact with this class of transcription factors in a comparable way to their interaction with CLOCK and BMAL. How does 6-4 photolyase bind to TEF-2 and thereby enhance its transactivation function? One piece of evidence for how this mechanism may operate comes from my results that 6-4 photolyase may participate in the stabilization of the TEF-2 protein. This suggests that protein modifications such as phosphorylation or ubiquitination, which have already been implicated in the regulation of transcription factor turn over and stability^{224,225}, might also be involved in the case of the interaction between 6-4 photolyase and TEF-2.

6-4 photolyase is a member of cryptochrome/photolyase family, a family of photoreceptors which share a highly conserved FAD domain. The results described in my project further implicate 6-4 photolyase in mediating light-regulated processes in the cell. The role of 6-4 photolyase in repressing transcriptional activation by CLOCK and BMAL places it as a central circadian clock component, playing a similar role as the cryptochromes. Furthermore, like cryptochromes such as *cry1a*, the expression of this

photolyase gene is robustly induced upon light exposure via the D-box enhancer promoter elements. The primary zeitgeber for the clock is light and so this implicates light-induced expression of 6-4 photolyase as a key step in resetting the phase of the clock in response to the environmental day-night cycle. Finally, the ability of 6-4 photolyase to enhance TEF-2 transcriptional activation of the D-box suggests that this protein plays a key part of a feedback mechanism which adapts the transcriptome to counter the effects of light exposure. Therefore, my results combined with previous findings point to photolyases being tightly linked with cellular responses to light at multiple levels.

4.3 Co-evolution of cryptochrome (circadian clock) and photolyase (DNA repair)

The Cryptochrome/photolyase family (CPF) represents a family of photoreceptors that during evolution, has evolved its functionality divergently to adapt to a complicated and changing environment. Specifically, it has been revealed that in *Phaeodactylum tricorutum*, a member of the CPF family, termed PtCPF1, displays DNA repair activity of 6-4 photoproducts and in parallel, this protein represses transactivation of the CLOCK-BMAL complex and thereby regulates the circadian clock, a result that is consistent with my own findings on zebrafish 6-4 photolyase¹⁹⁰. Moreover, the presence of a single protein belonging to the CPF family with a dual function called OtCPF1, has also been reported in the green alga, *Ostreococcus tauri*. Specifically, OtCPF1 has been shown to repair 6-4 photoproducts and to be involved in the maintenance of the circadian clock by regulating CLOCK-BMAL-activated transcription¹⁹¹. It has also been revealed that rhythmically expressed PtCPD (*Potorous tridactylus* CPD) photolyase can functionally substitute for CRY proteins in the mammalian circadian oscillator¹⁸⁹. In addition, human cryptochromes have been implicated in maintaining the functionality of monitoring UV-induced DNA damage²²⁶. In this project, I have presented additional confirmatory evidence that fish CPD photolyase is involved in the repair of diverse types of DNA damage, thereby

enhancing cell survival in response to environmental stress. Furthermore, as well as catalyzing the repair of UV-induced 6-4 photoproducts, 6-4 photolyase appears to serve as a repressor of CLOCK-BMAL activated transcription via the E-box enhancer and an activator of TEF-2 regulated transcription via the D-box enhancer.

Besides the functional convergence of cryptochrome and photolyase, it has also been elucidated that cryptochrome and photolyase share common transcriptional regulatory elements. Specifically, promoter analysis in fish models has revealed that all cryptochrome and photolyase genes possess conserved D-box enhancers (5'-TTTTGTAAC-3') involved in transcriptional mediation by light, and canonical E-box enhancer elements (5'-CACGTG-3') acting as circadian clock modulated enhancer elements^{150,155}.

Therefore, photolyases and cryptochromes are both photoreceptors, close relatives, share highly conserved domains, display functional overlap and divergent functionality during evolution. For all these reasons, it is plausible to speculate that photo-activated DNA repair and photo-entrained circadian rhythmicity evolved from a common progenitor⁵.

4.4 Why is CPD photolyase (but not 6-4 and DASH photolyase) conserved in Somalian cavefish?

Previous studies have demonstrated that mammals do not possess photolyase genes and UV-induced DNA damage is repaired by a more complex repairing system-NER pathway as a substitute for the more efficient photoreactivation. A theory termed the "Nocturnal Bottleneck theory", that has been described previously, has been proposed to potentially account for the loss of photoreactivation function in placental mammals. The absence of light to drive photoreactivation and photolyase enzymatic repair function as well as the lack of exposure to UV radiation during the periods of the day-night cycle when placental mammal ancestors would normally need to leave their burrows might have led to loss of photolyase genes in this lineage.

From an evolutionary perspective, like the mammalian ancestors in the Nocturnal Bottleneck theory, the Somalian cavefish has inhabited its constant dark environment for millions of years, thereby light-driven photoreactivation is not essential and so there has been limited selective advantage to maintain certain photolyase genes such as the 6-4 and DASH photolyases. In this regard, these fish also display a major change of circadian clock function with a complete absence of photic entrainment, which would again be consistent with loss of 6-4 photolyase function. As an alternative explanation to loss of selective pressure, these protective mechanisms may be energetically expensive, and consequently, if there is no longer considerable UV-induced DNA damage to repair, or any need to maintain a functional photic entrainment pathway for the circadian clock, there will be a positive selection pressure to eliminate 6-4 photolyase function

In contrast, due to its role in enhancing cell survival in response to oxidative stress, CPD photolyase function has been maintained. Consistent with these results, it has been previously described that compared to *Astyanax* surface fish, the *Astyanax* cavefish have a significantly higher basal level of CPD photolyase, display considerably lower DNA damage and, as a result, higher DNA repair activity even in the darkness. In particular, the *Astyanax* cavefish in the wild exhibit much higher baseline levels of CPD photolyase gene expression than both surface fish and lab-raised cavefish, indicating that the capacity for DNA repair would be even greater in the cave environment²¹⁰. All these findings point to a view that indeed, CPD photolyase is still involved in repairing damaged DNA in the constant dark cave environment.

4.5 Perspectives

My project has provided important new insight into the range of function for both CPD and 6-4 photolyase, based on evolution of cavefish species, mutant photolyase medaka lines and gain of photolyase function mammalian cell culture models. Now, there are important new directions for the project to follow. One concerns exploring the mechanisms whereby CPD photolyase is able to contribute to the repair of oxidatively damaged DNA. For tackling this issue, I plan to perform *in vitro* experiments using purified, bacterially synthesized mutant and wild type CPD photolyase proteins. In collaboration with the laboratory of Tilman Lamparter (KIT, Campus South) these will then be tested in *in vitro* binding and photoreactivation reactions. This will enable me to explore which types of DNA damage CPD photolyase can interact with, whether ROS treatment can generate “dark” CPD photoproducts in the absence of light and also whether redox state can influence the catalytic activity of the photolyase enzyme. My other major issue is to compare the interaction of cryptochromes with CLOCK and BMAL with that I have observed for 6-4 photolyase. Furthermore, it will be valuable to study how 6-4 photolyase interacts with the PAR bZip transcription factor TEF-2 and how this affects the steady state levels of this transcription factor. By these two approaches, I will aim to provide further insight into the functionality and evolution of the light-dependent cryptochrome and photolyase family of flavoproteins.

5. References:

1. Dunlap JC. Molecular bases for circadian clocks. *Cell*. 1999;96(2):271-290.
2. Oklejewicz M, Destici E, Tamanini F, Hut RA, Janssens R, van der Horst GTJ. Phase Resetting of the Mammalian Circadian Clock by DNA Damage. *Current Biology*. 2008;18(4):286-291.
3. Brash DE. UV mutagenic photoproducts in Escherichia coli and human cells: a molecular genetics perspective on human skin cancer. *Photochem Photobiol*. 1988;48(1):59-66.
4. Mitchell DL, Nairn RS. The biology of the (6-4) photoproduct. *Photochem Photobiol*. 1989;49(6):805-819.
5. Sancar A. Cryptochrome: The second photoactive pigment in the eye and its role in circadian photoreception. *Annu Rev Biochem*. 2000;69:31-67.
6. Sancar A. Structure and function of DNA photolyase and cryptochrome blue-light photoreceptors. *Chem Rev*. 2003;103(6):2203-2237.
7. Todo T. Functional diversity of the DNA photolyase/blue light receptor family. *Mutat Res*. 1999;434(2):89-97.
8. Thannickal VJ, Fanburg BL. Reactive oxygen species in cell signaling. *Am J Physiol Lung Cell Mol Physiol*. 2000;279(6).
9. RUPERT CS. Photoenzymatic repair of ultraviolet damage in DNA. I. Kinetics of the reaction. *J Gen Physiol*. 1962;45(4):703-724.
10. Douki T, Sage E. Dewar valence isomers, the third type of environmentally relevant DNA photoproducts induced by solar radiation. *Photochem Photobiol Sci*. 2016;15(1):24-30.
11. Friedberg EC W and S. DNA Repair and Mutagenesis. *ASM Press, Washington, DC*. Published online 1995.
12. Mitchell DL. The relative cytotoxicity of (6-4) photoproducts and cyclobutane dimers in mammalian cells. *Photochem Photobiol*. 1988;48(1):51-57.
13. Taylor JS. Unraveling the molecular pathway from sunlight to skin cancer. *Acc Chem Res*. 1994;27:76-82.
14. RUPERT CS. Photoenzymatic repair of ultraviolet damage in DNA. II. Formation of an enzyme-substrate complex. *J Gen Physiol*. 1962;45(4):725-741.
15. Wulff DL, Rupert CS. Disappearance of thymine photodimer in ultraviolet irradiated DNA upon treatment with a photoreactivating enzyme from baker's yeast. *Biochem Biophys Res Commun*. 1962;7(3):237-240.
16. Selby CP, Sancar A. A cryptochrome/photolyase class of enzymes with single-

- stranded DNA-specific photolyase activity. *Proc Natl Acad Sci U S A*. 2006;103(47):17696-17700.
17. Navarro E, Niemann N, Kock D, et al. The DASH-type Cryptochrome from the Fungus *Mucor circinelloides* Is a Canonical CPD-Photolyase. *Curr Biol*. 2020;30(22):4483-4490.e4.
 18. Eker AP KPHJYA. DNA photoreactivating enzyme from the cyanobacterium *Anacystisnidulans*. *J Biol Chem*. 1990;265 (14)(15):8009-8015.
 19. Sancar A. Structure and function of DNA photolyase. *Biochemistry*. 1994;33(1):2-9.
 20. Sancar A. Mechanisms of DNA Repair by Photolyase and Excision Nuclease (Nobel Lecture). *Angew Chem Int Ed Engl*. 2016;55(30):8502-8527.
 21. Tan C, Guo L, Ai Y, et al. Direct determination of resonance energy transfer in photolyase: structural alignment for the functional state. *J Phys Chem A*. 2014;118(45):10522-10530.
 22. Liu Z, Tan C, Guo X, et al. Dynamics and mechanism of cyclobutane pyrimidine dimer repair by DNA photolyase. *Proc Natl Acad Sci U S A*. 2011;108(36):14831-14836.
 23. Zhong D. Electron transfer mechanisms of DNA repair by photolyase. *Annu Rev Phys Chem*. 2015;66:691-715.
 24. Byrdin M, Lukacs A, Thiagarajan V, Eker APM, Brettel K, Vos MH. Quantum yield measurements of short-lived photoactivation intermediates in DNA photolyase: toward a detailed understanding of the triple tryptophan electron transfer chain. *J Phys Chem A*. 2010;114(9):3207-3214.
 25. Brettel K, Byrdin M. Reaction mechanisms of DNA photolyase. *Curr Opin Struct Biol*. 2010;20(6):693-701.
 26. Espagne A, Burdin M, Eker APM, Brettel K. Very fast product release and catalytic turnover of DNA photolyase. *Chembiochem*. 2009;10(11):1777-1780.
 27. Park HW, Kim ST, Sancar A, Deisenhofer J. Crystal structure of DNA photolyase from *Escherichia coli*. *Science*. 1995;268(5219):1866-1872.
 28. Kao YT, Saxena C, Wang L, Sancar A, Zhong D. Direct observation of thymine dimer repair in DNA by photolyase. *Proc Natl Acad Sci U S A*. 2005;102(45):16128-16132.
 29. Tan C, Liu Z, Li J, et al. The molecular origin of high DNA-repair efficiency by photolyase. *Nat Commun*. 2015;6.
 30. Schleicher E, Hitomi K, Kay CWM, Getzoff ED, Todo T, Weber S. Electron nuclear double resonance differentiates complementary roles for active site histidines in (6-4) photolyase. *J Biol Chem*. 2007;282(7):4738-4747.

31. Chang CW, Guo L, Kao YT, et al. Ultrafast solvation dynamics at binding and active sites of photolyases. *Proc Natl Acad Sci U S A*. 2010;107(7):2914-2919.
32. Kao YT, Saxena C, Wang L, Sancar A, Zhong D. Femtochemistry in enzyme catalysis: DNA photolyase. *Cell Biochem Biophys*. 2007;48(1):32-44.
33. MacFarlane IV AW, Stanley RJ. Cis-syn thymidine dimer repair by DNA photolyase in real time. *Biochemistry*. 2003;42(28):8558-8568.
34. Hassanali AA, Zhong D, Singer SJ. An AIMD study of the CPD repair mechanism in water: reaction free energy surface and mechanistic implications. *J Phys Chem B*. 2011;115(14):3848-3859.
35. Masson F, Laino T, Rothlisberger U, Hutter J. A QM/MM investigation of thymine dimer radical anion splitting catalyzed by DNA photolyase. *Chemphyschem*. 2009;10(2):400-410.
36. Hitomi K, DiTacchio L, Arvai AS, et al. Functional motifs in the (6-4) photolyase crystal structure make a comparative framework for DNA repair photolyases and clock cryptochromes. *Proc Natl Acad Sci U S A*. 2009;106(17):6962-6967.
37. Maul MJ, Barends TRM, Glas AF, et al. Crystal structure and mechanism of a DNA (6-4) photolyase. *Angew Chem Int Ed Engl*. 2008;47(52):10076-10080.
38. Zhong D. Ultrafast catalytic processes in enzymes. *Curr Opin Chem Biol*. 2007;11(2):174-181.
39. Zhao X, Liu J, Hsu DS, Zhao S, Taylor JS, Sancar A. Reaction mechanism of (6-4) photolyase. *J Biol Chem*. 1997;272(51):32580-32590.
40. Byrdin M, Villette S, Eker APM, Brettel K. Observation of an intermediate tryptophanyl radical in W306F mutant DNA photolyase from *Escherichia coli* supports electron hopping along the triple tryptophan chain. *Biochemistry*. 2007;46(35):10072-10077.
41. Byrdin M, Eker APM, Vos MH, Brettel K. Dissection of the triple tryptophan electron transfer chain in *Escherichia coli* DNA photolyase: Trp382 is the primary donor in photoactivation. *Proc Natl Acad Sci U S A*. 2003;100(15):8676-8681.
42. Schul W, Jans J, Rijksen YMA, et al. Enhanced repair of cyclobutane pyrimidine dimers and improved UV resistance in photolyase transgenic mice. *EMBO J*. 2002;21(17):4719-4729.
43. Wood RD. DNA repair in eukaryotes. *Annu Rev Biochem*. 1996;65:135-167.
44. de Laat WL, Jaspers NGJ, Hoeijmakers JHJ. Molecular mechanism of nucleotide excision repair. *Genes Dev*. 1999;13(7):768-785.
45. Hoeijmakers JHJ. Genome maintenance mechanisms for preventing cancer. *Nature*. 2001;411(6835):366-374.
46. Thoma F. Light and dark in chromatin repair: repair of UV-induced DNA lesions

- by photolyase and nucleotide excision repair. *EMBO J.* 1999;18(23):6585-6598.
47. Gregersen LH, Svejstrup JQ. The Cellular Response to Transcription-Blocking DNA Damage. *Trends Biochem Sci.* 2018;43(5):327-341.
 48. Poetsch AR. The genomics of oxidative DNA damage, repair, and resulting mutagenesis. *Comput Struct Biotechnol J.* 2020;18:207-219.
 49. Hayyan M, Hashim MA, Alnashef IM. Superoxide Ion: Generation and Chemical Implications. *Chem Rev.* 2016;116(5):3029-3085.
 50. Markkanen E. Not breathing is not an option: How to deal with oxidative DNA damage. *DNA Repair (Amst).* 2017;59:82-105.
 51. Paiva CN, Bozza MT. Are reactive oxygen species always detrimental to pathogens? *Antioxid Redox Signal.* 2014;20(6):1000-1034.
 52. Reuter S, Gupta SC, Chaturvedi MM, Aggarwal BB. Oxidative stress, inflammation, and cancer: how are they linked? *Free Radic Biol Med.* 2010;49(11):1603-1616.
 53. van Loon B, Markkanen E, Hübscher U. Oxygen as a friend and enemy: How to combat the mutational potential of 8-oxo-guanine. *DNA Repair (Amst).* 2010;9(6):604-616.
 54. Roots R, Okada S. Protection of DNA molecules of cultured mammalian cells from radiation-induced single-strand scissions by various alcohols and SH compounds. *Int J Radiat Biol Relat Stud Phys Chem Med.* 1972;21(4):329-342.
 55. Ward JF. Complexity of damage produced by ionizing radiation. *Cold Spring Harb Symp Quant Biol.* 2000;65:377-382.
 56. Lehner S. Biomolecular action of ionizing radiation. *CRC Press.* Published online 2007.
 57. Grollman AP, Moriya M. Mutagenesis by 8-oxoguanine: an enemy within. *Trends Genet.* 1993;9(7):246-249.
 58. Ward JF. Advances in DNA Damage and Repair. *Plenum New York.* Published online 1998:431-439.
 59. Michaels ML, Miller JH. The GO system protects organisms from the mutagenic effect of the spontaneous lesion 8-hydroxyguanine (7,8-dihydro-8-oxoguanine). *J Bacteriol.* 1992;174(20):6321-6325.
 60. Thomas D, Scot AD, Barbey R, Padula M, Boiteux S. Inactivation of OGG1 increases the incidence of G . C-->T . A transversions in *Saccharomyces cerevisiae*: evidence for endogenous oxidative damage to DNA in eukaryotic cells. *Mol Gen Genet.* 1997;254(2):171-178.
 61. Moore SPG, Toomire KJ, Strauss PR. DNA modifications repaired by base excision repair are epigenetic. *DNA Repair (Amst).* 2013;12(12):1152-1158.

62. Allgayer J, Kitsera N, Bartelt S, Epe B, Khobta A. Widespread transcriptional gene inactivation initiated by a repair intermediate of 8-oxoguanine. *Nucleic Acids Res.* 2016;44(15):7267-7280.
63. Ramon O, Sauvaigo S, Gasparutto D, Faure P, Favier A, Cadet J. Effects of 8-oxo-7,8-dihydro-2'-deoxyguanosine on the binding of the transcription factor Sp1 to its cognate target DNA sequence (GC box). *Free Radic Res.* 1999;31(3):217-229.
64. Hailer-Morrison MK, Kotler JM, Martin BD, Sugden KD. Oxidized guanine lesions as modulators of gene transcription. Altered p50 binding affinity and repair shielding by 7,8-dihydro-8-oxo-2'-deoxyguanosine lesions in the NF-kappaB promoter element. *Biochemistry.* 2003;42(32):9761-9770.
65. Khobta A, Anderhub S, Kitsera N, Epe B. Gene silencing induced by oxidative DNA base damage: association with local decrease of histone H4 acetylation in the promoter region. *Nucleic Acids Res.* 2010;38(13):4285-4295.
66. Larsen E, Kwon K, Coin F, Egly JM, Klungland A. Transcription activities at 8-oxoG lesions in DNA. *DNA Repair (Amst).* 2004;3(11):1457-1468.
67. Park JW, Han YI, Kim SW, et al. 8-OxoG in GC-rich Sp1 binding sites enhances gene transcription in adipose tissue of juvenile mice. *Sci Rep.* 2019;9(1).
68. Ruchko M v., Gorodnya OM, Pastukh VM, et al. Hypoxia-induced oxidative base modifications in the VEGF hypoxia-response element are associated with transcriptionally active nucleosomes. *Free Radic Biol Med.* 2009;46(3):352-359.
69. Pastukh V, Roberts JT, Clark DW, et al. An oxidative DNA "damage" and repair mechanism localized in the VEGF promoter is important for hypoxia-induced VEGF mRNA expression. *Am J Physiol Lung Cell Mol Physiol.* 2015;309(11):L1367-L1375.
70. Fleming AM, Ding Y, Burrows CJ. Oxidative DNA damage is epigenetic by regulating gene transcription via base excision repair. *Proc Natl Acad Sci U S A.* 2017;114(10):2604-2609.
71. Wang R, Hao W, Pan L, Boldogh I, Ba X. The roles of base excision repair enzyme OGG1 in gene expression. *Cell Mol Life Sci.* 2018;75(20):3741-3750.
72. Coluzzi E, Colamartino M, Cozzi R, et al. Oxidative stress induces persistent telomeric DNA damage responsible for nuclear morphology change in mammalian cells. *PLoS One.* 2014;9(10).
73. Fouquerel E, Barnes RP, Uttam S, Watkins SC, Bruchez MP, Opresko PL. Targeted and Persistent 8-Oxoguanine Base Damage at Telomeres Promotes Telomere Loss and Crisis. *Mol Cell.* 2019;75(1):117-130.e6.
74. von Zglinicki T. Oxidative stress shortens telomeres. *Trends Biochem Sci.* 2002;27(7):339-344.
75. Graham MK, Meeker A. Telomeres and telomerase in prostate cancer

- development and therapy. *Nat Rev Urol*. 2017;14(10):607-619.
76. Sedletska Y, Radicella JP, Sage E. Replication fork collapse is a major cause of the high mutation frequency at three-base lesion clusters. *Nucleic Acids Res*. 2013;41(20):9339-9348.
 77. David SS, O'Shea VL, Kundu S. Base-excision repair of oxidative DNA damage. *Nature*. 2007;447(7147):941-950.
 78. Premi S, Wallisch S, Mano CM, et al. Photochemistry. Chemiexcitation of melanin derivatives induces DNA photoproducts long after UV exposure. *Science*. 2015;347(6224):842-847.
 79. Ruven HJ, BRSCDJLPML van ZA. Ultraviolet-induced cyclobutane pyrimidine dimers are selectively removed from transcriptionally active genes in the epidermis of the hairless mouse. *Cancer Res*. 1993;53 (7)(1):1642-1645.
 80. Snopov SA, de Gruijl FR, Roza L, van der Leun JC. Immunochemical study of DNA modifications in the nuclei of UV-damaged lymphocytes. *Photochem Photobiol Sci*. 2004;3(1):85-90.
 81. Cooke MS, Evans MD, Dizdaroglu M, Lunec J. Oxidative DNA damage: mechanisms, mutation, and disease. *FASEB J*. 2003;17(10):1195-1214.
 82. Evans MD, Cooke MS. Oxidative damage to DNA in non-malignant disease: biomarker or biohazard? *Genome Dyn*. 2006;1:53-66.
 83. Brand RM, Wipf P, Durham A, Epperly MW, Greenberger JS, Falo LD. Targeting Mitochondrial Oxidative Stress to Mitigate UV-Induced Skin Damage. *Front Pharmacol*. 2018;9(AUG).
 84. Adar S, Hu J, Lieb JD, Sancar A. Genome-wide kinetics of DNA excision repair in relation to chromatin state and mutagenesis. *Proc Natl Acad Sci U S A*. 2016;113(15):E2124-E2133.
 85. Evans MD, Dizdaroglu M, Cooke MS. Oxidative DNA damage and disease: Induction, repair and significance. *Mutat Res Rev Mutat Res*. 2004;567(1):1-61.
 86. Delinasios GJ, Karbaschi M, Cooke MS, Young AR. Vitamin E inhibits the UVA1 induction of "light" and "dark" cyclobutane pyrimidine dimers, and oxidatively generated DNA damage, in keratinocytes. *Sci Rep*. 2018;8(1).
 87. Toriyama E, Masuda H, Torii K, Ikumi K, Morita A. Time kinetics of cyclobutane pyrimidine dimer formation by narrowband and broadband UVB irradiation. *J Dermatol Sci*. 2021;103(3):151-155.
 88. Karbaschi M, Macip S, Mistry V, et al. Rescue of cells from apoptosis increases DNA repair in UVB exposed cells: implications for the DNA damage response. *Toxicol Res (Camb)*. 2015;4(3):725-738.
 89. Kim J -K, Patel D, Choi B -S. Contrasting structural impacts induced by cis-syn

- cyclobutane dimer and (6-4) adduct in DNA duplex decamers: implication in mutagenesis and repair activity. *Photochem Photobiol.* 1995;62(1):44-50.
90. Koronowski KB, Sassone-Corsi P. Communicating clocks shape circadian homeostasis. *Science.* 2021;371(6530).
 91. Pittendrigh CS. Temporal organization: reflections of a Darwinian clock-watcher. *Annu Rev Physiol.* 1993;55:17-54.
 92. Roenneberg T, Daan S, Mrosovsky M. The art of entrainment. *J Biol Rhythms.* 2003;18(3):183-194.
 93. Roenneberg T, Foster RG. Twilight times: light and the circadian system. *Photochem Photobiol.* 1997;66(5):549-561.
 94. Schmutz I, Ripperger JA, Baeriswyl-Aebischer S, Albrecht U. The mammalian clock component PERIOD2 coordinates circadian output by interaction with nuclear receptors. *Genes Dev.* 2010;24(4):345-357.
 95. Brown SA, Ripperger J, Kadener S, et al. PERIOD1-associated proteins modulate the negative limb of the mammalian circadian oscillator. *Science.* 2005;308(5722):693-696.
 96. Mohawk JA, Green CB, Takahashi JS. Central and peripheral circadian clocks in mammals. *Annu Rev Neurosci.* 2012;35:445-462.
 97. Schibler U, Sassone-Corsi P. A web of circadian pacemakers. *Cell.* 2002;111(7):919-922.
 98. Menaker M, Moreira LF, Tosini G. Evolution of circadian organization in vertebrates. *Braz J Med Biol Res.* 1997;30(3):305-313.
 99. Chen L, Yang G. Recent advances in circadian rhythms in cardiovascular system. *Front Pharmacol.* 2015;6(APR).
 100. Hastings MH, Goedert M. Circadian clocks and neurodegenerative diseases: time to aggregate? *Curr Opin Neurobiol.* 2013;23(5):880-887.
 101. Kinouchi K, Sassone-Corsi P. Metabolic rivalry: circadian homeostasis and tumorigenesis. *Nat Rev Cancer.* 2020;20(11):645-661.
 102. Marcheva B, Ramsey KM, Buhr ED, et al. Disruption of the clock components CLOCK and BMAL1 leads to hypoinsulinaemia and diabetes. *Nature.* 2010;466(7306):627-631.
 103. Turek FW, Joshu C, Kohsaka A, et al. Obesity and metabolic syndrome in circadian Clock mutant mice. *Science.* 2005;308(5724):1043-1045.
 104. Partch CL, Green CB, Takahashi JS. Molecular architecture of the mammalian circadian clock. *Trends Cell Biol.* 2014;24(2):90-99.
 105. Reppert SM, Weaver DR. Molecular analysis of mammalian circadian rhythms.

- Annu Rev Physiol.* 2001;63:647-676.
106. Ye R, Selby CP, Ozturk N, Annayev Y, Sancar A. Biochemical analysis of the canonical model for the mammalian circadian clock. *J Biol Chem.* 2011;286(29):25891-25902.
 107. Xu H, Gustafson CL, Sammons PJ, et al. Cryptochrome 1 regulates the circadian clock through dynamic interactions with the BMAL1 C terminus. *Nat Struct Mol Biol.* 2015;22(6):476-484.
 108. Shearman LP, Sriram S, Weaver DR, et al. Interacting molecular loops in the mammalian circadian clock. *Science.* 2000;288(5468):1013-1019.
 109. Ye R, Selby CP, Chiou YY, Ozkan-Dagliyan I, Gaddameedhi S, Sancar A. Dual modes of CLOCK:BMAL1 inhibition mediated by Cryptochrome and Period proteins in the mammalian circadian clock. *Genes Dev.* 2014;28(18):1989-1998.
 110. Tamai TK, Young LC, Whitmore D. Light signaling to the zebrafish circadian clock by Cryptochrome 1a. *Proc Natl Acad Sci U S A.* 2007;104(37):14712-14717.
 111. Cahill GM. Clock mechanisms in zebrafish. *Cell Tissue Res.* 2002;309(1):27-34.
 112. Kobayashi Y, Ishikawa T, Hirayama J, et al. Molecular analysis of zebrafish photolyase/cryptochrome family: two types of cryptochromes present in zebrafish. *Genes Cells.* 2000;5(9):725-738.
 113. Whitmore D, Foulkes NS, Strähle U, Sassone-Corsi P. Zebrafish Clock rhythmic expression reveals independent peripheral circadian oscillators. *Nat Neurosci.* 1998;1(8):701-707.
 114. Ishikawa T, Hirayama J, Kobayashi Y, Todo T. Zebrafish CRY represses transcription mediated by CLOCK-BMAL heterodimer without inhibiting its binding to DNA. *Genes Cells.* 2002;7(10):1073-1086.
 115. Delaunay F, Thisse C, Marchand O, Laudet V, Thisse B. An inherited functional circadian clock in zebrafish embryos. *Science.* 2000;289(5477):297-300.
 116. Hughes S, Jagannath A, Hankins MW, Foster RG, Peirson SN. Photic regulation of clock systems. *Methods Enzymol.* 2015;552:125-143.
 117. Moore RY, Eichler VB. Loss of a circadian adrenal corticosterone rhythm following suprachiasmatic lesions in the rat. *Brain Res.* 1972;42(1):201-206.
 118. Richter CP. Inborn nature of the rat's 24-hour clock. *J Comp Physiol Psychol.* 1971;75(1):1-4.
 119. Stephan FK, Zucker I. Circadian rhythms in drinking behavior and locomotor activity of rats are eliminated by hypothalamic lesions. *Proc Natl Acad Sci U S A.* 1972;69(6):1583-1586.
 120. Moore RY, Speh JC, Patrick Card J. The retinohypothalamic tract originates from a distinct subset of retinal ganglion cells. *J Comp Neurol.* 1995;352(3):351-366.

121. Daan S. The Colin S. Pittendrigh Lecture. Colin Pittendrigh, Jürgen Aschoff, and the natural entrainment of circadian systems. *J Biol Rhythms*. 2000;15(3):195-207.
122. Foster RG. Shedding light on the biological clock. *Neuron*. 1998;20(5):829-832.
123. Berson DM, Dunn FA, Takao M. Phototransduction by retinal ganglion cells that set the circadian clock. *Science*. 2002;295(5557):1070-1073.
124. Sekaran S, Foster RG, Lucas RJ, Hankins MW. Calcium imaging reveals a network of intrinsically light-sensitive inner-retinal neurons. *Curr Biol*. 2003;13(15):1290-1298.
125. Do MTH, Yau KW. Intrinsically photosensitive retinal ganglion cells. *Physiol Rev*. 2010;90(4):1547-1581.
126. Hankins MW, Peirson SN, Foster RG. Melanopsin: an exciting photopigment. *Trends Neurosci*. 2008;31(1):27-36.
127. Schmidt TM, Do MTH, Dacey D, Lucas R, Hattar S, Matynia A. Melanopsin-positive intrinsically photosensitive retinal ganglion cells: from form to function. *J Neurosci*. 2011;31(45):16094-16101.
128. Provencio I, Rodriguez IR, Jiang G, Hayes WP, Moreira EF, Rollag MD. A novel human opsin in the inner retina. *J Neurosci*. 2000;20(2):600-605.
129. Hughes S, Jagannath A, Hankins MW, Foster RG, Peirson SN. Photic regulation of clock systems. *Methods Enzymol*. 2015;552:125-143.
130. Hughes S, Jagannath A, Hickey D, et al. Using siRNA to define functional interactions between melanopsin and multiple G Protein partners. *Cell Mol Life Sci*. 2015;72(1):165-179.
131. Graham DM, Wong KY, Shapiro P, Frederick C, Pattabiraman K, Berson DM. Melanopsin ganglion cells use a membrane-associated rhabdomic phototransduction cascade. *J Neurophysiol*. 2008;99(5):2522-2532.
132. Hartwick ATE, Bramley JR, Yu J, et al. Light-evoked calcium responses of isolated melanopsin-expressing retinal ganglion cells. *J Neurosci*. 2007;27(49):13468-13480.
133. Güler AD, Ecker JL, Lall GS, et al. Melanopsin cells are the principal conduits for rod-cone input to non-image-forming vision. *Nature*. 2008;453(7191):102-105.
134. Altimus CM, Güler AD, Alam NM, et al. Rod photoreceptors drive circadian photoentrainment across a wide range of light intensities. *Nat Neurosci*. 2010;13(9):1107-1112.
135. Lall GS, Revell VL, Momiji H, et al. Distinct contributions of rod, cone, and melanopsin photoreceptors to encoding irradiance. *Neuron*. 2010;66(3):417-428.

136. Lucas RJ, Lall GS, Allen AE, Brown TM. How rod, cone, and melanopsin photoreceptors come together to enlighten the mammalian circadian clock. *Prog Brain Res.* 2012;199:1-18.
137. Ding JM, Chen D, Weber ET, Faiman LE, Rea MA, Gillette MU. Resetting the biological clock: mediation of nocturnal circadian shifts by glutamate and NO. *Science.* 1994;266(5191):1713-1717.
138. Hannibal J, Møller M, Petter Ottersen O, Fahrenkrug J. PACAP and Glutamate Are Co-Stored in the Retinohypothalamic Tract. *J Comp Neurol.* 2000;418:147-155.
139. Meijer JH, Schwartz WJ. In search of the pathways for light-induced pacemaker resetting in the suprachiasmatic nucleus. *J Biol Rhythms.* 2003;18(3):235-249.
140. Gau D, Lemberger T, von Gall C, et al. Phosphorylation of CREB Ser142 regulates light-induced phase shifts of the circadian clock. *Neuron.* 2002;34(2):245-253.
141. Ginty DD, Kornhauser JM, Thompson MA, et al. Regulation of CREB phosphorylation in the suprachiasmatic nucleus by light and a circadian clock. *Science.* 1993;260(5105):238-241.
142. Schwartz WJ, Tavakoli-Nezhad M, Lambert CM, Weaver DR, de La Iglesia HO. Distinct patterns of Period gene expression in the suprachiasmatic nucleus underlie circadian clock photoentrainment by advances or delays. *Proc Natl Acad Sci U S A.* 2011;108(41):17219-17224.
143. Whitmore D, Foulkes NS, Sassone-Corsi P. Light acts directly on organs and cells in culture to set the vertebrate circadian clock. *Nature.* 2000;404(6773):87-91.
144. Vallone D, Gondi SB, Whitmore D, Foulkes NS. E-box function in a period gene repressed by light. *Proc Natl Acad Sci U S A.* 2004;101(12):4106-4111.
145. Davies WIL, Tamai TK, Zheng L, et al. An extended family of novel vertebrate photopigments is widely expressed and displays a diversity of function. *Genome Res.* 2015;25(11):1666-1679.
146. Gavriouchkina D, Fischer S, Ivacevic T, Stolte J, Benes V, Dekens MPS. Thyrotroph embryonic factor regulates light-induced transcription of repair genes in zebrafish embryonic cells. *PLoS One.* 2010;5(9):1-10.
147. Weger BD, Sahinbas M, Otto GW, et al. The light responsive transcriptome of the zebrafish: function and regulation. *PLoS One.* 2011;6(2).
148. Wang M, Zhong Z, Zhong Y, Zhang W, Wang H. The zebrafish period2 protein positively regulates the circadian clock through mediation of retinoic acid receptor (RAR)-related orphan receptor α (Ror α). *J Biol Chem.* 2015;290(7):4367-4382.
149. Vatine G, Vallone D, Appelbaum L, et al. Light directs zebrafish period2 expression via conserved D and E boxes. *PLoS Biol.* 2009;7(10).

150. Mracek P, Santoriello C, Idda ML, et al. Regulation of per and cry genes reveals a central role for the D-box enhancer in light-dependent gene expression. *PLoS One*. 2012;7(12).
151. Hirayama J, Cho S, Sassone-Corsi P. Circadian control by the reduction/oxidation pathway: catalase represses light-dependent clock gene expression in the zebrafish. *Proc Natl Acad Sci U S A*. 2007;104(40):15747-15752.
152. Zhao H, di Mauro G, Lungu-Mitea S, et al. Modulation of DNA Repair Systems in Blind Cavefish during Evolution in Constant Darkness. *Curr Biol*. 2018;28(20):3229-3243.e4.
153. Pagano C, Siauciunaite R, Idda ML, et al. Evolution shapes the responsiveness of the D-box enhancer element to light and reactive oxygen species in vertebrates. *Sci Rep*. 2018;8(1).
154. Gachon F. Physiological function of PARbZip circadian clock-controlled transcription factors. *Ann Med*. 2007;39(8):562-571.
155. Vatine G, Vallone D, Appelbaum L, et al. Light directs zebrafish period2 expression via conserved D and E boxes. *PLoS Biol*. 2009;7(10).
156. Ben-Moshe Z, Vatine G, Alon S, et al. Multiple PAR and E4BP4 bZIP transcription factors in zebrafish: diverse spatial and temporal expression patterns. *Chronobiol Int*. 2010;27(8):1509-1531.
157. Gachon F, Fonjallaz P, Damiola F, et al. The loss of circadian PAR bZip transcription factors results in epilepsy. *Genes Dev*. 2004;18(12):1397-1412.
158. Ossipow V, Fonjallaz P, Schibler U. An RNA polymerase II complex containing all essential initiation factors binds to the activation domain of PAR leucine zipper transcription factor thyroid embryonic factor. *Mol Cell Biol*. 1999;19(2):1242-1250.
159. Landschulz WH, Johnson PF, McKnight SL. The leucine zipper: a hypothetical structure common to a new class of DNA binding proteins. *Science*. 1988;240(4860):1759-1764.
160. O'Shea EK, Rutkowski R, Kim PS. Evidence that the leucine zipper is a coiled coil. *Science*. 1989;243(4890):538-542.
161. Hurst HC. Transcription factors 1: bZIP proteins. *Protein Profile*. 1995;2(2):101-168.
162. Struhl K. Helix-turn-helix, zinc-finger, and leucine-zipper motifs for eukaryotic transcriptional regulatory proteins. *Trends Biochem Sci*. 1989;14(4):137-140.
163. Drolet DW, Scully KM, Simmons DM, et al. TEF, a transcription factor expressed specifically in the anterior pituitary during embryogenesis, defines a new class of leucine zipper proteins. *Genes Dev*. 1991;5(10):1739-1753.

164. Ripperger JA, SLRSSU. CLOCK, an essential pacemaker component, controls expression of the circadian transcription factor DBP. *Genes Dev.* 2000;14(6)(15):679-689.
165. Mitsui S, Yamaguchi S, Matsuo T, Ishida Y, Okamura H. Antagonistic role of E4BP4 and PAR proteins in the circadian oscillatory mechanism. *Genes Dev.* 2001;15(8):995-1006.
166. Ohno T, Onishi Y, Ishida N. The negative transcription factor E4BP4 is associated with circadian clock protein PERIOD2. *Biochem Biophys Res Commun.* 2007;354(4):1010-1015.
167. Gachon F, Olela FF, Schaad O, Descombes P, Schibler U. The circadian PAR-domain basic leucine zipper transcription factors DBP, TEF, and HLF modulate basal and inducible xenobiotic detoxification. *Cell Metab.* 2006;4(1):25-36.
168. Yamaguchi S, Mitsui S, Yan L, Yagita K, Miyake S, Okamura H. Role of DBP in the circadian oscillatory mechanism. *Mol Cell Biol.* 2000;20(13):4773-4781.
169. Doi M, Nakajima Y, Okano T, Fukada Y. Light-induced phase-delay of the chicken pineal circadian clock is associated with the induction of cE4bp4, a potential transcriptional repressor of cPer2 gene. *Proc Natl Acad Sci U S A.* 2001;98(14):8089-8094.
170. Weng YJ, Hsieh DJY, Kuo WW, et al. E4BP4 is a cardiac survival factor and essential for embryonic heart development. *Mol Cell Biochem.* 2010;340(1-2):187-194.
171. Cowell IG. E4BP4/NFIL3, a PAR-related bZIP factor with many roles. *BioEssays.* 2002;24(11):1023-1029.
172. Gaddameedhi S, Selby CP, Kaufmann WK, Smart RC, Sancar A. Control of skin cancer by the circadian rhythm. *Proc Natl Acad Sci U S A.* 2011;108(46):18790-18795.
173. Kang TH, Lindsey-Boltz LA, Reardon JT, Sancar A. Circadian control of XPA and excision repair of cisplatin-DNA damage by cryptochrome and HERC2 ubiquitin ligase. *Proc Natl Acad Sci U S A.* 2010;107(11):4890-4895.
174. Lin C, Todo T. The cryptochromes. *Genome Biol.* 2005;6(5).
175. Cashmore AR, Jarillo JA, Wu YJ, Liu D. Cryptochromes: blue light receptors for plants and animals. *Science.* 1999;284(5415):760-765.
176. Hsu DS, Zhao X, Zhao S, et al. Putative human blue-light photoreceptors hCRY1 and hCRY2 are flavoproteins. *Biochemistry.* 1996;35(44):13871-13877.
177. Sancar A, Thompson C, Thresher RJ, et al. Photolyase/cryptochrome family blue-light photoreceptors use light energy to repair DNA or set the circadian clock. *Cold Spring Harb Symp Quant Biol.* 2000;65:157-171.

178. Ahmad M, Cashmore AR. HY4 gene of *A. thaliana* encodes a protein with characteristics of a blue-light photoreceptor. *Nature*. 1993;366(6451):162-166.
179. Todo T, Ryo H, Yamamoto K, et al. Similarity among the *Drosophila* (6-4)photolyase, a human photolyase homolog, and the DNA photolyase-blue-light photoreceptor family. *Science*. 1996;272(5258):109-112.
180. Todo T, Takemori H, Ryo H, et al. A new photoreactivating enzyme that specifically repairs ultraviolet light-induced (6-4)photoproducts. *Nature*. 1993;361(6410):371-374.
181. Ceriani MF, Darlington TK, Staknis D, et al. Light-dependent sequestration of TIMELESS by CRYPTOCHROME. *Science*. 1999;285(5427):553-556.
182. Reppert SM, Weaver DR. Coordination of circadian timing in mammals. *Nature*. 2002;418(6901):935-941.
183. Somers DE, Devlin PF, Kay SA. Phytochromes and cryptochromes in the entrainment of the *Arabidopsis* circadian clock. *Science*. 1998;282(5393):1488-1490.
184. Wang H, Ma LG, Li JM, Zhao HY, Xing Wang Deng. Direct interaction of *Arabidopsis* cryptochromes with COP1 in light control development. *Science*. 2001;294(5540):154-158.
185. Yang HQ, Tang RH, Cashmore AR. The signaling mechanism of *Arabidopsis* CRY1 involves direct interaction with COP1. *Plant Cell*. 2001;13(12):2573-2587.
186. Ahmad M, Jarillo JA, Smirnova O, Cashmore AR. Cryptochrome blue-light photoreceptors of *Arabidopsis* implicated in phototropism. *Nature*. 1998;392(6677):720-723.
187. Guo H, Yang H, Mockler TC, Lin C. Regulation of flowering time by *Arabidopsis* photoreceptors. *Science*. 1998;279(5355):1360-1363.
188. Lin C, Yang H, Guo H, Mockler T, Chen J, Cashmore AR. Enhancement of blue-light sensitivity of *Arabidopsis* seedlings by a blue light receptor cryptochrome 2. *Proc Natl Acad Sci U S A*. 1998;95(5):2686-2690.
189. Chaves I, Nijman RM, Biernat MA, et al. The Potorous CPD photolyase rescues a cryptochrome-deficient mammalian circadian clock. *PLoS One*. 2011;6(8).
190. Coesel S, Mangogna M, Ishikawa T, et al. Diatom PtCPF1 is a new cryptochrome/photolyase family member with DNA repair and transcription regulation activity. *EMBO Rep*. 2009;10(6):655-661.
191. Heijde M, Zabulon G, Corellou F, et al. Characterization of two members of the cryptochrome/photolyase family from *Ostreococcus tauri* provides insights into the origin and evolution of cryptochromes. *Plant Cell Environ*. 2010;33(10):1614-1626.

192. Brudler R, Hitomi K, Daiyasu H, et al. Identification of a new cryptochrome class. Structure, function, and evolution. *Mol Cell*. 2003;11(1):59-67.
193. Gerkema MP, Davies WIL, Foster RG, Menaker M, Hut RA. The nocturnal bottleneck and the evolution of activity patterns in mammals. *Proc Biol Sci*. 2013;280(1765).
194. Davis DD, Walls GL. The Vertebrate Eye and Its Adaptive Radiation. *J Mammal*. 1942;23(4):453.
195. Balsalobre A, Damiola F, Schibler U. A serum shock induces circadian gene expression in mammalian tissue culture cells. *Cell*. 1998;93(6):929-937.
196. Balsalobre A, Marcacci L, Schibler U. Multiple signaling pathways elicit circadian gene expression in cultured Rat-1 fibroblasts. *Curr Biol*. 2000;10(20):1291-1294.
197. Brown SA, Zimbrunn G, Fleury-Olela F, Preitner N, Schibler U. Rhythms of mammalian body temperature can sustain peripheral circadian clocks. *Curr Biol*. 2002;12(18):1574-1583.
198. Davies WIL, Collin SP, Hunt DM. Molecular ecology and adaptation of visual photopigments in craniates. *Mol Ecol*. 2012;21(13):3121-3158.
199. Yokoyama S. Molecular evolution of vertebrate visual pigments. *Prog Retin Eye Res*. 2000;19(4):385-419.
200. Painter RB. DNA damage and repair in eukaryotic cells. *Genetics*. 1974;78(1):139-148.
201. Cook JS, Regan JD. Photoreactivation and photoreactivating enzyme activity in an order of mammals (Marsupialia). *Nature*. 1969;223(5210):1066-1067.
202. Yasui A, Eker APM, Yasuhira S, et al. A new class of DNA photolyases present in various organisms including aplacental mammals. *EMBO J*. 1994;13(24):6143-6151.
203. Doyle S, Menaker M. Circadian photoreception in vertebrates. *Cold Spring Harb Symp Quant Biol*. 2007;72:499-508.
204. Whitmore D, Foulkes NS, Sassone-Corsi P. Light acts directly on organs and cells in culture to set the vertebrate circadian clock. *Nature*. 2000;404(6773):87-91.
205. Loew ER, McFarland WN. The underwater visual environment. *The Visual System of Fish*. Published online 1990:1-43.
206. Trajano E, Bichuette M, Kapoor B. Biology of subterranean fishes. Published online 2010.
207. Alunni A, Menuet A, Candal E, Pénigault JB, Jeffery WR, Rétaux S. Developmental mechanisms for retinal degeneration in the blind cavefish *Astyanax mexicanus*. *J Comp Neurol*. 2007;505(2):221-233.

208. Stemmer M, Schuhmacher LN, Foulkes NS, Bertolucci C, Wittbrodt J. Cavefish eye loss in response to an early block in retinal differentiation progression. *Development*. 2015;142(4):743-752.
209. Yoshizawa M, Yamamoto Y, O'Quin KE, Jeffery WR. Evolution of an adaptive behavior and its sensory receptors promotes eye regression in blind cavefish. *BMC Biol*. 2012;10.
210. Beale A, Guibal C, Tamai TK, et al. Circadian rhythms in Mexican blind cavefish *Astyanax mexicanus* in the lab and in the field. *Nat Commun*. 2013;4.
211. Cavallari N, Frigato E, Vallone D, et al. A blind circadian clock in cavefish reveals that opsins mediate peripheral clock photoreception. *PLoS Biol*. 2011;9(9).
212. Tarttelin EE, Frigato E, Bellingham J, et al. Encephalic photoreception and phototactic response in the troglobiont Somalian blind cavefish *Phreatichthys andruzzii*. *J Exp Biol*. 2012;215(Pt 16):2898-2903.
213. Ishikawa-Fujiwara T, Shiraishi E, Fujikawa Y, Mori T, Tsujimura T, Todo T. Targeted Inactivation of DNA Photolyase Genes in Medaka Fish (*Oryzias latipes*). *Photochem Photobiol*. 2017;93(1):315-322.
214. Mosmann T. Rapid colorimetric assay for cellular growth and survival: application to proliferation and cytotoxicity assays. *J Immunol Methods*. 1983;65(1-2):55-63.
215. Fritsch-Decker S, An Z, Yan J, et al. Silica Nanoparticles Provoke Cell Death Independent of p53 and BAX in Human Colon Cancer Cells. *Nanomaterials (Basel)*. 2019;9(8).
216. Hansjosten I, Rapp J, Reiner L, et al. Microscopy-based high-throughput assays enable multi-parametric analysis to assess adverse effects of nanomaterials in various cell lines. *Arch Toxicol*. 2018;92(2):633-649.
217. Pagano C, Martino O di, Ruggiero G, et al. The tumor-associated YB-1 protein: new player in the circadian control of cell proliferation. *Oncotarget*. 2017;8(4):6193-6205.
218. Beale A. The circadian clock of the Mexican blind cavefish, *Astyanax mexicanus*. *PhD thesis (UCL, London)*. Published online 2013.
219. Özer Z, Reardon JT, Hsu DS, Malhotra K, Sancar A. The other function of DNA photolyase: stimulation of excision repair of chemical damage to DNA. *Biochemistry*. 1995;34(49):15886-15889.
220. Domankevich V, Eddini H, Odeh A, Shams I. Resistance to DNA damage and enhanced DNA repair capacity in the hypoxia-tolerant blind mole rat *Spalax carmeli*. *J Exp Biol*. 2018;221(Pt 8).
221. Jostes RF. Genetic, cytogenetic, and carcinogenic effects of radon: a review. *Mutat Res*. 1996;340(2-3):125-139.

222. Allegrucci G, Sbordoni V, Cesaroni D. Is radon emission in caves causing deletions in satellite DNA sequences of cave-dwelling crickets? *PLoS One*. 2015;10(3).
223. Lahiri K, Vallone D, Gondi SB, Santoriello C, Dickmeis T, Foulkes NS. Temperature regulates transcription in the zebrafish circadian clock. *PLoS Biol*. 2005;3(11):2005-2016.
224. Zheng N, Shabek N. Ubiquitin Ligases: Structure, Function, and Regulation. *Annu Rev Biochem*. 2017;86:129-157.
225. Varshavsky A. The Ubiquitin System, Autophagy, and Regulated Protein Degradation. *Annu Rev Biochem*. 2017;86:123-128.
226. Özgür S, Sancar A. Purification and properties of human blue-light photoreceptor cryptochrome 2. *Biochemistry*. 2003;42(10):2926-2932.